



MÉMOIRE
PRÉSENTÉ À
L'UNIVERSITÉ DU QUÉBEC À CHICOUTIMI
COMME EXIGENCE PARTIELLE
DE LA MAÎTRISE EN INGÉNIERIE

PAR
Marwan Hamed

Paramètres de fraisage pour les alliages coulées Al-Cu et Al-Si

Quebec, Canada

© [Marwan Hamed], [2019]



THESIS

PRESENTED TO

UNIVERSITY OF QUEBEC AT CHICOUTIMI

IN PARTIAL FULFILLMENT OF THE REQUIREMENT FOR

THE DEGREE OF MASTER IN ENGINEERING

BY

Marwan Hamed

Milling Parameters For Al-Cu and Al-Si Cast Alloys

Quebec, Canada

© [Marwan Hamed], [2019]

*Dedicated to my parents,
my sister Rana, my cousin zīha
and my best friend Marwan Sallam...*

#19

ACKNOWLEDGMENT

First and foremost, I would like to thank God Almighty for giving me the strength, knowledge, ability and opportunity to undertake this research study and to persevere and complete it satisfactorily. Without his blessings, this achievement would not have been possible.

I would like to express my sincere gratitude to my supervisor, Prof. Fawzy Hosny Samuel, Professor at Université du Québec à Chicoutimi (Canada) for his guidance, advice and support throughout my research work; it has been an honor to be his student. I would also like to thank my co-supervisor, Prof. Agnes M. Samuel, Research Professor at Université du Québec à Chicoutimi (Canada) for her continuous guidance, support, and helpful suggestions in improving the quality of my thesis. Without their continuous guidance and support it would have been impossible to complete my master's degree.

Financial support received from General Motors Powertrain Group (USA), Natural Sciences and Engineering Research Council of Canada (NSERC), and Corporativo Nemark (Mexico) is gratefully acknowledged. It is a pleasure to thank all those who have contributed in completion of this study: Herbert W. Doty Technical Specialist Materials Technology in General Motor and Salvador Valtierra Gallardo Process Technology Manager in Nemark , I would like to thank my friend and colleague , Eng. Hussien Barakat in TAMLA Group for his help at various stages of my work without him it would be difficult.

I would like to Thank all my friends for not squashing my dreams, but rather encouraging them. Thank you for empowering me, helping me know that I was on track, right where I needed to be. Thank you all for helping me to feel able, in balance and hopeful. Thank you for listening to me and brainstorm my ideas.

Lastly but most importantly My family is everything. I am what I am thanks to my mother, my father and my sister I want to thank my parents and share the love and care that you two have given me in all my life. You are the most perfect parents in this world, the biggest blessing for a child is his parents. I feel lucky all the time for having such amazing parents like you! Love and support of parents can get their son anywhere and everywhere in life. Thank you, mom and dad, for always supporting me.

I would like to take the chance and express my deep love toward my joyful sister Rana who has passed through lots of ups and downs through her life and still have such a pure heart , thank you for inspiring and supporting me and wishing me all the best , thank you my sister I wish you to be strong and wise.

I would like to express my thanks and appreciation to my mentor Mohamed Abdelaziz. You are a wonderful teacher, leader, and friend. You are everything one could look for in a good mentor. Thank you for guiding me on the right path. I will always be thankful to you and I wish you great success in your life.

Thank you all.....

Marwan Hamed
July #19

RÉSUMÉ

La présente étude a été réalisée dans le but d'étudier les caractéristiques d'usinabilité, c'est-à-dire les caractéristiques d'usinage d'un alliage Al-6%Cu-0,7%Si (dans les conditions de vieillissement T5 et T7), et de comparer ces caractéristiques à celles bien définies de l'alliage B319.0 (brut de coulé et traité T7) et A356.0 (brut de coulé et traité T6). Le surfaçage a été effectué sur 15 blocs préparés à partir de chaque alliage en utilisant de nouvelles plaquettes en carbure pour une distance d'usinage d'environ 120 m. Trente-cinq blocs (12 x 7 po x 1,5 po) ont été utilisés. Le fraisage a été effectué à l'aide d'une machine à grande vitesse 5 axes à commande numérique Huron KX Five. L'expérience comprenait la machine à commande numérique, les blocs à usiner, un dynamomètre de table avec des capteurs piézoélectriques chargés de détecter et de mesurer les forces de coupe, un amplificateur de signal et une unité de conversion analogique-numérique. Des plaquettes de coupe neuves et usées ont été utilisées pour chaque groupe d'alliages. Treize couches de matériaux ont été retirées de chaque bloc, chaque couche étant composée de 10 chemins et la profondeur de coupe étant de 1,35 mm.

Les résultats obtenus avec de nouvelles plaquettes ont montré que le traitement thermique appliqué n'affectait pas les forces de coupe des alliages à base d'Al-Cu. La présence de Cu dans l'alliage B319.0 a neutralisé dans une certaine mesure l'effet néfaste des particules de Si dur. Les forces de coupe maximales ont été obtenues lors de l'usinage de l'alliage A356.0 traité au T6, en raison de la présence d'une densité élevée de particules de silicium eutectiques dures (environ 41495 particules/mm²) ainsi que d'une précipitation dense de particules ultrafines de Mg₂Si. Ainsi, les 6% de Cu dans l'alliage à base d'Al-Cu peuvent être considérés comme un autolubrifiant, conduisant à des surfaces de finition beaucoup plus lisses par rapport à celles présentées par les alliages B319.0 et A356.0. Des observations similaires ont été rapportées sur l'usure des outils de forage. En outre, après une distance d'usinage de 120 m, de minuscules bavures ont été collées sur les bords extérieurs de la pièce à usiner, alors que dans le cas de l'alliage A356.0, elles étaient séparées du bloc.

Les inserts émoussés ont été obtenus en passant les inserts neufs sur un bloc de fonte blanche afin de réduire la netteté des nouveaux inserts en carbure. Ce processus a entraîné de graves dommages à l'insert et la formation de cavités profondes. La forme des plaquettes mates et les caractéristiques de coupe varient d'une plaquette à l'autre et il est donc difficile d'obtenir des résultats reproductibles. En raison de la mauvaise forme des plaquettes mates, les efforts de coupe nécessaires pour usiner une distance de 14 m étaient 40 à 50% plus élevés que ceux requis avec les nouvelles plaquettes pour usiner une distance de coupe de 120 m. Le profil de rugosité de surface avec des outils émoussés était presque le double de celui obtenu avec de nouvelles plaquettes. Cependant, les signaux étaient beaucoup plus

larges dans le premier cas avec moins de pics. En raison des graves irrégularités des bords des outils émoussés, ni la composition de l'alliage ni le traitement thermique ne sont pertinents. La finition de surface de tous les alliages était caractérisée par la présence de fissures et de trous peu profonds. Les contraintes résiduelles ont varié sur la largeur du bloc usiné. Toutes les contraintes étaient de type tension par rapport au type compression dans les épaulés non usinés. En raison des forces appliquées élevées requises lors de l'utilisation d'inserts émoussés, les contraintes résiduelles résultantes étaient presque le double de celles générées par les nouveaux inserts malgré la grande différence de distance d'usinage. En raison de l'utilisation d'une douche de liquide de refroidissement, les copeaux étaient brillants et ne présentaient aucun signe de brûlure. Dans tous les cas, les fraises étaient séparées des pièces à traiter (fraises positives).

ABSTRACT

The present study was carried out to study the machinability i.e. milling characteristics of an Al-6%Cu-0.7%Si alloy (in the as-cast, T5 and T7 aging conditions) and compare these characteristics to those of well-defined B319.0 (as-cast, T7-treated) and A356.0 (as-cast, T6-treated) alloys. Wet milling was carried out on 15 blocks prepared from each alloy using new carbide inserts for about 120m machining distance. Thirty-five blocks (12 in x 7 in x 1.5 in) were employed. The milling was carried out using a CNC Huron KX Five 5-axis high speed machine. The experiment comprised the CNC machine, the blocks to be machined, a table dynamometer with piezoelectric sensors that are responsible for detecting and measuring the cutting forces, a signal amplifier and an A/D converting unit. New and dull cutting inserts were used for each alloy group. Thirteen layers of material were removed from each block, where each layer consisted of 10 paths, and the depth of cut was 1.35 mm.

The results employing new inserts showed that the cutting forces for Al-Cu based alloys were not affected by the applied heat treatment. The presence of Cu in the B319.0 alloy neutralized to some extent the harmful effect of the hard Si particles. Maximum cutting forces were obtained from machining the T6-treated A356.0 alloy, due to the presence of a high density of hard eutectic silicon particles (approximately 41495 particles/mm²) in addition to a dense precipitation of ultra-fine Mg₂Si particles. Thus, the 6% Cu in the Al-Cu based alloy may be considered to act as a self-lubricant, leading to much smoother finishing surfaces compared to those exhibited by B319.0 and A356.0 alloys. Similar observations were reported on the wearing of the drilling tools. In addition, after covering 120m machining distance, tiny burrs were found adhered to the outer edges of the block workpiece, whereas the burr in the case of A356.0 alloy was separated from the block.

Dull inserts were obtained by passing the new inserts on a block of white cast iron to reduce the sharpness of the new carbide inserts. This process led to severe damage of the insert and formation of deep cavities. The shape of the dull inserts and cutting characteristics varied from one insert to another and hence it was difficult to produce reproducible results. Due to the bad shape of the dull inserts, the cutting forces required to machine 14 m of distance were 40-50% higher than those required using new inserts to machine 120 m of cutting distance. The profile of surface roughness using dull tools was almost twice that of the profile obtained using new inserts. However, the signals were much wider in the former case with less number of peaks. Due to the severe irregularities of the edges of the dull tools, neither the alloy composition nor the heat treatment is relevant. The surface finish of all alloys was characterized by the presence of cracks and shallow holes. Residual stresses varied along the width of the machined block. All stresses were of tension type compared to compression type in the un-machined shoulders. Due to the high applied forces required when using dull inserts, the resulted residual stresses were almost twice that generated by new inserts in spite of the large difference in the machining distance. Due to the use of showers of coolant, the chips in all cases were shiny with no signs of burning. In all cases, the burrs were separated from the workpieces (positive burr).

TABLE OF CONTENTS

ACKNOWLEDGMENT	I
RÉSUMÉ	III
ABSTRACT.....	V
1 INTRODUCTION	2
1.1 INTRODUCTION	2
1.2 REFERENCES	6
2 SURVEY OF THE LITERATURE AND OBJECTIVES	8
2.1 Al-Cu AND Al-Si-Cu/Mg ALLOYS	8
2.2 Al-Si ALLOYS	9
2.2.1 EFFECT OF ALLOYING ELEMENTS ADDITIONS TO Al-Si ALLOYS	12
2.3 ALUMINUM COPPER ALLOYS	16
2.4 MELT TREATMENT.....	18
2.5 HEAT TREATMENT	19
2.5.1 SOLUTION HEAT TREATMENT	20
2.5.2 QUENCHING.....	21
2.5.3 AGE HARDENING.....	21
2.6 MACHINABILITY.....	24
2.6.1 CUTTING FORCES GENERATED AND FACTORS AFFECTING THEM	27
2.6.2 TOOL LIFE AND TOOL WEAR.....	30
2.6.3 CHIP FORMATION.....	36
2.6.4 PRODUCT QUALITY	41
2.7 OBJECTIVES	42
2.8 REFERENCES.....	43
3 EXPERIMENTAL PROCEDURES.....	52
3.1 INTRODUCTION	52
3.2 MATERIALS AND CASTING PROCEDURES	52
3.3 HEAT TREATMENT	55
3.4 TENSILE TESTING.....	57
3.5 MACHINABILITY TESTING.....	58
3.5.1 MILLING PROCESS.....	58
3.5.2 CUTTING TOOL.....	60
3.5.3 MEASUREMENT OF CUTTING FORCES.....	61

3.5.4	EVALUATION OF SURFACE ROUGHNESS	69
3.6	RESIDUAL STRESS MEASUREMENT	71
3.7	MICROSTRUCTURE EXAMINATION	73
4	RESULTS AND DISCUSSION.....	75
4.1	INTRODUCTION	75
4.2	PART I - USE OF NEW INSERTS	76
4.2.1	MICROSTRUCTURE AND TENSILE PROPERTIES	76
4.2.2	CUTTING FORCES AND TOOL WEAR	80
4.2.3	MEASUREMENT OF RESIDUAL STRESSES.....	89
4.2.4	SURFACE ROUGHNESS AND BURR FORMATION.....	91
4.3	PART II - USE OF DULL INSERTS	96
4.3.1	TOOL SHAPE	96
4.3.2	CUTTING FORCES	98
4.3.3	SURFACE ROUGHNESS	98
4.3.4	SURFACE FINISH.....	101
4.3.5	RESIDUAL STRESSES	103
4.3.6	CHIP SHAPE AND BURRING	104
5	CONCLUSIONS.....	107
5.1	PART I - NEW INSERTS.....	107
5.2	PART II - DULL INSERTS.....	108
5.3	REFERENCES.....	111
APPENDIX.....	Error! Bookmark not defined.	

LIST OF FIGURES

FIGURE 1-1 ALUMINUM - GLOBAL END USE BY SECTOR 2018 [1]	2
FIGURE 1-2 ALUMINUM CONSUMPTION IN LIGHT VEHICLES IN NORTH AMERICA FROM 1975 TO 2028. [5]	4
FIGURE 2-1 ALUMINUM RICH PORTION OF THE AL-SI PHASE DIAGRAM [21].....	9
FIGURE 2-2(A) MICROSTRUCTURE OF HYPOEUTECTIC ALLOY (1.6-12.6% Si) 150X. (B)MICROSTRUCTURE OF EUTECTIC ALLOY (12.6% Si). 400 X. (C) MICROSTRUCTURE OF HYPEREUTECTIC ALLOY (>12.6% Si). 150X [7].	10
FIGURE 2-3 NUCLEATION OF THE DENDRITIC STRUCTURE OF ALPHA ALUMINUM IN AN AL-MG ALLOY (AFTER LIX ET AL. [63]).....	11
FIGURE 2-4 BLOCK LIKE Al_2Cu PHASE AND THE BLOCKY FORM OF Q-PHASE (AFTER E. SAMUEL ET AL. [64]).	12
FIGURE 2-5 THICK ARROW POINTS TO THE B- Al_5FeSi PHASE TRANSFORMING TO Π - $Al_8Mg_3FeSi_6$ PHASE, THIN ARROW REPRESENTS THE Mg_2Si PHASE (AFTER E. SAMUEL ET AL. [64]).....	13
FIGURE 2-6 : (A) B- Al_5FeSi PLATELETS; (B) SCRIPT-LIKE A- Al_8Fe_2Si ; (C) Π - $Al_8FeMg_3Si_6$ PHASE GROWING FROM B; (D) SCRIPT-LIKE Π -PHASE (AFTER J. A. TAYLOR [65]).	14
FIGURE 2-7 PORTION OF ALUMINUM-COPPER BINARY PHASE DIAGRAM. TEMPERATURE RANGES FOR ANNEALING, PRECIPITATION HEAT TREATING, AND SOLUTION HEAT TREATING ARE INDICATED. THE RANGE FOR SOLUTION TREATING IS BELOW THE EUTECTIC [18].	17
FIGURE 2-8 EFFECT OF PHOSPHORUS REFINEMENT ON THE MICROSTRUCTURE OF AL-22SI-1NI-1CU ALLOY. (A) UNREFINED. (B) PHOSPHORUS-REFINED. (C) REFINED AND FLUXED. ALL 100X [6].	18
FIGURE 2-9 SCHEMATIC OF SOLUTIONIZING AND AGING PROCESS.	19
FIGURE 2-10 TEM OBSERVATIONS OF THE EVOLUTION OF THE MICROSTRUCTURE DURING AGING: (A) GP ZONE; (B) θ'' ; (C) θ' ; (D) θ [25].	22
FIGURE 2-11 THE EFFECT OF AGING TEMPERATURE ON THE SEQUENCE OF PRECIPITATE [24].	22
FIGURE 2-12 ALUMINUM–COPPER PHASE DIAGRAM ALONG WITH METASTABLE PHASE BOUNDARIES AT ALUMINUM END [24].	22
FIGURE 2-13 ILLUSTRATION OF THE MACHINING ENVIRONMENT.	24
FIGURE 2-14 THE GEOMETRY OF ORTHOGONAL CUTTING [58].....	27
FIGURE 2-15 CUTTING FORCE VARIATION WITH CUTTING SPEED [56].....	28

FIGURE 2-16 BEHAVIOR OF CUTTING FORCES GENERATED BY DIFFERENT CUTTING TOOLS IN TURNING OF ALUMINUM [17].	29
FIGURE 2-17 VISUALIZATION OF BASIC TERMS IN ORTHOGONAL CUTTING [57].	30
FIGURE 2-18 TEMPERATURE GRADIENT ACROSS TOOL AND WORKPIECE DURING MACHINING [27].	32
FIGURE 2-19 TYPES OF TOOL WEAR ACCORDING TO STANDARD ISO 3685:1993 [57].	34
FIGURE 2-20 FLANK WEAR EVOLUTION WHEN DRILLING AL-SI ALLOYS AND MMC USING PCD TIPPED DRILLS [27].	35
FIGURE 2-21 EXAMPLES OF (A) SHOWS CONTINUOUS CHIP FORMATION. (B) SHOWS CONTINUOUS CHIP FORMATION WITH BUE , (C) SHOWS DISCONTINUOUS CHIP FORMATION [52].	36
FIGURE 2-22 EFFECT OF FEED RATE ON THE MORPHOLOGY OF CONTINUOUS CHIPS DURING MACHINING OF UNS A97075-T6 (AL-ZN) AND UNS A92024-T3 (AL-CU) ALLOYS [61].	37
FIGURE 2-23 (A) BUE DEVELOPED DURING DRY TURNING OF AA2024-T351 AT CUTTING SPEED 60 M/ MIN , FEED = 0.1 MM AND RAKE ANGLE 0 DEGREES; (B) SURFACE FINISH WITHOUT BUE; (C) SURFACE FINISH WITH BUE ON THE TOOL EDGE [52].	38
FIGURE 2-24 DISCONTINUOUS CHIPS OBTAINED FROM BRITTLE WORK MATERIAL, LOW CUTTING SPEEDS, LARGE FEED AND DEPTH OF CUT [52].	39
FIGURE 3-1 ELECTRIC RESISTANCE FURNACE.	54
FIGURE 3-2 BOOK MOLD AND CAST MACHINING BLOCK.	54
FIGURE 3-3 BLUE M FORCED AIR HEAT TREATMENT FURNACES.	56
FIGURE 3-4 T5, T6 AND T7 HEAT TREATMENT REGIMES.	56
FIGURE 3-5(A) MTS SERVOHYDRAULIC MECHANICAL TESTING MACHINE, (B) ATTACHABLE STRAIN GAUGE.	57
FIGURE 3-6 CNC HURON KX FIVE 5-AXIS MACHINE.	59
FIGURE 3-7 REMOVAL OF LAYERS FROM A CAST BLOCK (A) SCHEMATIC, AND (B) ACTUAL BLOCK.	59
FIGURE 3-8 (A) CONSTRUCTION OF A 3-COMPONENT DYNAMOMETER (FX , FY & FZ), (B) SENSOR ARRANGEMENT OF THE TABLE DYNAMOMETER.	62
FIGURE 3-9 RAW DATA EXTRACTED FROM THE CUTTING FORCE MEASURING SYSTEM SHOWING FX, FY, FZ AND FR FOR ALLOY A.	64
FIGURE 3-10 FREQUENCY DOMAIN BEFORE AND AFTER APPLYING DIGITAL FILTRATION.	65
FIGURE 3-11(A) DEFINING NUMBER OF CYCLES, (B) ILLUSTRATION OF CUTTING FORCES BEFORE AND AFTER CORRECTION.	67
FIGURE 3-12 MAXIMUM PEAK VALUES AND AVERAGE PEAK VALUES.	68

FIGURE 3-13 MITUTOYO SJ-410 MEASURING INSTRUMENT.....	69
FIGURE 3-14 MEASUREMENT OF RESIDUAL STRESSES IN THE BLOCK AT THE END OF THE MILLING PROCESS.	71
FIGURE 3-15 LEICA DM LM OPTICAL MICROSCOPE.	73
FIGURE 3-16 STRUERS TEGRAPOL-35 GRINDER-POLISHER.	73
FIGURE 4-1 OPTICAL MICROSTRUCTURES OF ALLOYS IN THE AS-CAST CONDITION: (A) HT200 ALLOY, (B) 319 ALLOY, (C) 356 ALLOY.....	77
FIGURE 4-2 BACKSCATTERED ELECTRON IMAGES OF: (A) ALLOY D; (B) ALLOY C IN T7 CONDITION, (C) ALLOY E IN T6 CONDITION. PFZ = PRECIPITATE FREE ZONES.	79
FIGURE 4-3 SCHEMATIC REPRESENTATION SHOWING THE INFLUENCE OF THE INCREASING AGING TEMPERATURE ON THE SIZE , DENSITY ,AND INTER-PARTICLE SPACING OF THE HARDENING PRECIPITATES : (A) AT A LOW AGING TEMPERATURE , AND (B) AT A HIGH AGING TEMPERATURE (L1 AND L2 INDICATE INTER-PARTICLE SPACING).	80
FIGURE 4-4 RESULTANT CUTTING FORCES OBTAINED FOR (A) ALLOYS A, B AND C IN THE AS-CAST, T5 AND T7 HEAT-TREATED CONDITIONS, RESPECTIVELY; COMPARISON OF RESULTANT CUTTING FORCES (B) FOR COMMERCIAL ALLOYS E AND D, AND (C) FOR ALLOY C WITH ALLOY D.....	83
FIGURE 4-5 (A) CUTTING EDGE OF NEW INSERT, (B) CUTTING EDGE AFTER MACHINING 120 M, (C) FACE OF NEW INSERT, (D) FACE OF THE INSERT AFTER MACHINING 120 M IN ALLOY A.	84
FIGURE 4-6 (A) CUTTING EDGE OF NEW INSERT (B) CUTTING EDGE AFTER MACHINING 120 M (C) FACE OF NEW INSERT (D) FACE OF THE INSERT AFTER MACHINING 120 M - ALLOY C.	85
FIGURE 4-7 (A) CUTTING EDGE AFTER MACHINING 120 M OF ALLOY C, (B) CUTTING EDGE AFTER MACHINING 120 M OF ALLOY D, (C) FACE OF THE INSERT AFTER MACHINING 120 M OF ALLOY C, (D) FACE OF THE INSERT AFTER MACHINING 120 M OF ALLOY D.....	88
FIGURE 4-8 PORTABLE X-RAY MACHINE [13].....	89
FIGURE 4-9 RESIDUAL STRESSES MEASURED BY X-RAY DIFFRACTION TECHNIQUE IN THE MILLING DIRECTION.	90
FIGURE 4-10 CRITERIA FOR DEFINING THE SURFACE ROUGHNESS:(A) RA, (B) RZ, RT ACCORDING TO ISO	4287. 92
FIGURE 4-11 MEASUREMENTS OF SURFACE ROUGHNESS FOR THE FIVE ALLOYS STUDIED.....	93
FIGURE 4-12 SURFACE ROUGHNESS AFTER MILLING FOR 120 M: (A) ALLOY A, (B) ALLOY C.	93
FIGURE 4-13 SURFACE ROUGHNESS AFTER MILLING FOR 120 M: (A) ALLOY D, (B) ALLOY E.	93
FIGURE 4-14 BURRING FORMATION AFTER 120 M MILLING DISTANCE: (A) ALLOY C, (B) ALLOY E.	94

FIGURE 4-15 CHIP SHAPE AFTER 120 M MILLING DISTANCE OBTAINED FROM: (A) ALLOY C,(B) ALLOY E. 95

FIGURE 4-16 SHAPE OF THE CUTTING INSERTS FOR DIFFERENT CONDITIONS: (A) FRESH TOOL, (B) DULL TOOL- SIDE, (C) DULL TOOL- EDGE, AND (D) DULL TOOL AFTER MACHINING ALLOY E... 97

FIGURE 4-17 CUTTING FORCES FOR BOTH NEW AND DULL INSERTS (14 M OF MACHINING DISTANCE). 98

FIGURE 4-18 PROFILES OF THE MACHINING SURFACE OF ALLOY E: (A) FRESH INSERTS - 120 M MACHINING DISTANCE, AND (B) DULL INSERTS - 14 M MACHINING DISTANCE. 100

FIGURE 4-19 COMPARISON OF ROUGHNESS PARAMETERS FOR THE FIVE ALLOYS USING NEW INSERTS (120 M MACHINING DISTANCE) AND DULL INSERTS (14 M MACHINING DISTANCE).. 101

FIGURE 4-20 COMPARISON OF SURFACE FINISH OF ALLOY C: (A) NEW INSERTS AND (B) DULL INSERTS. 102

FIGURE 4-21 SURFACE FINISHING USING DULL INSERTS: (A) ALOY A, (B) ALLOY C, (C) ALLOY E.102

FIGURE 4-22 RESIDUAL STRESSES MEASURED IN THE TRANSVERSE DIRECTION FOR ALLOY C..... 103

FIGURE 4-23 SHAPE OF THE CHIPS OBTAINED USING DULL INSERTS: (A) ALLOY A, (B) ALLOY C AND (C) ALLOY E. 104

FIGURE 4-24 EXAMPLES OF BURR FORMS DURING MILLING OPERATION [31]..... 105

FIGURE 4-25 BURR FORMS USING DULL TOOLS: (A) ALLOY C, (B) ALLOY E..... 105

LIST OF TABLES

TABLE 2-1 CLASSIFICATION OF CAST ALUMINUM ALLOYS	8
TABLE 2-2 FACTORS INFLUENCING MACHINING OPERATION.....	26
TABLE 3-1 CHEMICAL ANALYSIS OF THE ALLOYS.....	53
TABLE 3-2 ROUGHNESS EVALUATION PARAMETERS.....	70
TABLE 3-3 MEASUREMENT CONDITIONS FOR DETERMINATION OF RESIDUAL STRESSES USING X-RAY TECHNIQUE	72
TABLE 4-1 TENSILE PROPERTIES OF THE STUDIED ALLOYS.....	77
TABLE 4-2 EVALUATION OF THE MAX HARDNESS VALUES HV AT 10 μ M BELOW THE MACHINED SURFACE.....	91

LIST OF EQUATIONS

EQUATION 1 CUTTING FORCE IN X DIRECTION.....	62
EQUATION 2 CUTTING FORCE IN Y DIRECTION.....	62
EQUATION 3 CUTTING FORCE IN Z DIRECTION.....	62
EQUATION 4 RESULTANT CUTTING FORCE.....	62

CHAPTER 1
INTRODUCTION

CHAPTER 1

1 INTRODUCTION

1.1 INTRODUCTION

From the early 1900s, aluminum and its alloys have gained increasing attention. Aluminum is a promising material, due to its exceptional mechanical and physical properties. These properties comprise its light weight due to its low density, good formability, high corrosion resistance, high electrical and thermal conductivity, high stiffness and better high temperature strength. Aluminum alloys are versatile materials that find application in several industries. Figure 1-1 shows the main consumer segments being transportation, construction and packaging. [1]The economic output of the aluminum industry is \$174 billion [2]. The economic impact of the industry finds its basis in job creation and recycling of aluminum. Some 692,000 U.S. jobs were created related to the production, processing and use of aluminum in diverse applications [2]. Aluminum is 100 percent recyclable, making the metal one of the most recyclable of all materials. According to the Aluminum Association, recycling of aluminum has a positive environmental impact in reducing the cost of the energy consumption by 90% compared to that required for primary production of aluminum. [1]

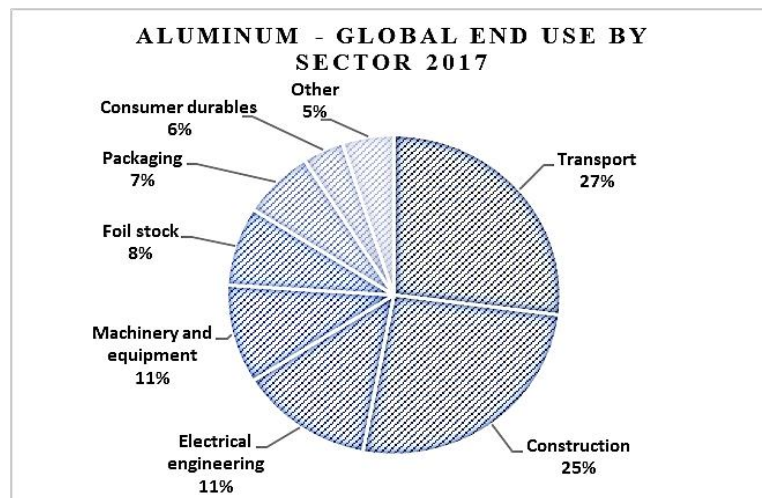


Figure 1-1 Aluminum - global end use by sector 2018 [1]

According to the 2018 annual report of Norsk Hydro, the highest usage of aluminum is in the transportation sector, 27 percent [2]. The main objective in the automotive industry is to increase fuel economy and reduce air pollution. Aluminum alloys can achieve these targets due to their light weight compared to steel and cast iron, materials previously used in automotive vehicles. Each pound of aluminum replaces nearly two pounds of steel. Aluminum also has a higher energy absorption capacity in relation to crash testing. The specific energy absorption of aluminum was found to be twice that of steel during an experimental study performed on structural steel (DP600) and structural aluminum (AA5754) U-beams in high speed crash testing. [3]. With these advantages, the use of aluminum alloys in the automotive industry has developed rapidly within the last decades. Parts such as radiators, wheels, cylinder heads, engine blocks, hoods, doors and car body are now made of aluminum. The reduction in the vehicle's overall weight results in reduction in fuel consumption and air pollution. Passenger vehicles with aluminum intensive design (AIV) have been reported to show a 17 percent reduction in CO₂ emissions [4].

Automotive castings producers specializing in the production of complex aluminum structural components play an important role in vehicle manufacturing. With a view to improving the quality of these components, the development of new alloys is continuously being investigated to meet with the increasing demands of new designs that operate at higher service temperatures which require alloys which can maintain their strength at these high temperatures. Increasing the alloy strength is often at the expense of machinability and may affect manufacturing costs. The integration of a new alloy requires carrying out several

machining tests, in order to understand the behavior of the alloy from the point of view of the quality of the machined parts and wear of the cutting tools.

As Figure 1-2 indicates, the consumption of aluminum in light vehicles has exhibited an increasing trend since 1975, and is expected to increase to 565 pounds per vehicle by 2028 in North America [5]. As a result of this increasing demand, industrialists, specifically automakers, are willing to invest money in order to improve existing commercial alloys as well as creating new alloys. The improvement regarding existing alloys is achieved by either enhancing their mechanical properties such as hardness, tensile strength and impact toughness, or by optimizing manufacturing techniques which is achieved by understanding the machinability characteristics of the alloy in question.

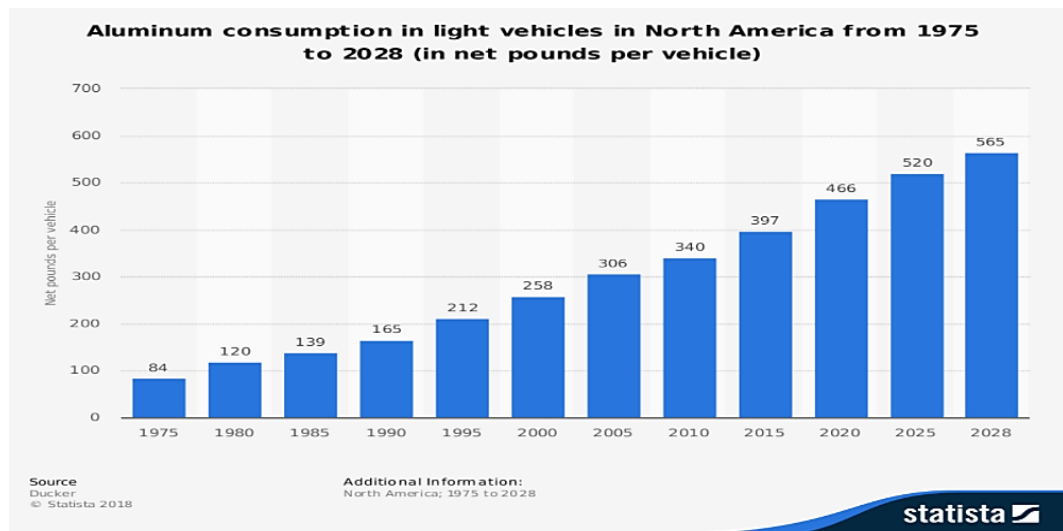


Figure 1-2 Aluminum consumption in light vehicles in North America from 1975 to 2028. [5]

Machining is an important and essential part of the manufacturing process. With the progress in technology development over the last decades, it is easy nowadays to attain a final product with precise dimensions as well as an impressive surface quality. The three main machining processes are milling, turning and drilling. These operations should be

controlled, monitored and optimized to achieve cost effective and sustainable products. This may be achieved by understanding the cutting process and the factors affecting it such as cutting parameters, cutting tool selection, lubrication, etc. The cutting process is suitable for machining almost all materials (ferrous and non-ferrous, soft and hard, ductile and brittle, etc.) [6,7].

With regard to the machinability of aluminum alloys, it is also important to take into consideration the condition of the workpiece (casting) which is controlled by factors such as the alloy composition, microstructure, porosity, heat treatment and properties. According to Elgallad et al. [8] and Tash [9], the machinability of conventionally cast Al-Cu alloys depends primarily on the shape, size and distribution of the eutectic and Al_2Cu precipitation present in the microstructure. The present research study was carried out to investigate the effect of heat treatment conditions on the mechanical properties and the machinability behavior, in particular the milling characteristics, of a recently developed Al-Cu cast alloy, in order to compare its performance with those of well-defined Al-Si based reference alloys, namely 356-T6 and 319-T7 alloys used in automotive components. The machinability characteristics were investigated using a cutting tool with sharp cutting inserts, and compared with those obtained with dull cutting inserts. The results obtained using dull inserts is a supportive evidence for the importance of avoiding the use of the dull inserts while performing machining operations.

1.2 REFERENCES

- [1] "Hydro Annual report 2018," Norsk Hydro ASA, Oslo Norway, 2019.
- [2] "The Aluminum Association," 2019. [Online]. Available:
<https://www.aluminum.org/aluminum-advantage/economic-impact-aluminum>.
- [3] Clark, G & Almond, D & Reynolds, Neil & Hughes, Darren & Pharaoh, M & Williams,
"Comparative energy absorption of U-beams in high-speed crush testing: Thermoplastic
composite, steel & aluminum," in *International SAMPE Technical Conference.*, 2013.
- [4] S. Das, "Life Cycle Energy and Environmental Assessment of Aluminum-Intensive Vehicle
Design," *SAE International Journal of Materials and Manufacturing*, vol. 123, no. 5, 2014.
- [5] "Statista," Ducker, 2018. [Online]. Available:
[https://www.statista.com/statistics/496185/pounds-of-aluminum-per-car-in-north-america/..](https://www.statista.com/statistics/496185/pounds-of-aluminum-per-car-in-north-america/)
[Accessed 15 April 2019].
- [6] E.M. Trent, *Metal Cutting*, Butherworth-Heinemann, Oxford, UK, 3rd edition, 1991, 188-241.
- [7] P. Kovac, L. Sidjanin, *Tribology in Industry*, XVII (1995) 1, 12-16.
- [8] E.M. Elgallad, F.H. Samuel, A.M. Samuel, H.W. Doty, *Journal of Materials Processing
Technology*, 210 (2010) 13, 1754-1766.
- [9] M. Tash, F.H. Samuel, F. Mucciardi, H.W. Doty, S. Valtierra, *Materials Science and
Engineering A*, 434 (2006) 207– 217.

Chapter 2

SURVEY OF THE LITERATURE AND OBJECTIVES

Chapter 2

2 SURVEY OF THE LITERATURE AND OBJECTIVES

2.1 Al-Cu AND Al-Si-Cu/Mg ALLOYS

Aluminum and its alloys have been widely used in many high technology industries such as automotive, marine and aerospace, due to their exceptional mechanical and physical properties. These properties comprise lightweight based on the low density of aluminum, good formability, high corrosion resistance, high electrical and thermal conductivity, high stiffness and improved high temperature strength. Aluminum cast alloys are designated by a three-digit system followed by a decimal place. This classification is based on major alloying element(s). The classification system proposed by the Aluminum Association is commonly recognized worldwide. The alloys are also classified according to the percentage of alloying elements present: (i) major alloying elements including silicon, copper and magnesium; (ii) minor alloying elements such as nickel and tin; (iii) microstructure-modifying additives, like strontium, boron, sodium, phosphorus, chromium, etc. and (iv) impurity elements, such as iron, for example [1]. Table 2-1 below lists the different family of aluminum alloys corresponding to the major alloying element(s)

Table 2-1 Classification of cast aluminum alloys.

Series	Main alloying element/s
1xx	99% Pure Al alloys
2xx	Al-Cu alloys
3xx	Al-Si alloys with additions of Mg or Cu or both
4xx	Al-Si alloys
5xx	Al-Mg alloys
7xx	Al-Zn alloys with additions of Mg, Cu, Cr, Mn or combinations
8xx	Al-Sn alloys

The overall physical properties of an alloy depend on the properties of the major alloying elements. The weight or volume fraction and the morphology of major phases present has a significant effect on the properties of the alloy. [2]

2.2 Al-Si ALLOYS

The aluminum silicon alloys (Al-Si) are the largest group of cast alloys due to their properties such as, elevated wear resistance, low thermal expansion, high thermal and electrical conductivity, and high strength-to-weight ratio, and high hardness. These properties make them very suitable for use in the production of several automotive parts such as radiators, wheels, cylinder heads, engine blocks, hoods, doors and car body applications. [3] According to the Aluminum Association, classification the aluminum silicon cast alloys belong to 3XX.X and 4XX.X series. The former are Al-Si alloys containing Cu and/orMg, while the 4XX.X series are Al-Si alloys.

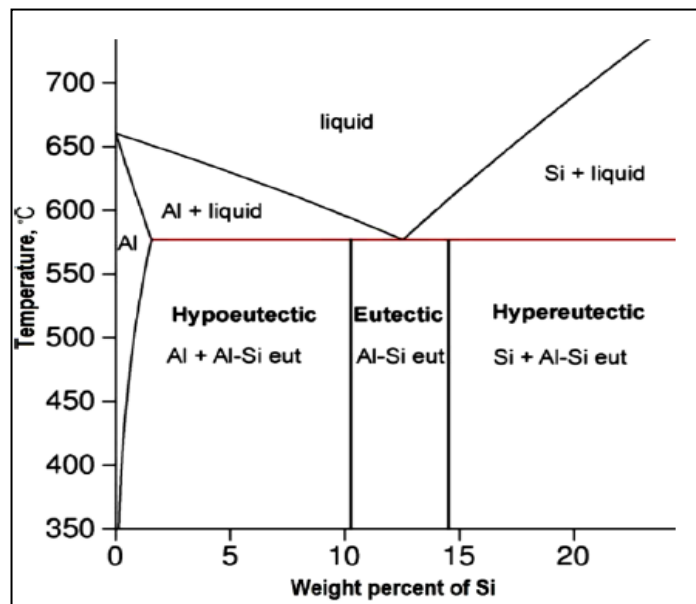


Figure 2-1 Aluminum rich portion of the Al-Si phase diagram [21].

The phase diagram of Al-Si alloy is a simple binary diagram, the maximum solid solubility of silicon in aluminum is 1.65% [4]. The Al-Si eutectic occurs at 12.2% Si, at a temperature of 577 °C. The range of silicon content in Al-Si commercial alloys varies from 5 up to 23 wt% as illustrated in Figure 2-1 [5]. The Si concentration of alloys used in the automotive industry often ranges between 5 and 10 wt.%. Its presence enhances the fluidity and improves feeding which reduces shrinkage porosity, thus parts having complex designs with varying thickness can be achieved. Silicon also increases the alloy strength as well as stiffness, but reduces the ductility [6]. Al-Si alloys are classified according to their Si content: hypoeutectic alloys contain 5 to 10% silicon; in eutectic alloys the Si content ranges from 11 to 14%; while hypereutectic alloys contain 14 up to 25 wt% Si. The corresponding microstructures that form are shown in Figure 2-2 [7].

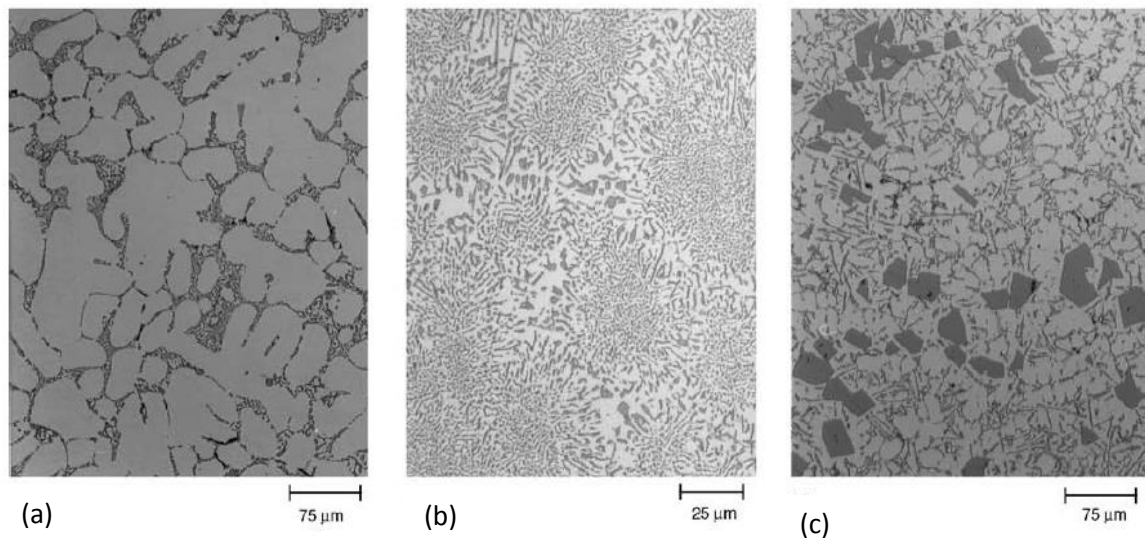


Figure 2-2(a) Microstructure of hypoeutectic alloy (1.6-12.6% Si) 150X. (b) Microstructure of eutectic alloy (12.6% Si). 400 X. (c) Microstructure of hypereutectic alloy (>12.6% Si). 150X [7].

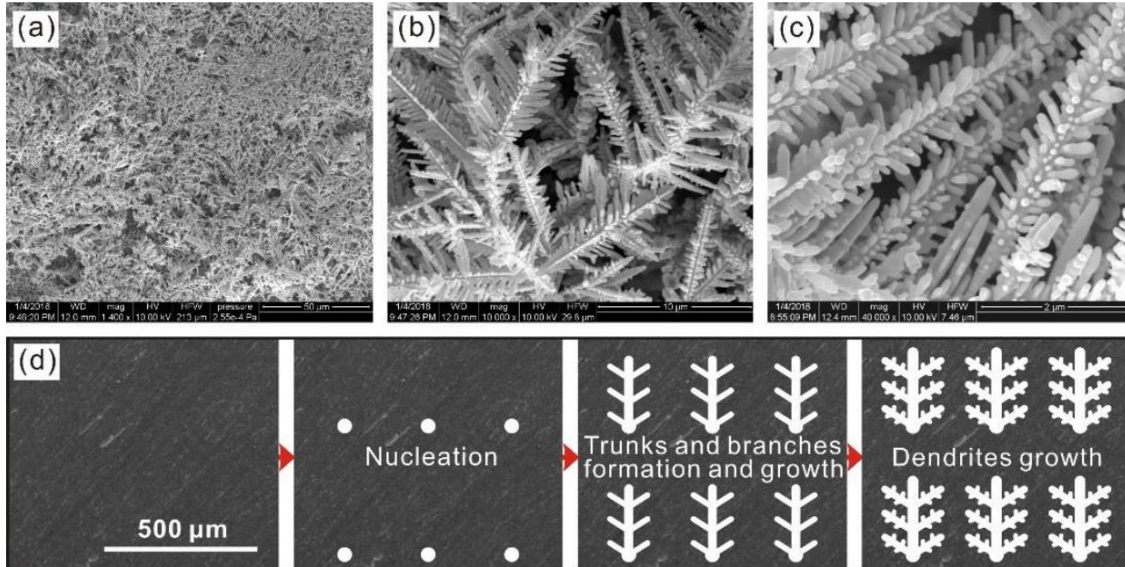


Figure 2-3 Nucleation of the dendritic structure of alpha Aluminum in an Al-Mg alloy (after Lix et al. [63]).

The main phases present in Al-Si alloys are the primary α -Al phase and silicon. The hypoeutectic alloys are characterized by having alpha-aluminum that solidifies first in dendritic morphology (tree-like structure) surrounded by eutectic Al-Si, while in hypereutectic alloys, the primary silicon solidifies first and surrounded by eutectic Al-Si [8]. The dendritic structure of the alpha aluminum crystals is defined by two terms, primary dendrite arm spacing (PDAS) and secondary dendrite arm spacing (SDAS). The cooling rate during solidification is the key factor that controls the values for PDAS and SDAS [5] [9]. The eutectic Al-Si structure as well as pure silicon particles are formed in the liquid surrounding the dendrite structure. Figure 2-3 shows nucleation of the α -Al dendrites in an Al-Mg alloy [63].

2.2.1 EFFECT OF ALLOYING ELEMENTS ADDITIONS TO Al-Si ALLOYS

The characteristics of Al-Si alloys are enhanced by the addition of certain alloying elements. Properties such as hardness and tensile strength may be greatly improved by the addition of alloying elements such as Cu and Mg in minor quantities, through the formation of the strengthening precipitates CuAl_2 and Mg_2Si within the microstructure after heat treatment.

2.2.1.1 EFFECT OF COPPER ADDITION TO AL-Si BASED ALLOYS

Addition of copper to Al-Si alloys has a positive impact on the mechanical properties. Tensile strength and hardness of the alloy are enhanced at both elevated and room temperature [10]. The increased matrix hardness has an impact on improving the machinability of the alloy. The enhancement in the properties of the alloys is optimized by a selective heat treatment procedure. The heat treatment process will result in fine spheroidal copper precipitates that are homogeneously dispersed in the aluminum matrix. Addition of copper will result in reduction of both ductility and resistance to corrosion of the alloy. Sigworth [11] concluded that addition of copper up to 1.8% has a significant effect on enhancing Al-9%Si-0.5%Mg cast alloy, accompanied by a slight reduction in the ductility. Copper phases are precipitated during solidification mainly in three different forms (i) fine eutectic Al- Al_2Cu , (ii) block-like Al_2Cu , and (iii) Q- $\text{Al}_{15}\text{Mg}_8\text{Cu}_2\text{Si}_6$.

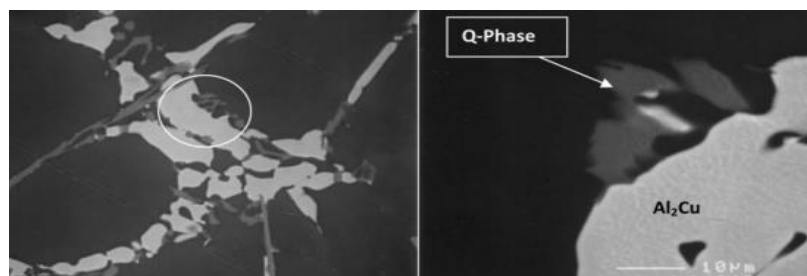


Figure 2-4 Block like Al_2Cu phase and the Blocky form of Q-phase (after E. Samuel et al. [64]).

2.2.1.2 EFFECT OF MAGNESIUM ADDITION TO Al-Si ALLOYS

Addition of Mg has the same strengthening effect as Cu but with increased reduction in the ductility. Mechanical properties such as tensile strength, yield strength as well as hardness are enhanced but the presence of Mg in Al-Si alloys has a great effect on reducing their ductility [12]. According to Dunn and Dickert [13], the addition of 0.55% Mg to the A380 and 383 cast alloys enhanced the mechanical properties, however it was clear that the Mg caused a reduction in the ductility of the alloy. Samuel et al. [68] studied the effect of Mg addition to 319 alloys containing iron. The authors reported that a large portion of the β -Al₅FeSi iron intermetallic phase is transformed to the π -Al₈Mg₃FeSi₆ Chinese script phase, as shown in Figure 2-5.

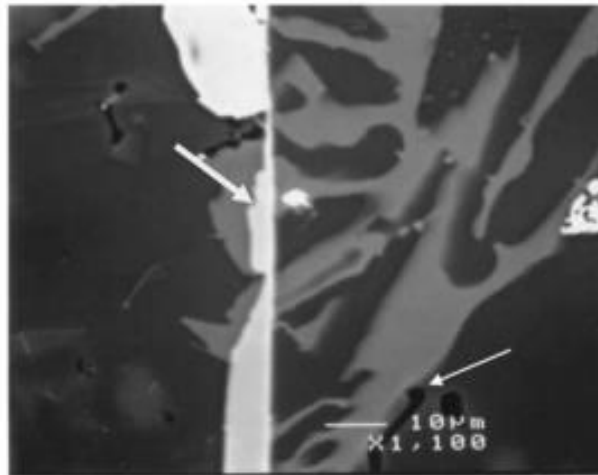


Figure 2-5 Thick arrow points to the β -Al₅FeSi phase transforming to π -Al₈Mg₃FeSi₆ phase, thin arrow represents the Mg₂Si phase (after E. Samuel et al. [64]).

2.2.1.3 EFFECT OF IRON ADDITION TO AL-SI ALLOYS

Iron (Fe) is an impurity element that is present in aluminum from the extraction process. The solid solubility of Fe in aluminum is low (0.05%), so that any amount in excess tends to form different intermetallic compounds. These Fe-intermetallics provide an increase in the yield strength (~ 7 MPa/vol%). However, their effect on strength depends on their size, chemistry, as well as their distribution. Iron constituents can also cause cracking and notches, which will result in a negative impact on fatigue resistance [15]. The remaining undissolved iron has high potential to combine with other alloying elements to form different types of intermetallic phases. Some of the more commonly observed phases are displayed in the optical microstructures of Al-5Si-1Cu-0.5Mg-Fe alloy shown in Figure 2-6, revealing the morphologies of these Fe-containing intermetallics.

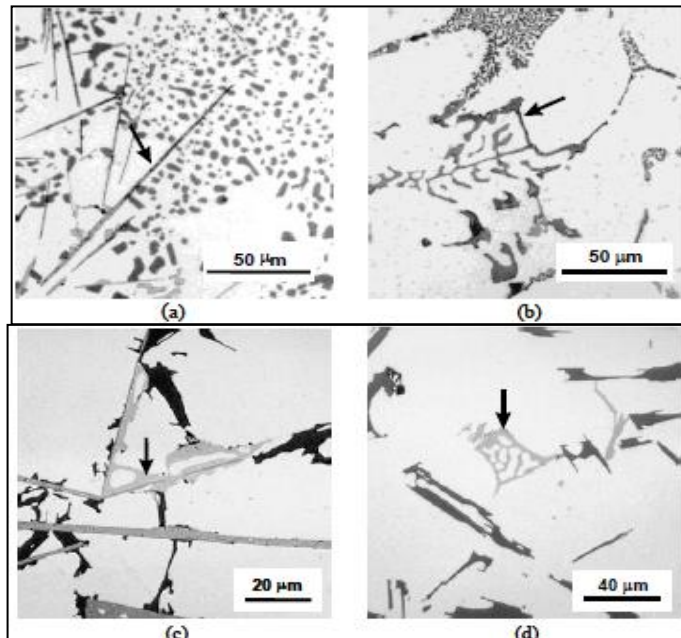


Figure 2-6 : (a) β -Al₅FeSi platelets; (b) script-like α -Al₈Fe₂Si; (c) π -Al₈FeMg₃Si₆ phase growing from β ; (d) script-like π -phase (after J. A. Taylor [65]).

The iron intermetallic constituents formed depend on the chemical composition of the alloy as follows:

- (i) In the absence of Si in the alloy as a dominant alloying element, Fe tends to combine with Al forming Al_3Fe and Al_6Fe ;
- (ii) In the presence of Si in the alloy, the orthorhombic Chinese script like $\alpha\text{-Al}_8\text{Fe}_2\text{Si}$ and the monoclinic platelet-like $\beta\text{-Al}_5\text{FeSi}$ appearing as needles in a two-dimensional micrograph - are formed;
- (iii) In the presence of Si and Mg in the alloy, an alternate phase, $\pi\text{-Al}_8\text{FeMg}_3\text{Si}_6$ can form. Another phase that forms when Mn is also present with Si is the cubic $\text{Al}_{15}(\text{Fe},\text{Mn})_3\text{Si}_2$, also called the $\alpha\text{-Fe}$ phase.

2.3 ALUMINUM COPPER ALLOYS

Aluminum-copper (Al-Cu) alloys are widely used in both wrought and cast form. The Al-Cu cast alloys belong to the 2XX.X series. Alloys such as 201, 203, 206 have a Cu content of 4-5 wt%, while alloys such as 240 and 222 contain 8 wt% Cu and 10 wt% Cu, respectively [16]. The Al-Cu binary alloy system has maximum solubility of 5.7 wt% Cu at the eutectic temperature of 548°C, as shown in the phase diagram. The chemical composition of the Al-Cu alloy gives it the privilege to record the highest strength of all Al cast alloys. The eutectic is formed at 33.2% Cu at temperature of 548 °C. Alloys containing a copper content below 33.2 wt% are termed hypoeutectic alloys, where the primary α -Al dendritic phase solidifies first, followed by solidification of the remaining liquid in the interdendritic regions to form the eutectic Al + CuAl₂ eutectic. The copper content in the CuAl₂ or θ phase lies between 52.5 and 54.1% [17].

These alloys are suited for applications where high strength and hardness are required at both room and elevated temperature. Al-Cu alloys exhibit excellent strength, thus making them suitable for automotive, marine, and aerospace applications. Because of the elevated density of Cu, 8.92 g/cm³, however, the high Cu content of Al-Cu alloys increases the weight of the cast parts manufactured from these alloys. The Al-Cu alloys generally have lower resistance to corrosion compared to other Al alloys, as well as poor resistance to hot cracking.

The marginal presence of silicon - less than 0.1 wt% - in some Al-Cu alloys may be considered as an impurity. Such a low Si level has a detrimental effect on the alloy castability and fluidity. Thus, producing castings with complex designs incorporating thin sections and pressure-tight parts is barely achievable. As a result, an appropriate gating and feeding system design is necessary. A combination of tensile properties and ductility can be attained with controlled additions of impurities (Si and Fe). Grain refining elements are usually added in the melt treatment stage to improve properties of the cast alloy. Alloys containing 4-5.5%Cu exhibit a significant improvement in strength following heat treatment [18]. Silver accelerates the aging response and reduces the risk of stress corrosion.

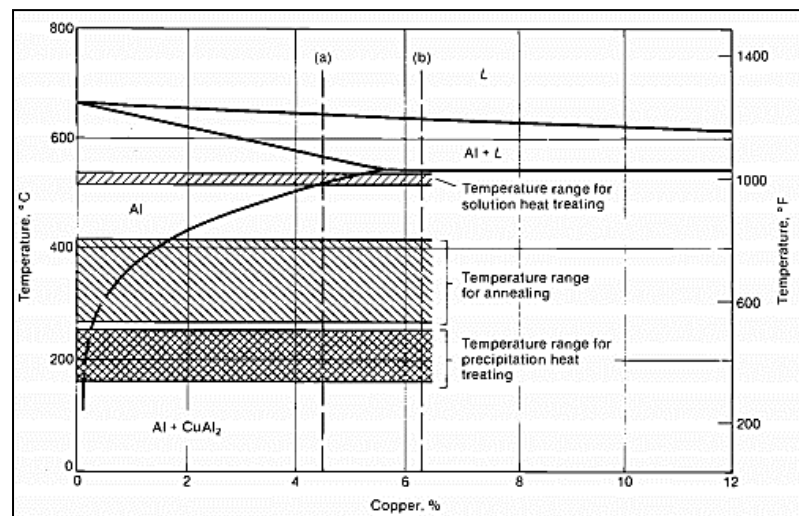


Figure 2-7 Portion of aluminum-copper binary phase diagram. Temperature ranges for annealing, precipitation heat treating, and solution heat treating are indicated. The range for solution treating is below the eutectic [18].

Also, copper has a significant impact on the strength and hardness of aluminum castings at both ambient and elevated service temperatures (up to 300 °C) [19]. So, the mechanical properties of these alloys may be improved via solution heat treatment and age hardening through the formation of CuAl₂ precipitates. The morphology of these precipitates changes according to the heat treatment process applied [18].

2.4 MELT TREATMENT

Mechanical properties can be further enhanced during the melt treatment process, where morphologies and distribution of phases present, as well as the grain size can have a significant effect on the properties. Minor alloying elements, known as microstructure modifiers, are often added to the melt. Elements such as strontium (Sr) and sodium (Na) modify the needle-like morphology of the eutectic silicon in Al-Si alloys to a fine fibrous form, while the effect of phosphorus addition to hypereutectic Al-Si alloys refines the coarse structure of primary silicon crystals, by reducing their size by a factor of 10. The unrefined structure of the silicon crystals has a harmful effect on tool life when machining is carried out. Phosphorus is added to the molten metal in the form of phosphorus-containing compounds or metallic forms such as phosphorus pentachloride and phosphor-copper, respectively. Inert gas fluxing is applied to activate aluminum phosphide nuclei [6].

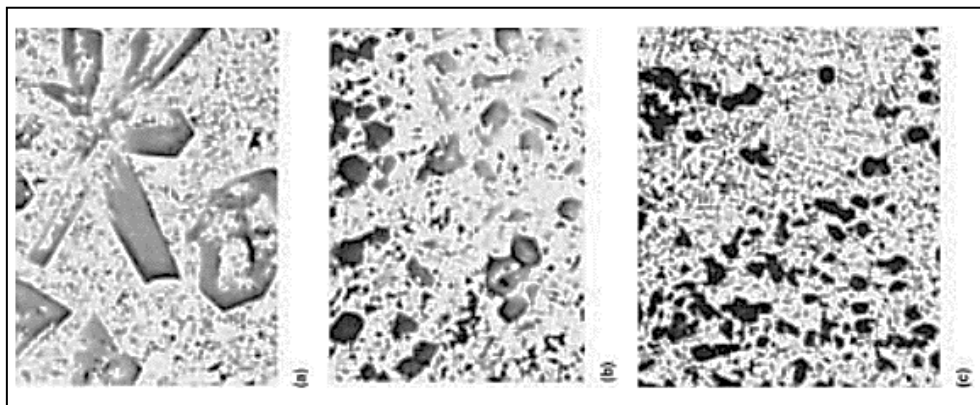


Figure 2-8 Effect of phosphorus refinement on the microstructure of Al-22Si-1Ni-1Cu alloy. (a) Unrefined. (b) Phosphorus-refined. (c) Refined and fluxed. All 100x [6].

2.5 HEAT TREATMENT

Thermal treatment is technique used to enhance the mechanical properties of heat-treatable alloys. The enhancement is achieved through modifications to the microstructure of an alloy brought about by the heat treatment steps. These comprise a controlled sequence of heating and cooling processes where time and temperature are the main parameters. The T6 and T7 tempers are the common heat treatment processes that are applied to Al alloys to enhance their properties. The strengthening effect is gained from the precipitation of secondary hard phases embedded within the soft aluminum matrix [18]. The T6 and T7 treatments are expressed in Figure 2-9 , showing three stages: (i) solution heat treatment, followed by (ii) quenching, and then (iii) age hardening or precipitation heat treatment.

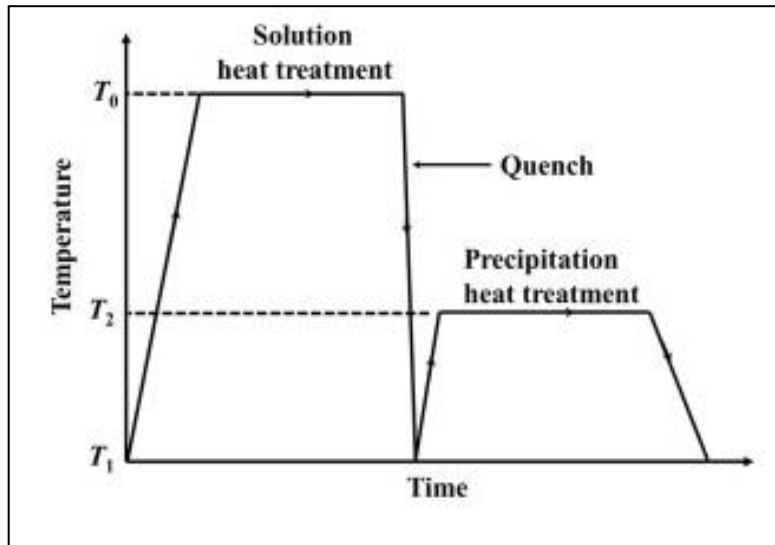


Figure 2-9 Schematic of solutionizing and aging process.

2.5.1 SOLUTION HEAT TREATMENT

The alloy is heated and held to a temperature close to the eutectic temperature, where alloying elements such as Cu and Mg are dissolved into solid solution. The amount of the solutes present usually exceeds their solid solubility limit. The main target of the solution heat treatment stage is to obtain a homogeneous supersaturated solid solution (SSSS) where most of the hard phases such as CuAl_2 and Mg_2Si are dissolved. The solution treatment temperature depends on the alloy composition and solid solubility limits. The chemical composition of an alloy will control the different phases formed during solidification. Phases containing iron such as $\pi\text{-Al}_8\text{FeMg}_3\text{Si}_6$ and $\alpha\text{-Al}_8\text{Fe}_2\text{Si}$ are harder to dissolve due to the limited solubility of iron in aluminum (0.05%). Furthermore, the solution treatment temperature must be lower than the melting points of the phases present to avoid incipient melting, which would lead to porosity formation and a reduction in the mechanical properties.

The solution treatment temperature ranges between 510 °C and 550 °C for an Al-4.5 wt% Cu alloy, for the Cu to be completely dissolved in solid solution [16]. Wang et al. [20] recorded an improvement in the mechanical properties of an Al-Si-Cu-Mg cast alloy when solution heat treatment was carried out at 520 °C without the occurrence of incipient melting of the phases present. However, as a precaution, Abdelaziz [21] used a temperature of 495 °C for Al-Si-Cu-Mg alloys to avoid any possibility of incipient melting [22].

2.5.2 QUENCHING

The supersaturated solid solution (SSSS) obtained with solution heat treatment is then subjected to a rapid cooling process termed quenching. During quenching, the SSSS structure is preserved at ambient temperature with many vacancies in its lattice structure. These vacancies are active nucleation sites for precipitates to form. Selection of quenching rate is based on the quenching sensitivity of the alloy. A high quenching rate is desirable to avoid precipitation of the hardening solutes (CuAl_2 and Mg_2Si) to maintain them in solid solution form within the SSSS microstructure. The rate of quenching has an impact on residual stresses, intergranular corrosion resistivity and strength of the material [23].

2.5.3 AGE HARDENING

The main target of the aging stage is to maximize the formation of fine homogeneously dispersed hardening precipitates characterized by high matrix coherency and tight spacing between adjacent precipitates. Solute atoms form clusters due to the supersaturation of vacancies in the SSSS, which allows diffusion. Clusters fit coherently in the structure of the aluminum lattice. These clusters of solute atoms are called GP zones. These are metastable regions where enough energy is present to enable precipitates to form. Clusters of solute atoms are formed and precipitation occurs due to rejection of solute atoms from the super-saturated solid solution. The formed precipitates are transitional metastable phases. The morphology of the phase is affected by the aging temperature and aging time. The sequence of formation of CuAl_2 precipitates is as follows:



As aging time proceeds the GP zones are dissolved and the θ'' phase starts to form, leading to increase in hardness and strength. With further increase in aging time, the strength

and hardness start to deteriorate due to dissolution of θ'' which is transformed to θ' , when the alloy is said to be overaged. Finally, the stable form of θ precipitates is observed. Clusters have a disk-like morphology, they grow in diameter and thickness as the precipitation sequence is followed, as illustrated in Figure 2-10 [24].



Figure 2-10 TEM observations of the evolution of the microstructure during aging: (a) GP zone; (b) θ'' ; (c) θ' ; (d) θ [25].

Figure 2-12 illustrates the effect of aging temperature on the sequence of precipitates. The temperature of the precipitates formed depends on the Cu concentration (wt%) in the matrix phase. As Figure 2-11 illustrates, the precipitation temperatures increase as the Cu content in the matrix increases.

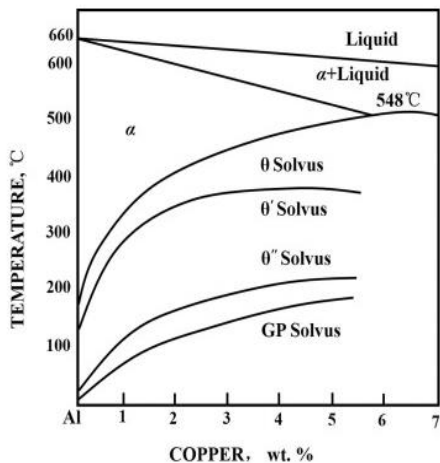


Figure 2-12 Aluminum-copper phase diagram along with metastable phase boundaries at aluminum end [24].

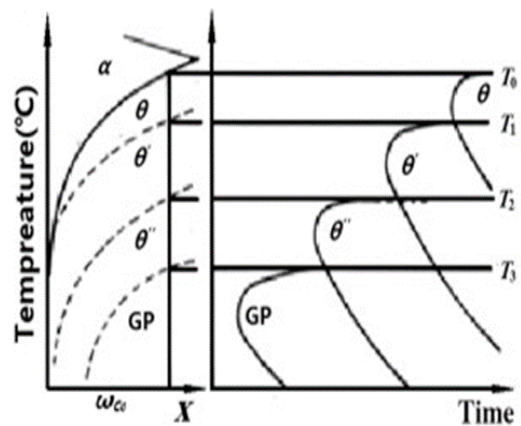


Figure 2-11 The effect of aging temperature on the sequence of precipitate [24].

- i. $T_1 < T < T_0$ the only precipitate that is possible is the stable non-coherent phase of θ .
- ii. When $T_2 < T < T_1$ both GP zones and θ'' vanish; as the aging process proceeds, the outcome of precipitates is $\theta' \rightarrow \theta$.
- iii. When $T_3 < T < T_2$ GP zones completely disappear with progress of the aging process, the outcome of precipitates is $\theta'' \rightarrow \theta' \rightarrow \theta$.
- iv. When $T < T_3$ the main precipitates present are the GP zones; with the progress of aging process, the outcome of precipitates is GP zones $\rightarrow \theta'' \rightarrow \theta' \rightarrow \theta$.

The fine precipitates fill the defective zones at grain boundaries, point dislocations and fill most of the imperfections within the lattice structure. The precipitates cause local distortion and strain fields that hinder dislocation movement, resulting in an enhancement of the mechanical properties.

2.6 MACHINABILITY

Machinability of a material can be expressed in many terms. It is the study of the interactions between tool, considering its material and design, and the workpiece considering its material composition and heat treatments applied. These interactions are tested through a selected machining operation such as milling, turning or drilling, etc. The machining operation is controlled by a set of cutting parameters like cutting speed, feed rate depth of cut for a specific machining environment as shown in Figure 2-13.

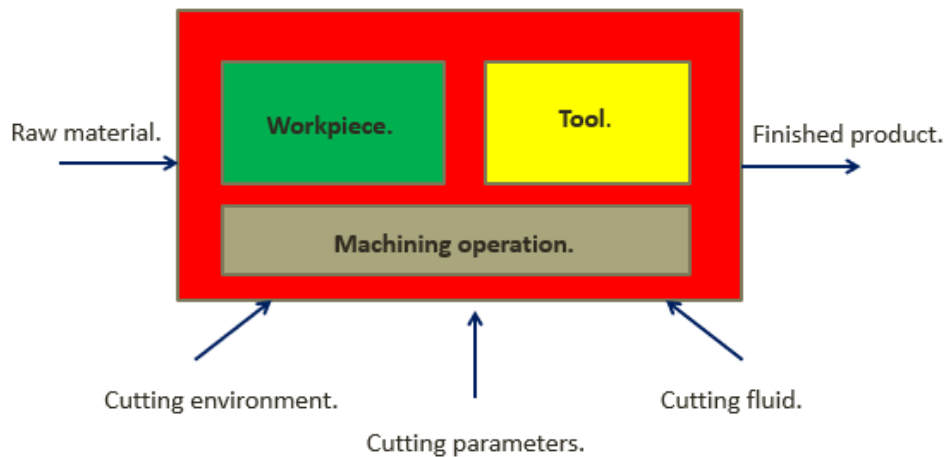


Figure 2-13 Illustration of the machining environment.

Machinability is also defined as the material response to machining. According to the American Iron and Steel Institute (AISI), machinability can also be expressed in terms of how easy or difficult a material can be to machine compared to a 160 Brinell hardness B1112 cold drawn steel, machined at 180 surface feet per minute. Machinability of a certain material is evaluated based on one or more of the following factors: (a) tool life, (b) cutting forces, (c) chip formation, and (d) quality of the machined surface. In the following sections, machinability of aluminum alloys is explained referring to the above-mentioned machinability criteria.

Machining is the leading type of forming process; however, due to technology developments, this type of production has changed over the last decades. Nowadays it is easy to attain a final product with precise dimensions as well as impressive surface quality. Machining operations should be controlled, monitored and optimized to achieve cost effective and sustainable products. The machining process is monitored and optimized by a clear understanding of the cutting process and the factors affecting it such as cutting parameters, cutting tool selection, lubrication, etc. Machinability of an alloy is assessed based on the following:

i. Cutting forces generated

The cutting forces usually express the overall power consumption; the greater the cutting force the higher the power consumption of the machine.

ii. Tool life and tool wear

Tool life can be expressed as the duration where the cutting edge is applicable to produce products prior to tool failure, while tool wear may be expressed as an inevitable gradual failure of the tool. The tool condition directly impacts the material removal rate (MMR) which is the volume of material removed per unit time.

iii. Product quality

The quality of the product includes the surface roughness and dimensional tolerance. The roughness of the machined surface has a great impact in mechanical meshing between parts and is thus critical.

iv. Chip formation

Chips are formed as three different types (i) continuous chips, (ii) discontinuous chips, and (iii) continuous chips with built up edges (BUE). The formed chips have a major role in cutting heat dissipation from the workpiece.

Table 2-2 Factors influencing machining operations.

Factors	Influence on the machining operation
Cutting parameters: cutting speed, feed rate, depth of cut	Cutting forces, tool life, heat generation, surface finish.
Tool design: tool angles rake, relief and clearance angle	Influence chip flow direction, reduction in tool wear.
Tool wear	Dimensional accuracy, surface quality, cutting forces, heat generation.
Continuous chips	Good surface finish, stabilized cutting forces, undesirable results in increase in the down time in automated machining due to clogging.
Discontinuous chips	Desirable due to ease of chip disposal, may affect the surface quality, fluctuation of the cutting forces resulting in vibration and tool chatter.
Built up edge chips	Affect tool geometry resulting in poor surface finish, desirable only when thin as it may protect the cutting tool edge.
Temperature rise	Influence tool life by enhancing crater wear, may cause thermal damage to the workpiece.

To be able to evaluate the machinability of an alloy, it is necessary to have a clear understanding of the factors and parameters that influence the machining operation as a whole. These factors, summarized in the Table 2.2 below, will be discussed in the following sections.

2.6.1 CUTTING FORCES GENERATED AND FACTORS AFFECTING THEM

Machining of aluminum alloys generates cutting forces usually lower than that of steel by 70 %, this is due to the lower mechanical properties of aluminum alloys compared to those of ferrous alloys [19]. Aluminum has a low density compared to steel, which reduces the inertia force that prohibits high speed machining, resulting in overall reduction of the specific cutting forces. The variation of the cutting forces among aluminum alloys depends on the chemical composition, and hence the physical properties [25] [26]. Heat treatments and/or the addition of alloying elements that affect the mechanical properties (hardness or strength) of the alloy positively may reduce the machining forces as the chip-tool contact area is reduced [27] [28] [29].

By increasing machining cutting speed, the machining forces are reduced since the increase in the cutting force will increase cutting temperature, leading to a reduction in the shear stress in the primary shear zone as well as the secondary shear zone (Figure 2-14). The stress at the secondary shear plane are usually 30% less than those of the primary shear [30] [31]. Overall increase in the cutting speed will reduce cutting forces but in some cases high speed cutting causes excessive increase in the deformation rates that may result in increased machining forces [32] [33].

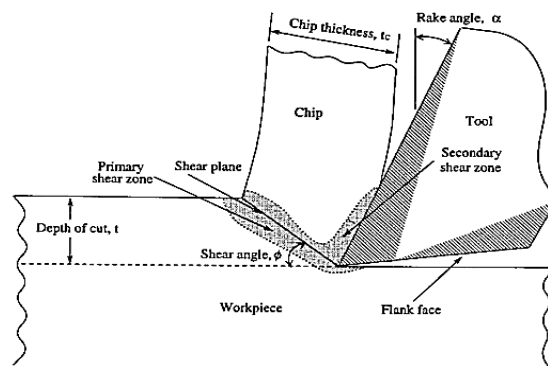


Figure 2-14 The geometry of orthogonal cutting [58].

High speed machining of alloys containing hard particles will result in elevated cutting forces due to excessive flank wear occurring to the cutting tool [34]. Figure 2-15 shows the effect of cutting speed on the generated cutting forces. Hard particles act as abrasive material on the cutting tool. Lahres et al. [35] found that, during high speed dry milling of AlSiMg cast alloy, material from the work pieces sticking on the cutting edges of the tool lead to flank wear; however, this problem can be reduced by the application of minimum quantity lubrication (MQL). Any increase in the depth of cut and/or feed rate will increase the area of the primary as well as the secondary shear planes - increase chip tool contact area- which in its turn will deteriorate the shearing process of the material and will result in increasing the cutting forces [36].

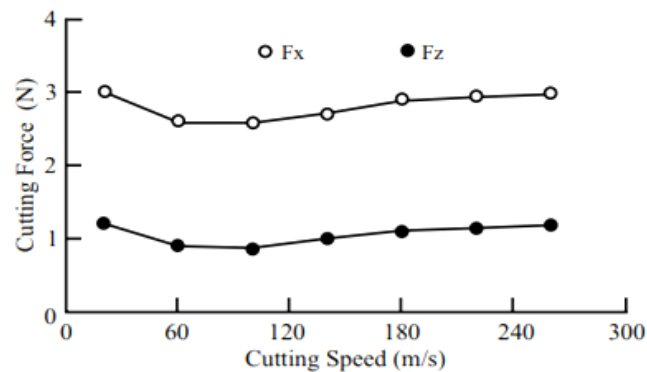


Figure 2-15 Cutting force variation with cutting speed [56].

Tool design and tool geometry, such as rake angle and nose radius, have a great impact on the cutting forces. Any geometrical changes that occur in the tool geometry due to wear or built-up-edge (BUE) will strongly affect the machining cutting forces. Tools with increased rake angle reduce chip-tool contact area, therefore they will result in reducing the machining forces [37] [38]. Shankar et al. [39] reported that machining 6061-T6 aluminum alloy with a tool that has a reduction in the rake angle, results in increasing

the cutting force [39]. Also, tools with a large nose radius usually generate small rake angles that may increase the cutting forces [40].

Tang et al [39] concluded that flank wear generates high machining forces; this conclusion is based on the milling of aluminum alloy 7050-T7451. Flank wear increases contact area between tool and workpiece. According to ISO 513, the letter N is used as the standard designation for cemented carbide tools that are employed for machining aluminum alloys. Coated or diamond cutting tools do not react chemically with aluminum alloys, therefore such types of tools are less adhesive which will result in reduced cutting forces as reported by Roy et al. [40] during machining of pure aluminum by various types of tools, namely (1) uncoated silicon carbide, (2)TiC (titanium carbide)—CVD, (3)-TiN—CVD, (4)Al₂O₃ (aluminum oxide)—CVD, (5)-AlON (aluminum oxynitride), (6) TiB₂ (titanium diboride)—PVD, and (7) diamond—HFCVD (hot filament chemical vapor deposition) as shown in Figure 2-16.

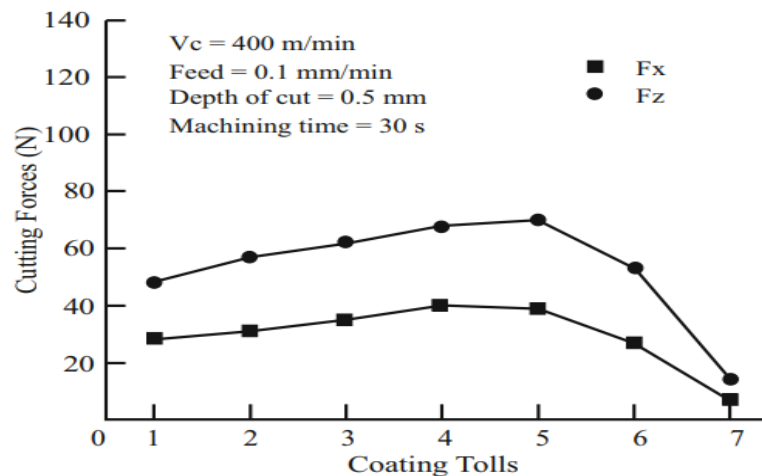


Figure 2-16 Behavior of cutting forces generated by different cutting tools in turning of aluminum [17].

2.6.2 TOOL LIFE AND TOOL WEAR

Various tool materials with different tool geometry can be used for machining aluminum alloys, such as high-speed steel (HSS), cemented carbides, and diamond-based tools. The proper selection of a tool is a must prior to the start of the selected machining operations. Moreover, the selection of tool material mainly depends on the chemical composition of the alloys and the presence of hard material embedded within the alloy matrix. HSS tools are satisfactory for machining all aluminum alloys except Al-Si alloys, because these alloys are abrasive and should be machined with silicon carbide tools or diamond based tools due to their low chemical affinity for aluminum, which would enhance the surface finish of the workpiece [19]. Figure 2-17 illustrates the basic terms used for a cutting process.

Machining with cutting speeds within the range of 600 to 800 m/min and a carbide tool with rake angle ranging from 6 to 20 degrees is suitable for the turning of aluminum alloys that are free of hard particles. Toropov et al. [41] used N10 grade tools with different rake angles of -5° , 0° , 5° , 10° , and 20° and a cutting speed of 800 m/min during turning of Al6061-T6. The authors aimed at studying the effect of rake angle on burr height, and concluded that tools with rake angles of 10° , and 20° produce smaller burr height than those of -5° , 0° and 5° rake angles.

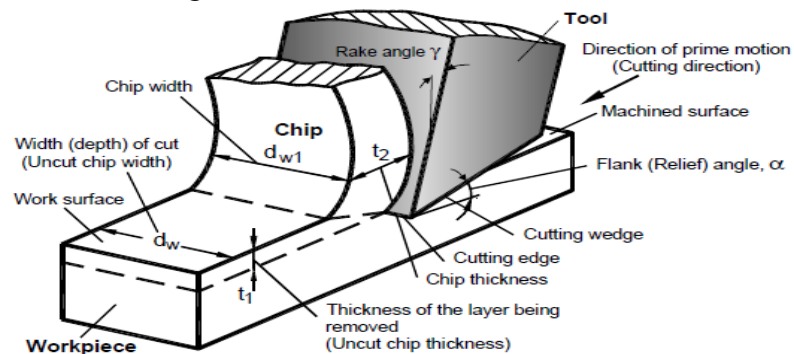


Figure 2-17 Visualization of basic terms in orthogonal cutting [57].

It is recommended for aluminum alloys containing about 12-16 vol% of hard particles of either Si or SiC to be machined with tools having rake angles of 0° to 7° and cutting speeds of 20 to 450 m/min regardless the type of tool material [27][25]. Ciftci et al. [42] performed turning tests on Al-2014 alloy matrix composites containing 8 and 16 vol% SiC using K10 (N10) inserts (5° rake angle) and cutting speeds ranging from 20 to 80 m/min.. A turning test was performed by Manna and Bhattacharayya [43] on Al/SiC (12 wt% Si and 15 vol% SiC) at a cutting speed of 235m/min using uncoated tungsten carbide K10 (now designated N10) with a rake angle of 5° .

For drilling operations of aluminum alloys it is recommended to use helical drills with helix angles of about 40° to 48° and point angles of 118° to 140° . Tools with deep flow grooves will facilitate chip flow and prevent the material from sticking on the drill's rake face [19] [44] [45].

Diamond based tools are very efficient for machining high strength aluminum alloys at cutting speeds above 700m/min [27] [41], whereas polycrystalline diamond (PCD) tools are more suitable for machining alloys containing 10 to 20 vol% of ceramic particles or Si contents varying from 12 to 21 wt% because they are resistant to the thermally activated wear mechanisms [46]. The hardness of PCD tools is four times greater than silicon or ceramic particles. PCD tools have higher thermal conductivity compared to cemented carbides; therefore, less generation of cutting temperature is attained [47].

Diamond coated tools have been proved to improve the machinability of aluminum alloys due to their magnificent properties, high hardness at high temperatures, low friction coefficient, low adhesiveness, high thermal conductivity, and chemical stability. Diamond

coated tools reduce BUE, abrasive wear as well as cutting forces; they also produce a good surface finished product.

Tool wear is a non-desirable change that alters the tool geometry from its original shape. The geometrical changes resulting from wear affect the performance of the tool. Tool wear has a great impact on the machining process as well as on the quality of the work piece being machined. The cutting force increases in machining operations due to gradual wear of the tool, as a result of the friction and relative movement of the tool and workpiece. Tool wear can be of different types such as (i) abrasive wear, (ii) adhesive wear,(iii) wear due to oxidation, (iv) tool wear as a result of diffusion and chemical decomposition, and (v) tool wear due to cyclic loading fatigue. The low melting point of aluminum leads to unelevated machining temperatures thus, thermally activated wear mechanisms such as oxidation, diffusion, fatigue and chemical decomposition do not usually occur. Figure 2-18 illustrates the temperature gradient during the interaction between tool and workpiece in orthogonal cutting.

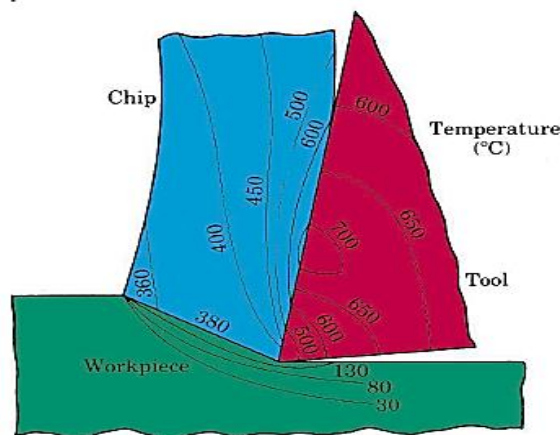


Figure 2-18 Temperature gradient across tool and workpiece during machining [27].

Abrasive and adhesive tool wear are the most common mechanisms that occur while machining aluminum alloys. As the tool cuts through the workpiece, the soft material of the workpiece slides over the cutting edge of the tool. If the material of the workpiece contains small hard particles, the contact of these hard particles against the cutting edges of the tool may cause the machining temperature to increase, which lowers the resistance of the cutting tool thus adhesive and abrasive wear are accelerated. During machining process friction, temperature and pressure are usually generated. Parts of the soft material of the work piece tend to adhere to the hard material of the tool, and form what is called a built up edge (BUE).

Abrasive and adhesive wear usually occur when machining an alloy containing hard particles such as silicon carbide (SiC). Normally the percentage of these hard SiC particles of in the workpiece lies in the range of 10 to 20% of the alloy volume. The hardness of the SiC particles is higher than that of the cemented carbide tool material; therefore this causes the machinability of the aluminum alloys to decrease [38].

Figure 2-19 shows the common types of tool wear which include flank wear, crater wear, plastic deformation, nose wear, thermal cracking, mechanical fatigue cracking, chipping, fracture and BUE. Flank wear, crater wear and nose wear are the common ones that usually occur when machining aluminum alloys.

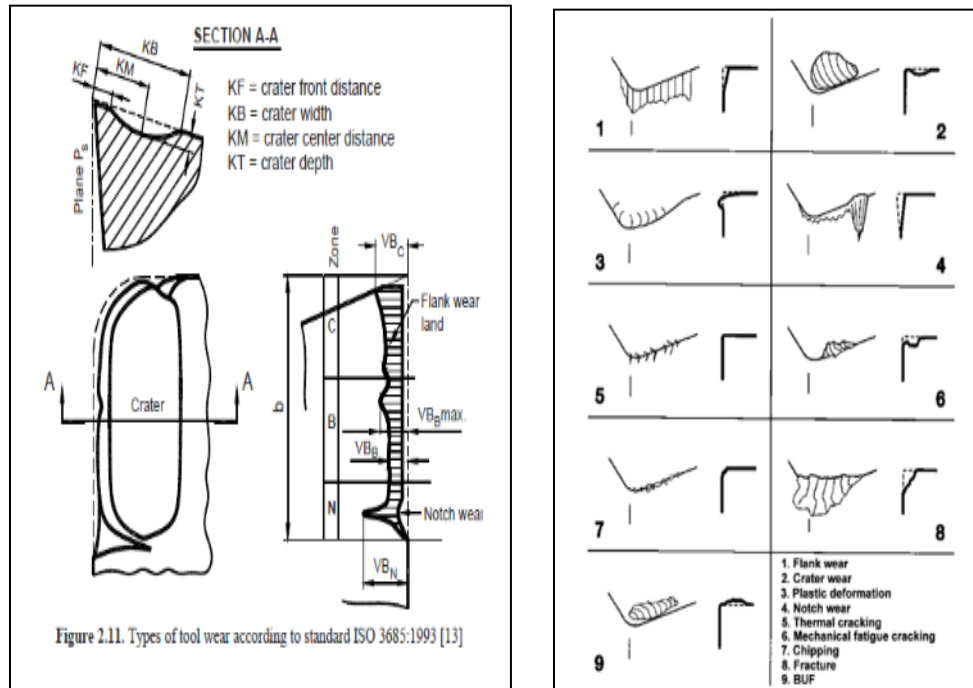


Figure 2-19 Types of tool wear according to standard ISO 3685:1993 [57].

Flank wear occurs on the flank side of the tool due to abrasive wear of the cutting edge against the machined surface of the workpiece. Flank wear is non-uniform along the cutting tool edges, rate of flank wear increases with the size and volume percentage of hard precipitates in the matrix of the alloy [48]. Therefore, the less the dispersion of hard particles of $\text{Al}_2\text{O}_3\text{p}$ and SiCp in the case of Al metal matrix composites (MMCs), the less the flank wear. Crater wear occurs on the rake surface of the tool, due to friction between the rake face and chips flowing across it, resulting in scars on the rake face. Coelho et al. [26] investigated the during drilling of hypoeutectic Al-Si alloy, hypereutectic Al-Si alloy and AA261-15vol% SiCp MMC; these materials contain hard particles of Si or SiCp. As Figure 2-20 shows, a progressive flank wear was noted when the test was carried out using PCD tools [49].

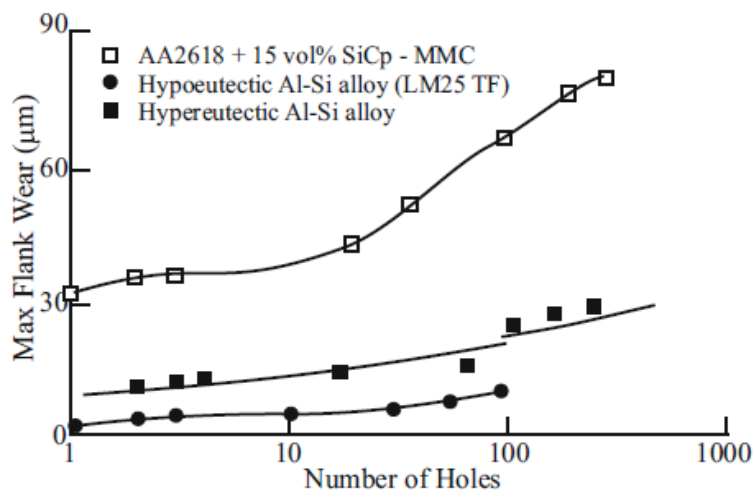


Figure 2-20 Flank wear evolution when drilling Al-Si alloys and MMC using PCD tipped drills [27].

Tool wear will cause deformation in tool geometry that will mainly reduce the sharpness of the primary and secondary cutting edges, which will have consequences on the cutting forces and the product quality, as the latter is associated with the surface quality of the product and its dimensional tolerance.

2.6.3 CHIP FORMATION

The process of chip formation is a critical issue in any machining process. The form of the chips greatly affects the machining operation as they have a great impact not only on tool life, but also on the integrity of the machined surface. Chips play an important role in heat dissipation from the workpiece, since most of the heat generated during the machining process is dissipated through the layers of material removed (i.e., chips). Chip formation is affected by many variables such as the workpiece material and its mechanical properties, the machining ambient temperature, and the cutting parameters like cutting speed and feed rate. Tool geometry and tool condition also have a great impact on the chip formation process. The types and form of chips as well as the factors affecting them are discussed.

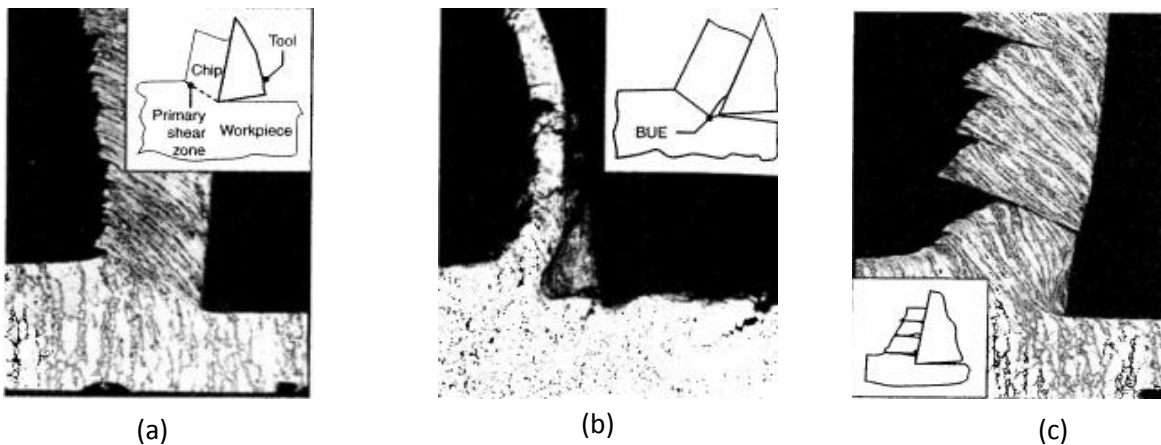


Figure 2-21 Examples of (a) shows continuous chip formation. (b) shows continuous chip formation with BUE , (c) shows discontinuous chip formation [52].

Chips can normally be categorized in three main groups: (i) continuous chips, (ii) continuous chips with built up edges (BUE), and (iii) discontinuous chips, as shown in Figure 2-21. The types and form of chips as well as the factors affecting them are discussed in the following sections.

2.6.3.1 CONTINUOUS CHIPS

Continuous chips are formed while machining a ductile material with relatively low hardness properties. Machining material like aluminum at high speed and/or high rake angles is likely to form continuous chips where plastic deformation of the material takes place along the primary shear zone. When ductile material is machined at low speed and low rake angles, distortion occurs, resulting in poor surface finish and induced surface residual stresses. Generally, machining ductile material at high-speed produces a good surface finish with continuous chips, as seen in Figure 2-22. However, continuous chips are not always desirable as they become entangled with the machine and the workpiece, when it becomes necessary to stop the machining operation for chip disposal.

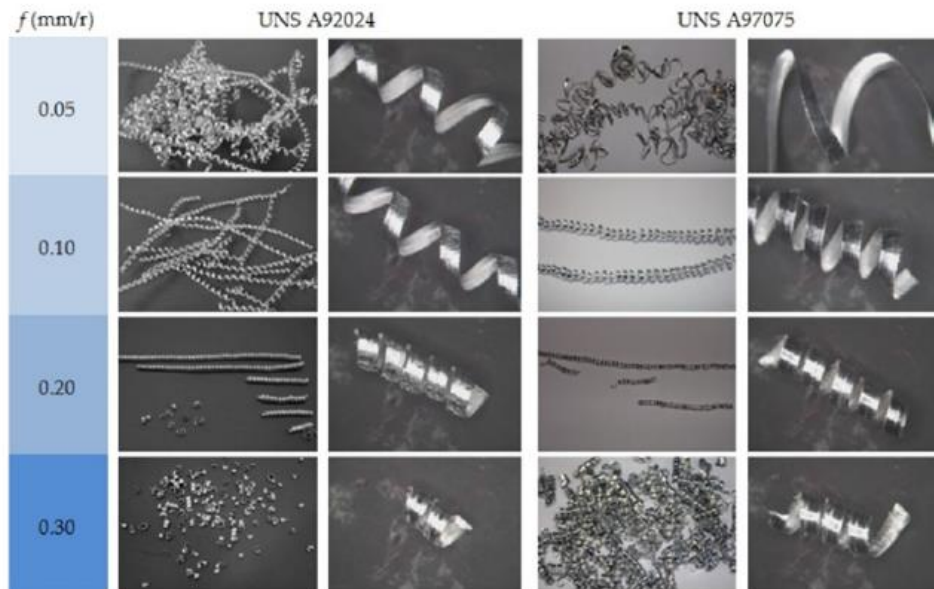


Figure 2-22 Effect of feed rate on the morphology of continuous chips during machining of UNS A97075-T6 (Al-Zn) and UNS A92024-T3 (Al-Cu) alloys [61].

Continuous chips also lead to blockage in chip flow regions of the tool, which might break the tool. This problem can be solved by the use of chip breakers or by changing cutting parameters such as cutting speed, feed and depth of cut.

2.6.3.2 CONTINUOUS CHIPS WITH BUE

These chips are like the continuous chips but some layers of material from the workpiece are gradually attached and deposited on the tip of the tool. This phenomenon is known as built up edge (BUE). BUE formation is cyclic, where the BUE grows larger on the tool tip until it breaks apart. The broken parts of the BUE become embedded on the machined surface of the workpiece, resulting in poor surface quality (see Figure 2-23), resulting in poor surface quality. The BUE changes the geometry of the cutting edge and dulls it; therefore, it has an impact on surface quality. A stable BUE is desirable as it reduces the tool wear by protecting the rake face, as the cutting speed affect the size of the BUE. Reduction of BUE formation can be attained by increasing the cutting speed, decreasing the depth of cut, increasing the rake angle, using tools that have a sharp edge and lower chemical affinity for the workpiece material. [50] [51].

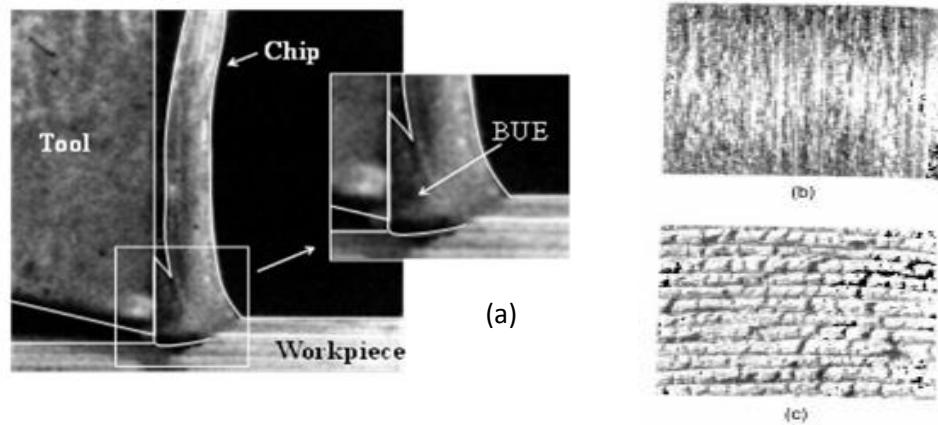


Figure 2-23 (a) BUE developed during dry turning of AA2024-T351 at cutting speed 60 m/ min , feed = 0.1 mm and rake angle 0 degrees; (b) surface finish without BUE; (c) surface finish with BUE on the tool edge [52].

2.6.3.3 DISCONTINUOUS CHIPS

Discontinuous chips are formed when machining a brittle material, as it does not have the ability to undergo the high shear strains during cutting. Discontinuous chips are shown of brittle material are shown in Figure 2-24. The presence of hard inclusions and precipitates in the workpiece material will result in the formation of discontinuous chips. Very low and very high cutting speeds, low rake angles and large depth of cut also result in discontinuous chip formation. With such chips, reduction in the cutting force values is observed, but with high fluctuations. Consequently, the stiffness of the tool holder of the machine must be high enough to avoid chatter and vibrations that may lead to an irregular surface finish [51].

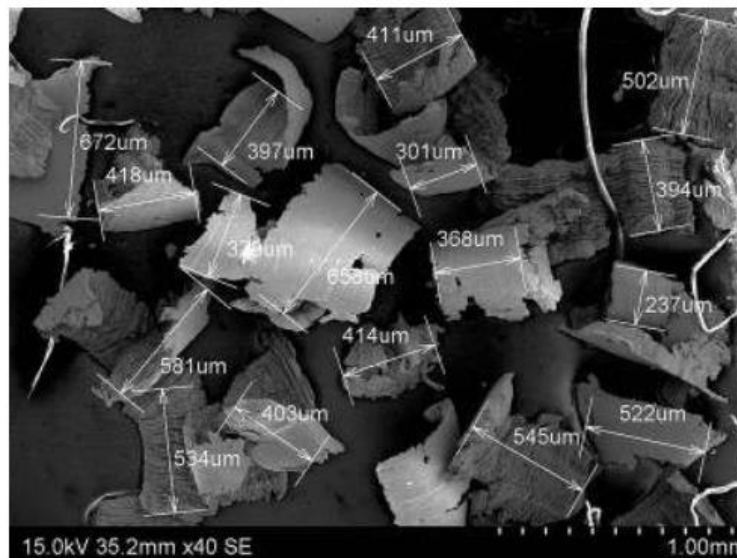


Figure 2-24 Discontinuous chips obtained from brittle work material, low cutting speeds, large feed and depth of cut [52].

2.6.3.4 FACTORS AFFECTING CHIP FORMATION

As discussed earlier, chip formation is affected by many parameters such as workpiece material, the heat treatment process, the alloying elements added, and the tool material and tool geometry. Coatings of titanium nitride TiN, titanium carbide TiC, aluminum oxide Al₂O₃ or titanium diboride TiB₂ are recommended to reduce the effect of BUE due to their great chemical affinity for aluminum [52]. Kelly and Cotterel [44] recommended using sharp tools with large rake angles and polished rake faces to achieve effective chip control. Trent and Wright [27] concluded that addition of Cu as an alloying element facilitates the formation of short-segmented chips in aluminum alloys. Addition of free cutting elements is a method of controlling chip formation due the low solubility of free cutting elements in the aluminum matrix. Dasch et al. [53] suggested the addition of up to 5 wt% of free cutting elements such as lead or antimony. Pure aluminum is very soft and ductile, having an increased tendency to adhere to the cutting tool edge. Machining soft material results in formation long continuous chips and BUE. The BUE will results in poor surface finish with high roughness values (Ra, Rt). Alloying elements that make the alloy heat treatable, enhance machinability by increasing the hardness of the soft aluminum aluminum matrix, and thus result in: (i) controlled chip and burr formation, (ii) reduction in BUE, and (iii).improved surface roughness.

Insoluble alloying elements such as bismuth and lead increase the ability of high speed machining due to their effect in chip breaking. Presence of hard intermetallic compounds like CuAl₂ or FeAl₃ they act as chip breaker without noticeable reduction in cutting tool lifetime. Presence of hard silicon precipitates or complex intermetallic

compounds of manganese or chromium also act as chip breakers with significant reduction in tool life.

2.6.4 PRODUCT QUALITY

The quality of the machined workpiece surface is limited by parameters, which control the material removing rate such as depth of cut, and feed rate [54]. When machining a ductile material, the material tends to stick to the tool surface, resulting in a surface with high roughness. As the hardness of a material increases, the tendency of the material to adhere to the cutting edge of the tool is decreased. In the case of Al alloys or composites, the microstructural characteristics and mechanical properties i.e., hardness of the alloy have a considerable effect on the roughness of the machined surface. The presence of hard brittle Si particles, SiC particulate or iron intermetallics embedded in the soft aluminum matrix tends to decrease the formation of BUE [43]. The BUE normally scratches the machined surface, thus increasing its roughness and increasing burr formation. High speed machining of ductile materials tends to reduce formation of BUE and cut down burr formation to a certain extent. Based on the discussed review of the literature the present study is focused on the following objectives.

2.7 OBJECTIVES

The mechanical properties (tensile and hardness) and machinability characteristics of a newly developed Al-Cu alloy for use in automotive applications were investigated, to compare the performance of the alloy with those of well established Al-Si based 356 and 319 alloys, taking into consideration the effects of alloy composition and heat treatment conditions (as-cast, T5 and T7). The study was conducted based on the following objectives.

- 1- Determine the tensile properties, namely, ultimate tensile strength (UTS), yield strength (YS) and percentage elongation (%El) of the newly developed Al-Cu cast alloy in the as-cast, and T5 and T7 heat-treated conditions.
- 2- Investigate the machinability characteristics of the Al-Cu cast alloy, and compare these characteristics to those of well-defined Al-Si based reference alloys, namely, 356 (Al-Si-Mg) alloy in the peak-aged condition and 319 (Al-Si-Cu) alloy in the overaged condition.
- 3- The machinability aspect investigated, namely, the milling characteristics will be performed using cutting tools with sharp cutting inserts. The results will be compared with the findings obtained employing dull cutting inserts, to emphasize the importance of the cutting tool condition while performing machining operations.
- 4- The study will include calculation of cutting forces, surface roughness, residual stresses, tool wearing, chip and burr formation.

2.8 REFERENCES

- [1] D. Apelian, "Aluminum cast alloys: enabling tools for improved performance," NADCA, 2009.
- [2] M. Warmuzek, *Aluminum-Silicon Casting Alloys: Atlas of Microfractographs*, ASM International, Materials Park, OH, 2015.
- [3] G. Armstrong, *Alloy selection for automotive aluminum castings*, SAE Technical paper, 1978.
- [4] H.V. Guthy. M.M. Makhlof, "The aluminum–silicon eutectic reaction: mechanisms and crystallography," *Journal of Light Metals*, Volume 1, , no. 4, pp. 199-218, 2001.
- [5] M.Abdelaziz, *Effect of ceramic nano particles on wear and corrosion properties of aluminum silicon hypereutectic cast alloy (A390)*, MSc, Cairo University, 2012.
- [6] J. Davis, "Alloying: Understanding the Basics," in *Aluminum and Aluminum Alloys*, 2001, pp. 351-416.
- [7] ASM International, "Aluminum-Silicon Casting Alloys," 2004.
- [8] M. I. R. Perna, *High Performing Cast Aluminium-Silicon Alloys*, LICENTIATE THESIS, Sweden: JÖNKÖPING UNIVERSITY, 2017.
- [9] M.Javidani and D.Larouche, "Application Of Cast Al-Si Alloys in Internal Combustion Engine Components," *International Materials Reviews*, vol. 59, no. 3, pp. 132-158, 2014.
- [10] M.Zeren, "Effect of Copper and Silicon Content on Mechanical Properties in Al-CU-Si-Mg

- Alloys," *Journal of Material Processing Technology*, vol. 2, no. 169, pp. 292-298, 2005.
- [11] G.Sigworth, Aluminum casting alloys, Special communication, 2008.
- [12] H.Ammar, *Influence of metallurgical parameters on the mechanical properties and quality indices of Al-Si-Cu-Mg casting alloys*, PhD, Université du Québec à Chicoutimi, 2010.
- [13] R.Dunn and W.Dickert, "Magnesium effect on the strength of A380.0 and 383.0 Aluminum die casting alloys," *Die Casting Eng.*, pp. 2-20, 1975.
- [14] A.M. Samuel, F.H. Samuel and H.W. Doty, "Observation on the formation of B-Al₅ FeSi phase in 319 type Al-Si Alloys.," *Journal of Materials Science.*, vol. 31, no. 20, pp. 5529-5539, 1996.
- [15] D. S. Mackenzie and G. E. Totten, "Physical Metallurgy and Processes," in *Handbook of Aluminum*, CRC Press, 2003.
- [16] J.E. Hatch, *Aluminum: Properties and Physical Metallurgy*, American Society for Metals, Ohio, 1990.
- [17] R.M. Brick, *Structure and Properties of Alloys*, 3rd Edition, McGraw-Hill, 1965.
- [18] "Heat Treating of Aluminum Alloys," in *ASM Handbook*, ASM International®, 1991, pp. 841-879.
- [19] P. Johne, *Machining of Products*, Düsseldorf: European Aluminium Association, (1994).
- [20] P.S.Wang ,S-L. Lee, J.-C.Lin and M.-T. Jahn, "Effect of solution temperature on mechanical properties of 319.0 aluminum casting alloy containing trace beryllium.," *Journal of Materials Research.*, vol. 15, no. 9, pp. 2027-2035, 2000.

- [21] M. Abdelaziz, *Microstructural and mechanical characterization of transition elements-containing Al-Si-Cu-Mg alloys for elevated temperature applications*, PhD Thesis, Université du Québec à Chicoutimi., 2018.
- [22] E. Sjolander and S. Seifeddin., "The heat treatment of Al-Si-Cu-Mg casting alloys .," *Journal of Materials Processing Technology.*, vol. 210 (10), 1249-1259, 2010.
- [23] D. Scott MacKenzie, N. Bogh, T. Croucher, "Heat Treating of Nonferrous Alloys: Quenching of Aluminum Alloys," in *ASM Handbook, Volume 4E*, ASM International, 2016, pp. 148-171.
- [24] Gaofeng Quan, Lingbao Ren, Zhou Mingyang, "Comprehensive Materials Finishing - Solutionizing and Age Hardening of Aluminum Alloys," in *Reference Module in Materials Science and Materials Engineering*, vol. 2, 2017, pp. 372-397.
- [25] G. Campatelli and A. Scippa, "Prediction of milling cutting force coefficients for aluminum 6082-T4.," *Procedia CIRP*, vol. 1, p. 563-568, 2012.
- [26] X. Zhang, M. Haikuo, X. Huang, Z. Fu, D. Zhu, H. Ding, "Cryogenic milling of aluminium-lithium alloys: thermo-mechanical modelling towards fine-tuning of part surface residual stress," . *Procedia CIRP*, vol. 31, 160-165, 2015.
- [27] P.K. Wright and E.M. Trent, "Metal Cutting, 4th Edn," Butterworth-Heinemann, 2000, p. 439.
- [28] P.E. DeGarmo, J.T. Black, R.A. Kohser, "DeGarmo's Materials and Processes in Manufacturing," Wiley, 2007, p. 1032.

- [29] N. Fang N, Q. Wu, "The effects of chamfered and honed tool," *Int J of Machine Tools and Manufacture*, vol. 45 (10), 2005.
- [30] I. Zaghbani and V. Songmene, "A force-temperature model including a constitutive law for dry high speed milling of aluminium alloys," *J Mater Process Technology*, vol. 209, 2532-2544, 2009.
- [31] D.S. Kilic and S. Raman, "Observations of the tool–chip boundary conditions in turning of aluminum alloys, " *Wear* 262 (7-8), 889-904, 2007.
- [32] S. Larbi, S. Djebali, A. Bilek, "Study of High Speed Machining by Using Split Hopkinson Pressure Bar," *Procedia Eng.*, vol. 114, 314–321, 2015.
- [33] R.F. Hamade and F. Ismail, "A case for aggressive drilling of aluminum," *J of Materials Processing Technology*, vol. 166 (1), 86–97, 2005.
- [34] S. Kannan and H.A. Kishawy, "Tribological aspects of machining aluminium metal matrix composites," *J of Materials Processing Technology*, vol. 198, 399-406, 2008.
- [35] P.S. Sreejith, "Machining of 6061 aluminum alloy with MQL, Dry and Flooded Lubrificant Conditions," *Materials Letters*, vol. 62 (2), p. 276–278, 2008.
- [36] C.K. Ng, S.N. Melkote, M. Rahman, A. Senthil Kumar, "Experimental study of micro- and nano-scale cutting of aluminum 7075-T6," *Int J Machine Tools and Manufacture*, vol. 46 (9), 929–936, 2006.
- [37] H. Saglam, F. Unsacar, S. Yaldiz, "Investigation of the effect of rake angle and approaching angle on main cutting force and tool tip temperature," *Int J Machine Tools and Manufacture*,

vol. 46 (2), pp. 132-141, 2006.

- [38] A. Gómez-Parra, M. Álvarez-Alcón, J. Salguero, M. Batista, M. Marcos, "Analysis of the evolution of the Built-Up Edge and Built-Up Layer formation mechanisms in the dry turning of aeronautical aluminium alloys," *Wear*, vol. 302 (1-2), 1209-1218, 2013.
- [39] M.R. Shankar, S. Chandrasekar, W.D. Compton, A.H. King, "Characteristics of aluminum 6061-T6 deformed to large plastic strains by machining," *Mater Sci Eng A*, vol. 410–411, 364–368, 2005.
- [40] Roy P, Sarangi SK, Ghosh A, Chattopadhyay AK, "Machinability study of pure aluminium and Al–12% Si alloys against uncoated and coated carbide inserts," *Int J Refract Met Hard Mater*, vol. 27 (3), p. 535–544, 2009. *Int. Journal of Refractory Metals & Hard Materials –*
- [41] A. Toropov, S.L. Ko, B.K. Kim, "Experimental study of burrs formed in feed direction when turning aluminum alloy Al6061-T6," *J Machining Tools Manufacturing*, vol. 45, 1015-1022, 2005.
- [42] I. Ciftci, M. Turker, U. Seker, "Evaluation of tool wear when machining SiCp-reinforced Al-2014 alloy matrix composites," *Mater Des*, vol. 25 (3), 251-255, 2004.
- [43] A. Manna, B. Bhattacharayya, "A study on different tooling systems during machining of Al/SiC-MMC," *Journal of Materials Processing Technology*, vol. 123 (3), 476–482, 2002.
- [44] J.F. Kelly, M.G. Cotterell, "Minimal lubrication machining of aluminium alloys.," *J Mater Process Technol*, vol. 120 (1-3), 327–334, 2002.
- [45] M. Nouari, G. List, F. Girot, D. Coupard, "Experimental analysis and optimisation of tool

- wear in dry machining of aluminium," *Wear*, vol. 255 (7-12), 1359-1368, 2003.
- [46] B.M. Lane, M. Shi, T.A. Dow, R. Scattergood, "Diamond tool wear when machining Al6061 and 1215 steel," *Wear*, vol. 268 (11-12), 1434–1441, 2010.
- [47] R.T. Coelho, S. Yamada, D.K. Aspinwall, M.L.H. Wise, "The application of polycrystalline diamond (PCD) tool materials when drilling and reaming aluminium based alloys including MMC," *Int J Mach Tools Manufact*, vol. 35 (5), 761–774, 1995.
- [48] D. Biermann, M. Heilmann, "Improvement of workpiece quality in face milling of aluminum alloys.," *J Mater Process Technology*, vol. 210 (14), 1968-1975, 2012.
- [49] R. Nur, D. Kurniawan, M.Y. Noordin, S. Izman, "Optimizing power consumption for sustainable dry turning of treated aluminum alloy," *Procedia Manufacturing*, vol. 2, 558-562, 2015.
- [50] S. Kouadri, K. Necib, S. Atlati, B. Haddag, M. Nouari, "Quantification of the chip segmentation in metal machining: Application to machining the aeronautical aluminium alloy AA2024-T351 with cemented carbide tools WC-Co," *Int. J. Mach. Tools & Manufacture*, vol. 64, 102-113, 2013.
- [51] M.C. Shaw, P.K. Wright, and S. Kalpakjian, in *Manufacturing, Engineering and Technology* (5th Edition), Chapter 21: Fundamentals of Machining, Prentice Hall, 2005.
- [52] P. Roy, S.K. Sarangi, A. Ghosh, A.K. Chattopadhyay, "Machinability study of pure aluminium and Al–12% Si alloys against uncoated and coated carbide inserts," *Int J Refract Met Hard Mater*, vol. 209, 631-638, 2009.

- [53] J.M. Dasch, C.C. Ang, C.A. Wong, R.A. Waldo, .D. Chester, Y-T. Cheng YT, B.R. Powell, A.M. Weiner, E. Konca, "The effect of free machining elements on dry machining of B319 aluminum alloy," *J Mater Process Technology*, vol. 209 (10), 4638-4644, 2009.
- [54] E-G Ng, D. Szablewski, M, Dumitrescu, M.A. Elbestawi, J.H. Sokolowski, "High speed face milling of a aluminium silicon alloy casting.," *CIRP Annals*, vol. 53 (1), 69–72, 2004.
- [55] H. Demir, S. Gündüz, "The effects of aging on machinability of 6061aluminum alloy," *Materials and Design*, vol. 30, 1480–1483, 2009.
- [56] R. Yousefi, Y. Ichida, "A study on ultra–high-speed cutting of aluminium alloy: formation of welded metal on the secondary cutting edge of the tool and its effects on the quality of finished surface," *Eng J Int Soc Precis Eng* , vol. 24, 371-376, 2000.
- [57] V.P. Astakhov, *Geometry of Single-point Turning Tools and Drills: Fundamentals and Practical Applications*, Springer-Verlag London Limited, 2010, Chapter 2, pp. 55-126.
- [58] W.Y.H. Liew, "The effect of air in the machining of aluminium alloy," *Tribology Letters*, vol. 17 (1), 41-49, 2004.
- [59] Badis Haddag, Samir Atlati, Mohammed Nouari and Abdelhadi Moufki, "Dry Machining Aeronautical Aluminum Alloy AA2024-T351: Analysis of Cutting Forces, Chip Segmentation and Built-Up Edge Formation," *Metals*, 2016, 6(9), 197; <https://doi.org/10.3390/met6090197>
- [60] Xide Li; Xiaoping Wu; Yilan Kang, "Micro-Optical Metrology in China," *Optics and Lasers in Engineering*, 2010.

- [61] Francisco Javier Trujillo Vilches, Lorenzo Sevilla Hurtado, Francisco Martín Fernández and Carolina Bermudo Gamboa, "Analysis of the Chip Geometry in Dry Machining of Aeronautical Aluminum Alloys," *Applied Sciences*, vol. 7 (2), p. 132, 2017;
- [62] Serope Kalpakjian, Steven Schmid, *Manufacturing, Engineering and Technology* (5th Edition), Prentice Hall, 2005.
- [63] X. Li, T. Shi, B. Li, C. Zhang, B. Zhong, Y. Lv, Q. Zhang, "One-Step Preparation of Super-Hydrophobic Micro-Nano Dendrites on Al Alloy for Enhanced Corrosion Resistance.," *Metals*, vol. 8, no. 11, p. 960, 2018; <https://doi.org/10.3390/met8110960>
- [64] E. Samuel, A. M. Samuel, H. W. Doty, S. Valtierra, F. H. Samuel, "Intermetallic phases in Al-Si based cast alloys: new perspective," *International Journal of Cast Metals Research*, vol. 27, no. 2, 107-114, 2014.
- [65] J. A. Taylor, "Iron-containing intermetallic phases in Al-Si based casting alloys," in *11th International Congress on Metallurgy & Materials SAM/CONAMET 2011*, Rosario, Argentina, 2011; *Procedia Materials Science*, vol. 1, 19-33, 2012.

CHAPTER 3

EXPERIMENTAL PROCEDURES

CHAPTER 3

3 EXPERIMENTAL PROCEDURES

3.1 INTRODUCTION

In this section, the methodology and experimental procedures used in this study are described and explained in detail. The aspects addressed in this chapter will cover the preparation of the alloys used, the casting procedures, details of the applied heat treatments; preparation of samples for tensile testing; and the details of the machining equipment and set-up and tools used for carrying out the milling experiments. It should be mentioned here that the tensile testing was carried out at ambient temperature.

3.2 MATERIALS AND CASTING PROCEDURES

For determining the potential of the new Al-Cu alloy to produce automotive castings, five alloys were tested to identify the one with the best machinability. Optimization of the manufacturing method is a major challenge in the development of a reliable cast component.

Three of these alloys were based on the Al-Cu HT200 alloy and were coded as Alloys A, B and C, with a silicon (Si) content lower than that used in conventional alloys, to improve machinability. The HT200 alloy belongs to the 2xx family of alloys, where copper is the highest alloying element by weight percentage (6 wt%). Their low Si and high copper (Cu) content thus characterize these alloys. Alloy A represents the HT200 alloy in

its as-cast condition, while Alloy B is used in the T5 heat-treated condition, and Alloy C corresponds to the alloy in the T7 heat-treated condition. The composition of the HT200 alloy is proprietary to Nemak who supplied the alloy for this study.

These alloys were compared to the well-known 319 and 356 alloys, coded D and E, respectively, which were considered as reference alloys, being commonly used in the automotive industry. These alloys belong to the 3xx family of Al-Si alloys, and contain a silicon level of ~7%. The compositions of the three alloys are provided in Table 3-1. All alloys were cast using a permanent mold. The 319 alloy (Alloy D) corresponds to the Al-Si-Cu system while the 356 alloy (Alloy E) corresponds to the Al-Si-Mg system, where the strengthening elements Cu and Mg provide precipitate hardening following aging treatment. The 319 alloy was used in the T7 heat-treated condition, while the 356 alloy was used in the T6 heat-treated condition.

Table 3-1 Chemical analysis of the alloys

Chemical Analysis (wt%)										
Alloy	Element									
	Cu	Si	Fe	Mn	Mg	Ti	Zr	V	Zn	Al
HT200	6.0	0.69	0.17	0.38	0.015	0.102	0.19	0.013	0.19	Bal
319	3.323	7.97	0.418	0.245	0.266	0.131	-	-		Bal
356	0.12	7.19	0.12	-	0.32	0.12	-	-		Bal

The ingots of the HT200, 319.0, and 356.0 alloys received were cut, cleaned, dried and melted using an electrical resistance furnace, employing a silicon carbide crucible of

120-kg capacity. The metal was melted at a temperature of 750°C, and the alloying additions were made in order to achieve the required chemical compositions as shown in Table 3-1.

Before pouring the melt into the respective molds, pure dry argon was injected into the melt at a constant rate of 20 m³/hr, for about 20 min, using a rotating impeller in order to reduce the amount of hydrogen absorbed in the melt, as well as to ensure that all additions made were homogeneously mixed and distributed within the melt. Prior to pouring, the surface of the melt was carefully skimmed to remove oxides and inclusions.

The melt was poured into two different permanent molds, i.e. an ASTM B-108 mold for preparing test bars for tensile testing, and a book mold, which provided cast blocks for machinability testing, respectively.

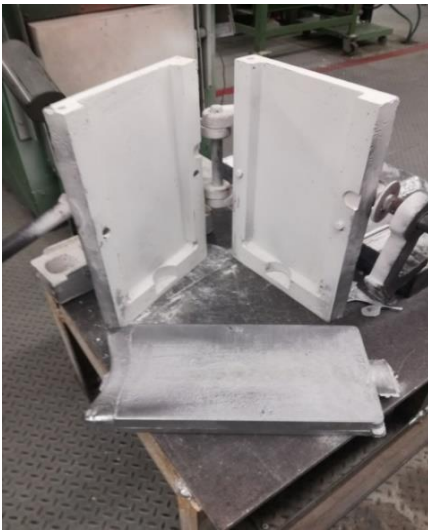


Figure 3-2 Book mold and cast machining block.



Figure 3-1 Electric resistance furnace. .

3.3 HEAT TREATMENT

The as-cast samples i.e., the tensile test bars and blocks were subjected to different heat treatment procedures. While alloys A, B, and C have the same HT200 alloy chemical composition, alloy A was used in the as-cast condition (i.e. without heat treatment), alloy B was heat treated using the T5 temper, and alloy C was subjected to the T7 heat treatment temper. The heat treatment conditions were as follows:

- 1- T5 temper treatment: Heating the as-cast alloy at 250°C for 5 hours followed by air cooling;
- 2- T7 temper treatment: Solution heat treatment of the as-cast alloy at 530°C for 8 hours, followed by quenching in warm water (60°C), then artificial aging at 250°C for 5 hours, and finally air cooling.

Alloy D (319.0) was heat treated according to the T7 temper procedure using the following conditions:

- 1- Solution heat treatment at 510°C for 8 hours;
- 2- Quenching in warm water at 60°C;
- 3- Artificial aging at 250°C for 5 hours; and
- 4- Air cooling.

Finally, alloy E (356.0) were investigated in the peak-aging condition (i.e. T6-treated) using the following conditions:

- 1- Solution heat treatment at 540°C for 8 hours;
- 2- Quenching in warm water at 60°C;
- 3- Artificial aging at 180°C for 5 hours; and
- 4- Air-cooling.

while Figure 3-3 shows a photo of the Blue M forced air heat treatment furnaces with programmable controller (± 2 °C variation) which were used to carry out the solution and aging treatments ,while Figure 3-4 shows a graphic representation of the heat treatment procedures used.

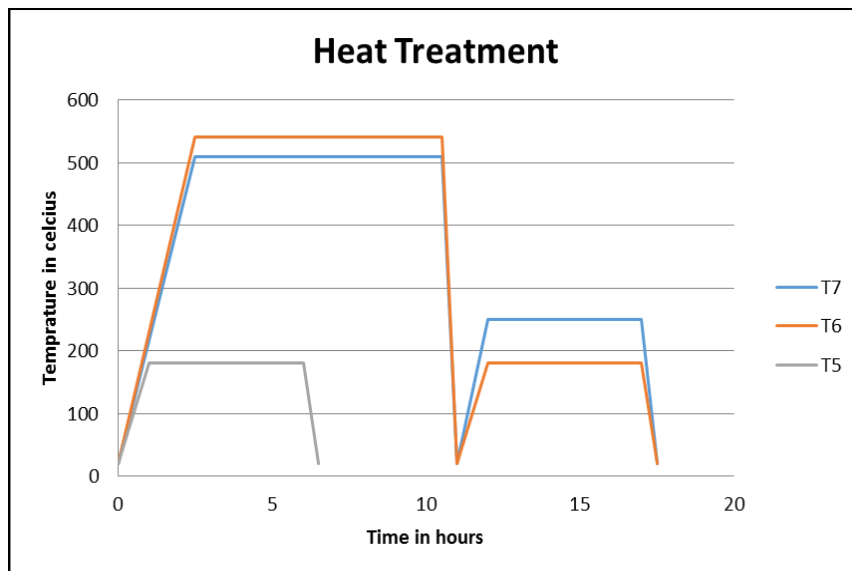


Figure 3-4 T5, T6 and T7 heat treatment regimes.



Figure 3-3 Blue M forced air heat treatment furnaces.

3.4 TENSILE TESTING

Tensile testing at room temperature was carried out on as-cast and heat treated test bars using an MTS Servo hydraulic mechanical testing machine, at a strain rate of $4 \times 10^{-1} \text{ s}^{-1}$. The elongation was measured using a strain gauge extensometer attached to the sample. A data acquisition system attached to the MTS machine shown in Figure 3-5 converts the measurement from the strain gauge to an accurate measure of the percentage elongation. From the stress-strain curve obtained for each specimen tested, the data acquisition system provided values of the ultimate tensile strength (UTS), yield strength (YS) at 0.2% offset strain and percentage elongation (%El). For each alloy composition, five test bars were used in the as-cast and heat-treated conditions, from which the average UTS, YS and %El values were determined.

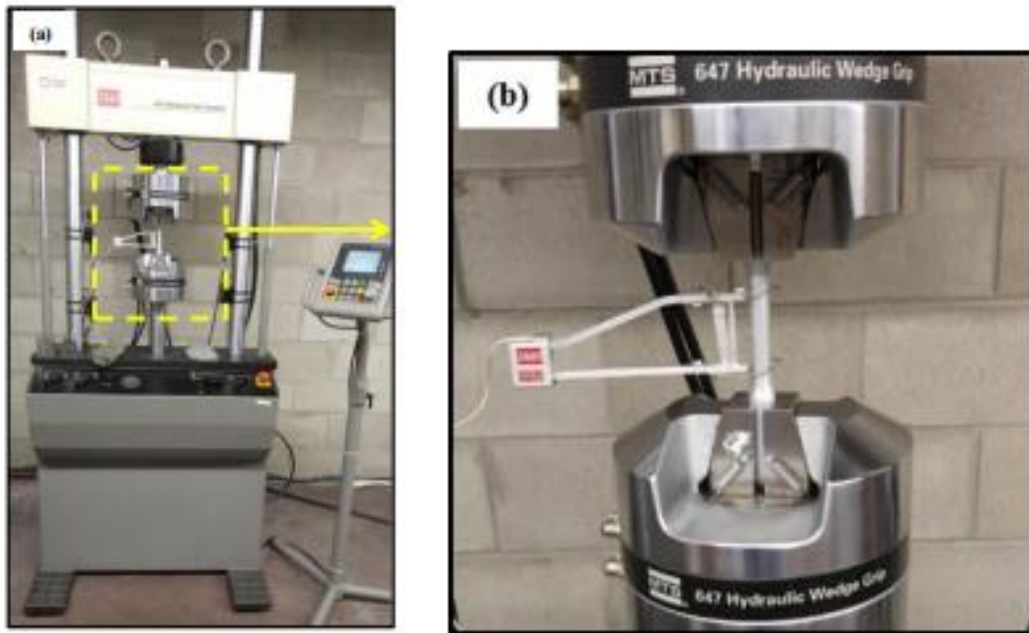


Figure 3-5(a) MTS Servohydraulic mechanical testing machine, (b) attachable strain gauge.

3.5 MACHINABILITY TESTING

This study is divided into two parts. Part one deals with the use of new inserts whereas Part two examine the effects of applying dull ones. Dull inserts are prepared by machining on a steel alloy. The steel alloy has an overall hardness higher than that of the cast aluminium machining blocks. The increased hardness will result in excessive wear along the cutting edge of the cutting inserts. After machining is performed, a non-uniform wear is developed along the cutting edges. The resulting wear profile is a magnification of the accumulative wear that might occur when several blocks of aluminium are machined. Performing the machining process using dull inserts will highlight the effect of the cutting tool condition on the investigation of machinability criteria. The investigations include calculation of the cutting forces, quality of the finished surface, tool wearing, residual stresses, chip and burr formation.

3.5.1 MILLING PROCESS

Face milling is the machining process that was used to examine the machinability of Alloys A, B, C, D and E. The milling process was carried out on the CNC HURON KX Five 5-axis high-speed machine shown in Figure 3-6 that is known for its excellent precision. A spindle speed of 121000 RPM was used. The experimental set-up consists of the CNC machine, the blocks to be machined, a table dynamometer with piezoelectric sensors that is responsible for detecting and measuring the cutting force, a signal amplifier and A/D converting unit. Five blocks of each alloy group were machined using the same cutting insert. A new cutting insert was used for each alloy group. For example, after machining the five blocks of alloy A, a new insert was used to machine the next five blocks of alloy B, and so on.



Figure 3-6 CNC HURON KX Five 5-axis machine.

Thirteen layers of material were removed from every block tested. Each layer consists of 10 paths, the depth of cut being 1.35 mm. Figure 3-7 shows (a) a schematic of the removal process, and (b) an actual block after removal of the layers. The cutting forces were recorded during the removal of the second and the seventh layer of each block. Analysis of the cutting forces was done using the Matlab Software. In addition, tool wear, built up edge (BUE), and characterization of the chips formed were the other aspects examined to understand the machinability of alloys A, B, C, D and E.

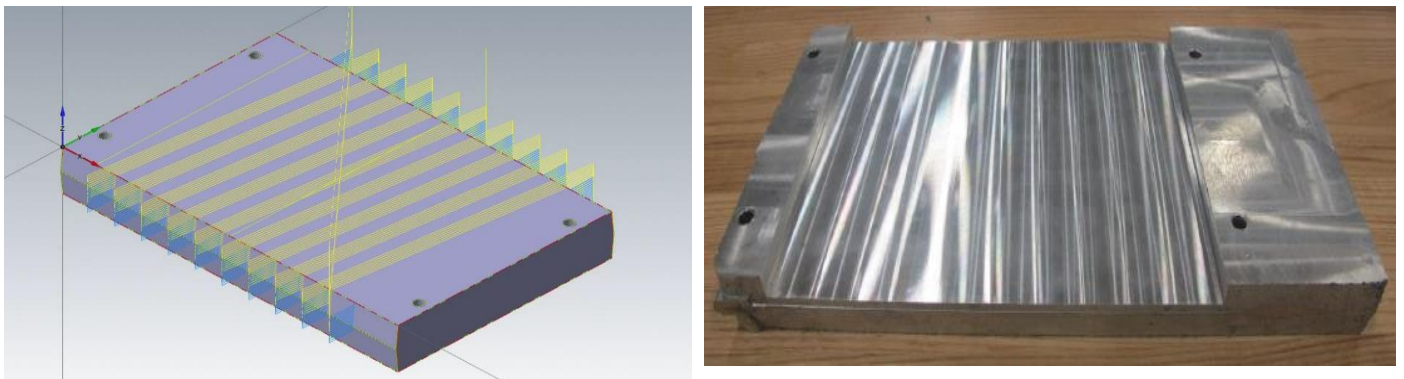
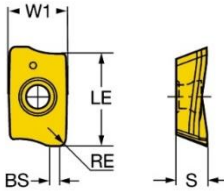


Figure 3-7 Removal of layers from a cast block (a) schematic, and (b) actual block.

3.5.2 CUTTING TOOL

A 25-mm machining tool was used with removable four inserts made of tungsten carbide material that has a relatively high hardness and wear resistance compared to the soft material of the aluminum alloy. Details of the insert are provided below. The carbide inserts have an elevated range of hardness that can withstand machining of hard silicon phases presented in Al-Si alloys especially at high machining speeds.

Sandvik Carbide Insert: R390-11 T3 08e-nl H13a



Operation type (CTPT) : **Light**

Coating (COATING) : **UNCOAT**

Insert size and shape (CUTINTSIZESHAPE) : **CoroMill 390 -11T3**

Wiper edge length (BS) : **1.5 mm**

Insert width (W1) : **6.8 mm**

Cutting edge effective length (LE) : **10 mm**

Corner radius (RE) : **0.8 mm**

Insert thickness (S) : **3.59 mm**

Hand (HAND) : **R**

Start values

N	fz 0.15 mm(0.05-0.25)
	vc 990 m/min(1000-960)



3.5.3 MEASUREMENT OF CUTTING FORCES

Cutting forces were measured to investigate the machinability of the utilised alloys. Measuring the cutting forces provides an evaluation of the machining process. Cutting forces are detected and measured using advanced sensitive sensors. The cutting force data is used in comparing and selecting different workpiece materials and tools. It is necessary to link the tool wear and chip formation with the cutting forces. The cutting forces measuring system consists of three stages: (i) the transducing stage which is achieved using a piezoelectric table dynamometer; (ii) the conditioning stage wherein data stabilization, primary filtration and amplification was achieved using a multichannel amplifier consisting of eight independent channels; and the read-out stage is achieved using data acquisition software reading and recording the data.

The 3-component dynamometer used in this experiment is piezoelectric type. The 9255B Kistler dynamometer has high rigidity and consequently results in having a high natural frequency which allows measurement of dynamic machining. The dynamometer contains four of the 3-component sensors that are well placed inside the dynamometer structure, therefore a multi- component force measurement can be done easily. The forces are measured in three directions X, Y and Z for F_x , F_y and F_z , where values for F_x , F_y and F_z are combined to obtain the resultant of the cutting force, F_r (see Figure 3-8).

The piezoelectric mechanism gives an output charge that is directly proportional to the measured load. This charge is passed to the multi-charge amplifying unit, where the charges are converted into voltage signals through a well-insulated cable. The data acquisition software changes this voltage form to proportional values in terms of forces verses time. The data is then saved in ‘.mdt’ format to be processed by the Matlab software. The 8 output signals of the forces are collected from the 8 channels, to be summed in the three main directions as Fx, Fy and Fz components using the following equations:

$$F_x = F_{x1+2} + F_{x3+4}$$

Equation 1 Cutting force in X direction.

$$F_y = F_{y1+2} + F_{y3+4}$$

Equation 2 Cutting force in Y direction.

$$F_z = F_{z1} + F_{z2} + F_{z3} + F_{z4}$$

Equation 3 Cutting force in Z direction.

$$F_r = \sqrt{F_x^2 + F_y^2 + F_z^2}$$

Equation 4 Resultant cutting force.

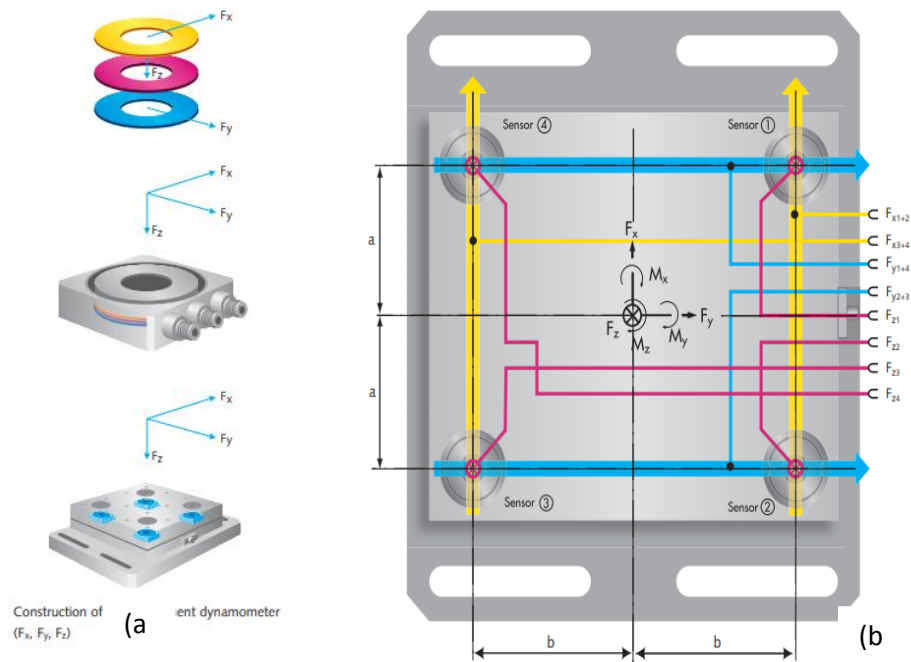


Figure 3-8 (a) Construction of a 3-component dynamometer (Fx , Fy & Fz), (b) Sensor arrangement of the table dynamometer

3.5.3.1 DATA PROCESSING PROCEDURE USING MATLAB SOFTWARE

The data processing procedure is achieved by applying a set of consecutive steps. Raw data is extracted or generated from the data acquisition system (table dynamometer, wiring connection, multichannel amplifier and the operating software). The data is extracted in the time domain (as shown in Figure 3-9), and then transferred to the frequency domain using Fourier transform, whereby the unnecessary frequencies are highlighted. Digital filtration is applied to eliminate these frequencies from the raw data. The eliminated frequencies represent noises generated from the motor of the machine. Cycle recognition is then applied, with one cycle equated to one machined path, followed by cycle correction or cycle calibration where the cutting force cycle is adjusted to initiate from zero.

The data processing process was achieved using MATLAB software, where a code was generated to apply the above-mentioned steps. To observe any trends, the following steps were carried out.

Frequency analysis: The raw forces data were transferred from time domain into frequency domain. The major frequencies with the highest magnitude that covered most of the domain were highlighted, as shown in Figure 3-10(a). As may be seen, the major frequency was 1500 Hz and 2500 in shear directions F_x . The forces in the time domain were filtered according to the selected major frequencies in the digital filtration stage. Figure 3-10(b) reveals that frequencies greater than 3000 Hz were eliminated using digital filtration, employing a low pass digital filter with 3000 Hz pass band frequency and a cut-off frequency of 5%.

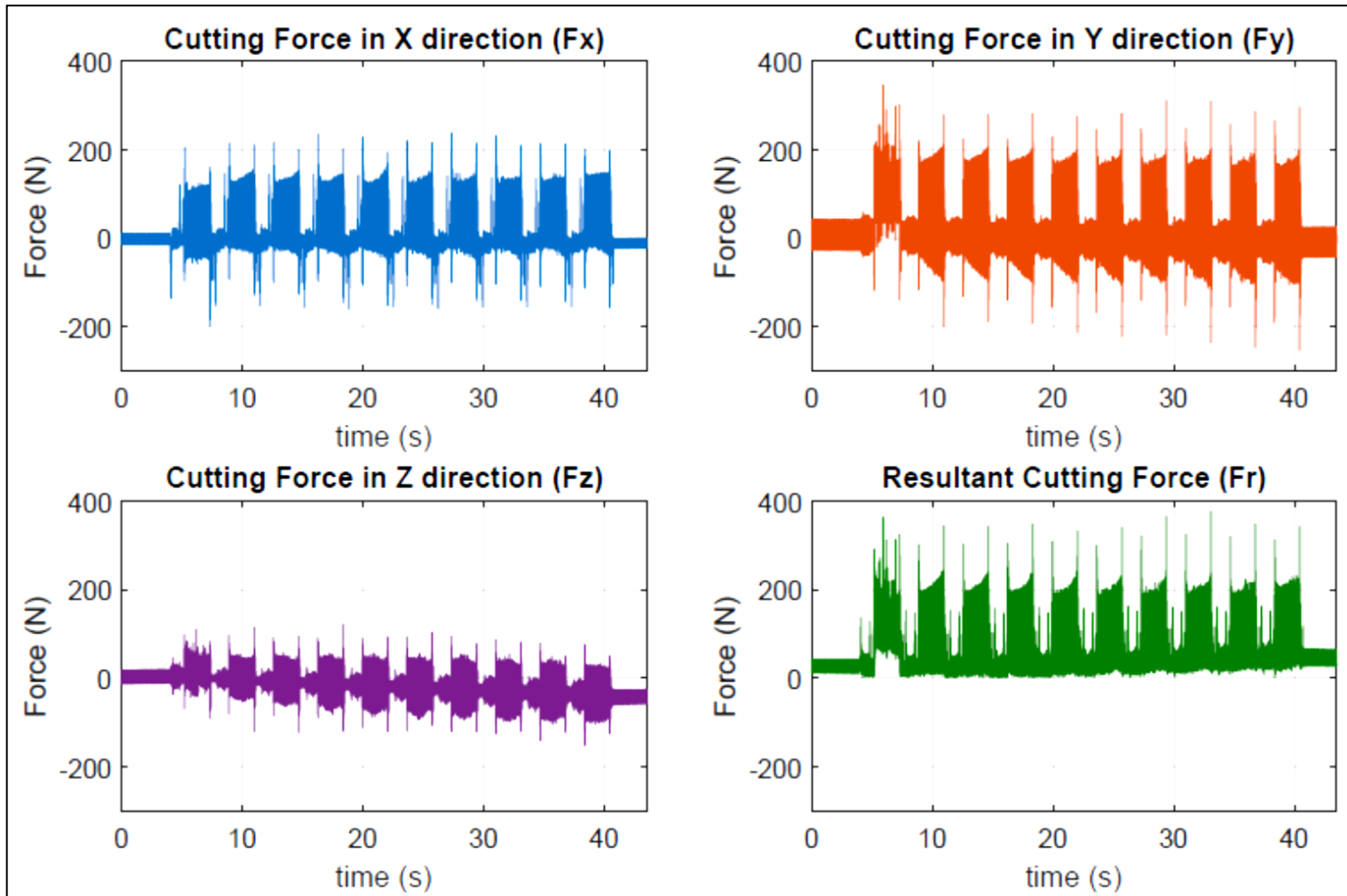


Figure 3-9 Raw data extracted from the cutting force measuring system showing F_x , F_y , F_z and F_r for alloy A.

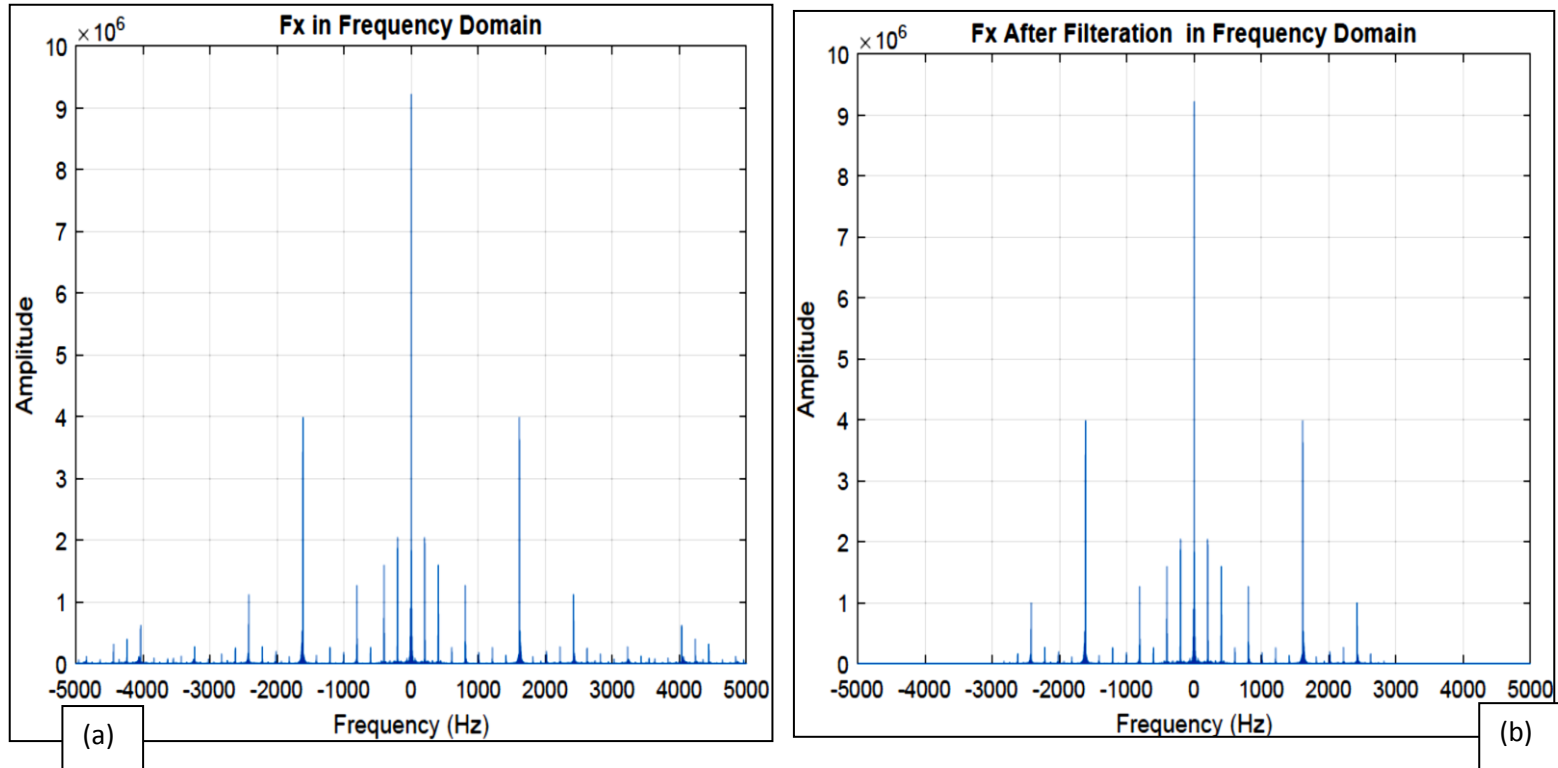
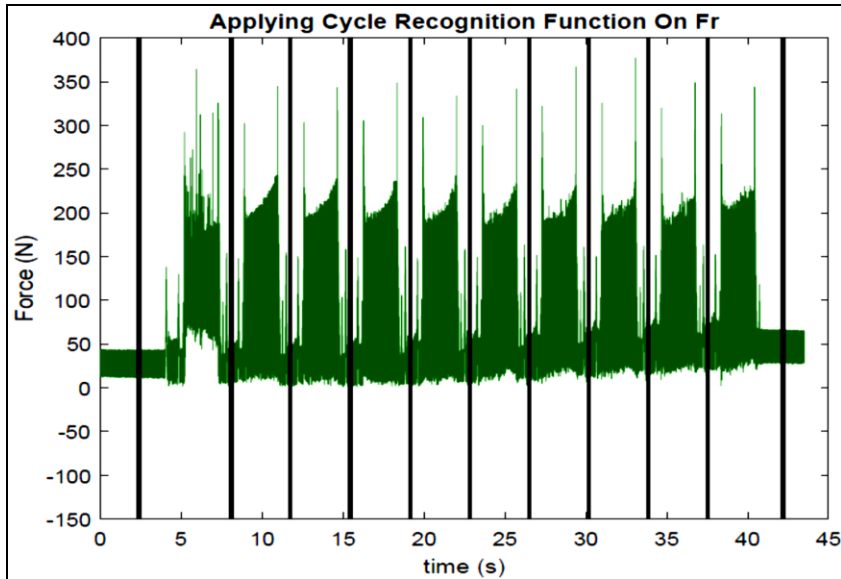
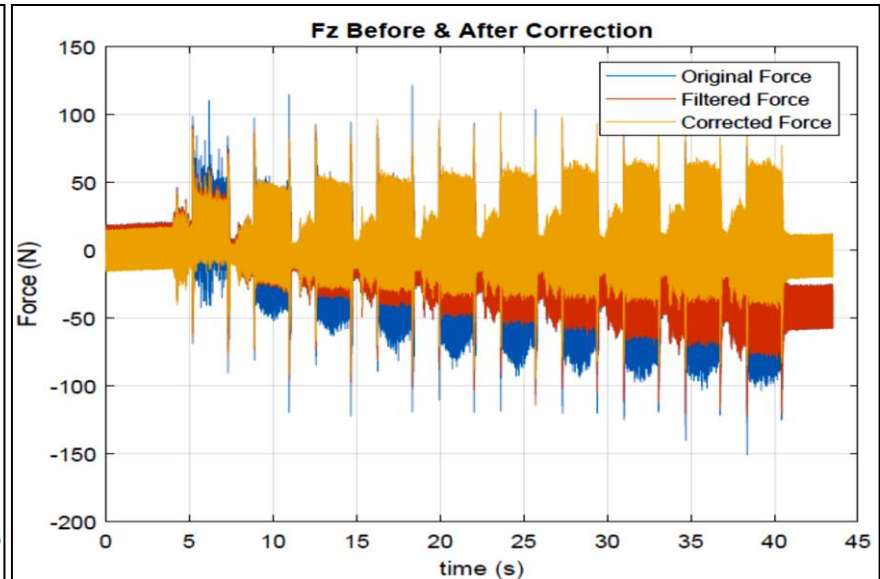


Figure 3-10 Frequency domain before and after applying digital filtration.

A cycle recognition function was used to specify the initial point and the final point of each cycle. The cycle was recognised by targeting the peaks as well as the valleys of each cycle. In Figure 3-11(a), the data between two black lines represents one cycle, which represents one machined path. The total number of cycles per one machined layer is ten cycles which were recognized by the values of the cutting forces during engagement and disengagement of the tool. Figure 3-11(b) represents the cycle correction stage. Cycle correction was done to ensure that all the recorded machining process cycles were readjusted to start from a certain reference: in our case zero was used as the datum line.



(a)



(b)

Figure 3-11(a) Defining number of cycles, (b) illustration of cutting forces before and after correction.

The extraction function for peaks and valleys was designed to collect the maximum and minimum peaks within each cycle. Maximum and minimum peaks were defined. Average values for peaks and valleys were calculated as a percentage of maxima and minima peaks, as shown in Figure 3-12. Data from the same alloy family were merged together in order to be able to visualize the total behaviour of the machining process for a specific alloy so that any trend could be easily observed and analysed.

Data from alloys A, B, C, D and E are plotted on scatter diagrams where the X axis represents the distance travelled by the tool in meters while the Y axis shows the magnitude of the force in Newton. Data from alloy D (319) and alloy E (356) were compared with data from alloy HT200 in the as-cast and heat-treated conditions to study the effect of alloying elements and heat treatment on the tensile properties of these alloys.

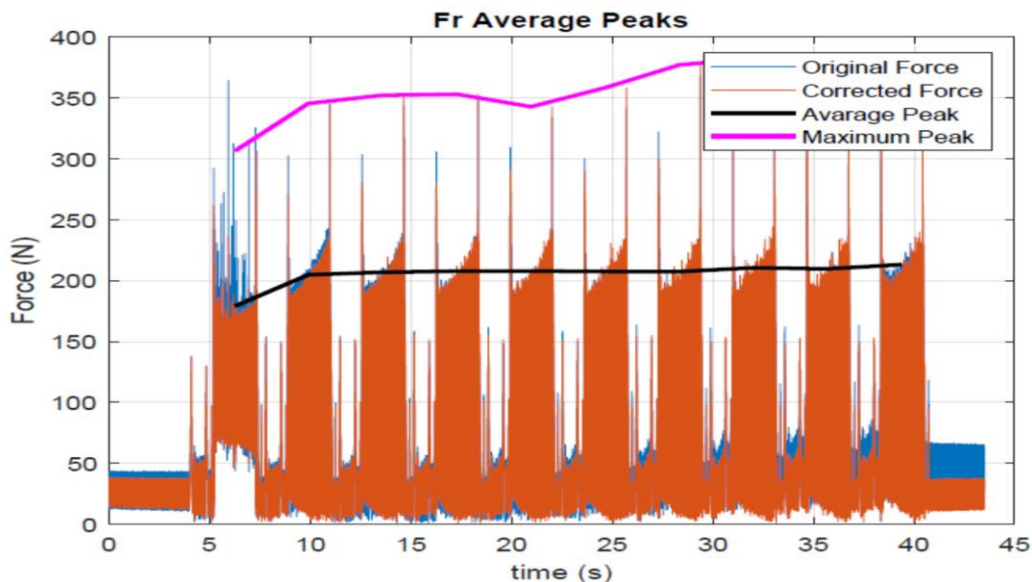


Figure 3-12 Maximum peak values and average peak values

3.5.4 EVALUATION OF SURFACE ROUGHNESS

A Mitutoyo SJ-410 Surftest model stylus tabletop surface roughness tester ($\pm 0.01\mu\text{m}$ accuracy) was used to measure the roughness of the machined surface, as shown in Figure 3-13. The surface roughness was measured at different locations. The stylus traces the surface of the machined workpiece and detects irregularities on the surface. The vertical displacement of the stylus is converted into digital values that are displayed and printed on the screen.

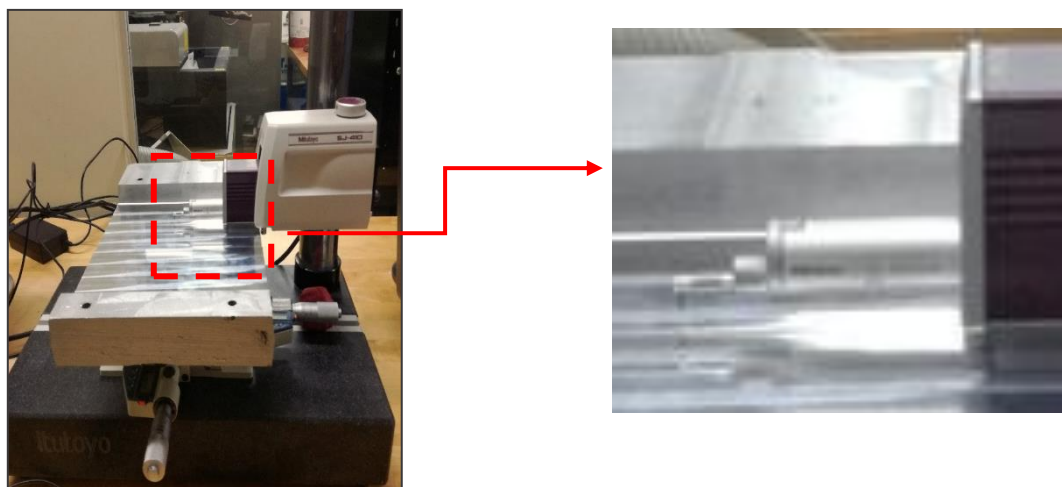


Figure 3-13 Mitutoyo SJ-410 measuring instrument.

The surface integrity is evaluated according to ISO 1997 standards. The following steps are carried out before measuring.

- 1- The workpiece is cleaned from the remaining oil and chips from the machining process, using a suitable solvent and a lint-free cloth.
- 2- A cone shaped probe with spherical tip (1 μm diameter) is selected. The selected stylus probe is checked for any signs of wear.
- 3- The instrument is calibrated prior to measuring the surface roughness, using the test specimen supplied by the manufacturer.
- 4- The collected data is processed, and statistical calculations are made using the operating software SurfTest Version 2.00.

Table 3-2 Roughness evaluation parameters

Measuring Tool	SurfTest	Version	Ver 2.00
Standard	ISO 1997	Digital Filter	GAUSS
Measured Profile	Roughness	Cut-Off	2.5mm
λ_s	25 μm	Filter	GAUSS

3.6 RESIDUAL STRESS MEASUREMENT

Measurement of residual stresses was carried out on the blocks at the end of the milling process, using the X-ray technique. Figure 3-14 shows the points where the X-ray measurements were carried out, in two directions, i.e., the milling direction and the transverse direction. The point P0 corresponds to the part of the block that was not machined. The insert on the top left shows the direction of the X-rays and the X and Y directions along which the measurements were recorded. It should be noted that the residual stress measurements were carried out for blocks that were subjected to the milling process using both new and dull inserts.

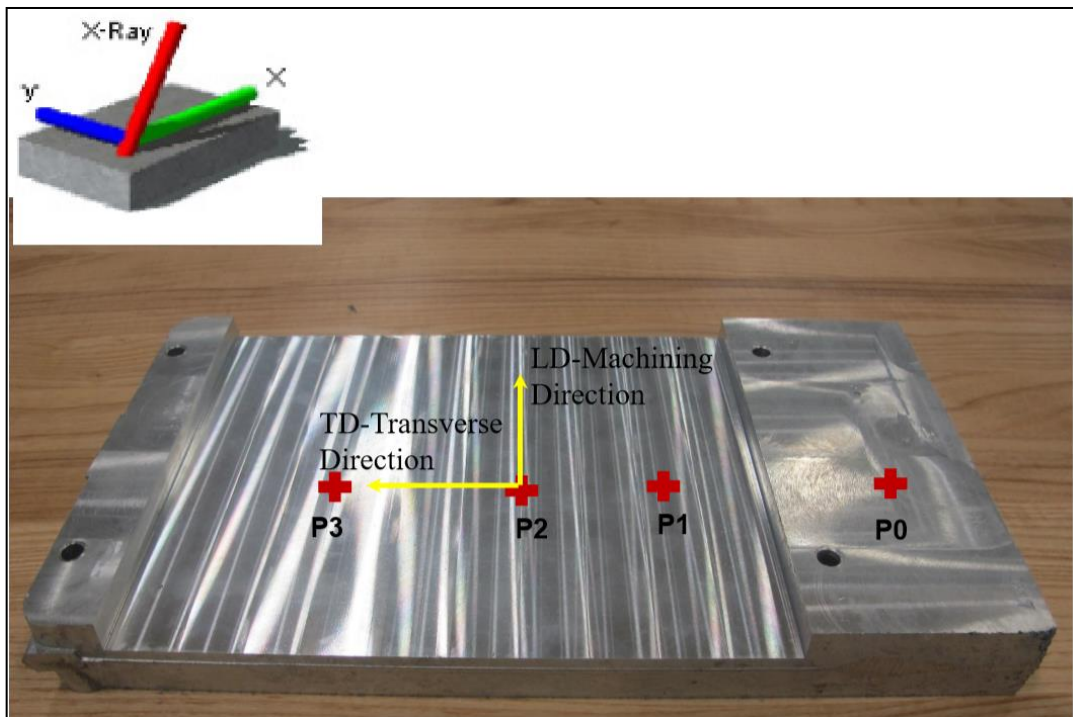


Figure 3-14 Measurement of residual stresses in the block at the end of the milling process.

The details and conditions under which the X-ray measurements of the residual stresses were carried out are summarized in Table 3-3 below.

Table 3-3 Measurement conditions for determination of residual stresses using X-ray technique

Measurement area	All (3,000 - 30,000 [mm])
Pitch	50 [um]
X-ray irradiation time(Setup)	20 [sec]
X-ray irradiation time(Meas.)	20 [sec]
X-ray irradiation time(Max)	85 [sec]
X-ray tube current	1,00 [mA]
X-ray tube voltage	30,00 [kV]
Sample distance(Monitor)	29,313 [mm]
Sample distance(Analysis)	28,593 / 27,969 [mm]
X-ray incidence angle	25,0 [deg]
Offset of alpha angle	0 [deg]
X-ray wavelength (K-Alpha)	2,29093 [Å] (Cr)
X-ray wavelength (K-Beta)	2,08480 [Å] (Cr)
Total measurement count	16253
Oscillation count	0
X-ray tube total use time	290,34 [h] (1045208 [sec])
Detection sensitivity	19,7 [%] (169649)
Peak strength (Ave)	172k / 46k
Level of ambient light	0,2 [%]
Temperature	28,94 [deg C]
K-Beta cut filter	Unused
Valid range of alpha angle	18,00 <--> 90,00 [deg]
Peak analysis method	Fitting Lorentz
Correction coefficient (Stress)	0,000xx + 1,000x + 0,000
Correction coefficient (FWHM)	0,000xx + 1,000x + 0,000
Correction coefficient (R.Gamma)	0,000xx + 1,000x + 0,000
Austenite calculation method	Integrated intensity ratio
R-value (Alpha)	---
R-value (Gamma)	---

3.7 MICROSTRUCTURE EXAMINATION

For metallographic observations, 25 x 25 mm samples were cut from the machined blocks. The samples were mounted in bakelite using a Struers Labopress-3 Mounting Press. The samples were then ground and polished to the desired fine finish using the Struers Tegrapol-35 Grinder-Polisher shown in Figure 3-15. The grinding stages were carried out using different grades of SiC abrasive papers # 240, # 320, # 400, # 600, # 800 and #1200. To produce samples with a mirror-like surface, the polishing was carried out in two stages (rough and fine polishing), using a solution of polycrystalline diamond powder particles suspended in water, employing diamond powder sizes of 6 μm and 3 μm , respectively. Struers oil was used in these polishing stages as a cooling and lubricating medium. After the polishing was completed, the samples were washed in alcohol and dried using compressed air.

The microstructures of the samples were examined using a Leica DM LM optical microscope-image analysis system, as shown in Figure 3-16. Grain size measurements were carried out employing the Clemex image analyzer software.



Figure 3-16 Struers Tegrapol-35 Grinder-Polisher.

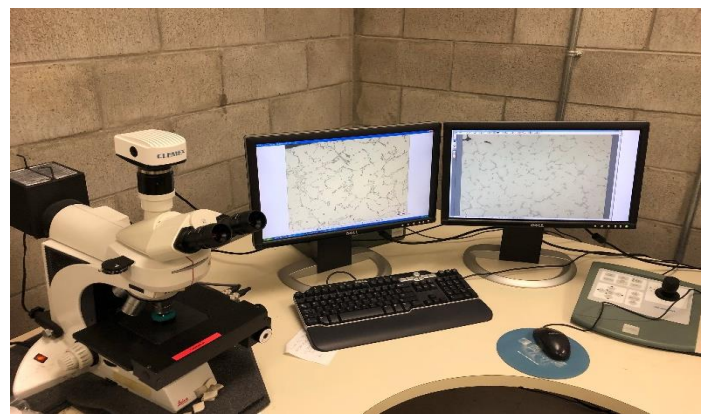


Figure 3-15 Leica DM LM optical microscope.

CHAPTER 4
RESULTS AND DISCUSSION

CHAPTER 4

4 RESULTS AND DISCUSSION

4.1 INTRODUCTION

The present chapter is devoted to the investigation of the metallurgical and mechanical parameters that control the milling behavior of the five alloys described in Table xx. The study is divided into two parts: Part I covers the milling results obtained with the use of new inserts whereas Part II examines the effect of applying dull inserts. The aspects investigated include calculation of the cutting forces, quality of the finished surface, tool wear, residual stresses, and chip and burr formation. The high-speed CNC machine described in Chapter 3 was used to perform the milling tests, and the techniques employed to study the different aspects included X-ray diffraction, field emission electron microscopy, stereographic and optical microscopy.

4.2 PART I - USE OF NEW INSERTS

4.2.1 MICROSTRUCTURE AND TENSILE PROPERTIES

Figure 1 shows the optical microstructures obtained from samples sectioned from the as-cast tensile bars of the three alloys A, D and E. The large amount of Cu in alloy A is reflected in the precipitation of coarse Al_2Cu phase throughout the entire matrix along with a few $\alpha\text{-Al}_{15}(\text{Fe},\text{Mn})_3\text{Si}_2$ phase particles, Figure 4-1(a). As reported previously [1-3], modification with Sr would lead to a divorced eutectic reaction where the Al-Si eutectic has been observed separated from the Al- Al_2Cu eutectic, as seen in the case of alloy D, Figure 4-1(b). In addition, the $\alpha\text{-Fe}$ phase particles are also rejected in front of the advancing Al-Si eutectic. Pucella et al. [4] reported on the inverse precipitation of $\alpha\text{-Fe}$ in Sr-modified alloys. In this case, the $\alpha\text{-Fe}$ phase precipitates within the $\alpha\text{-Al}$ during solidification of alloy, Figure 4-1(c). In other words, the $\alpha\text{-Fe}$ precipitates prior to the formation of the $\alpha\text{-Al}$ network. The importance of this reaction is to harden the soft $\alpha\text{-Al}$, leading to more-or-less uniform strength over the entire alloy.

Table 4-1 lists the tensile properties of the five alloys investigated following the heat treatments described in Table 2 in Chapter 3. The as-cast HT200 alloy itself shows relatively good characteristics, with almost 96% of the yield strength of the 319 alloy after T7 treatment, but with a significantly low ultimate tensile strength and elongation.

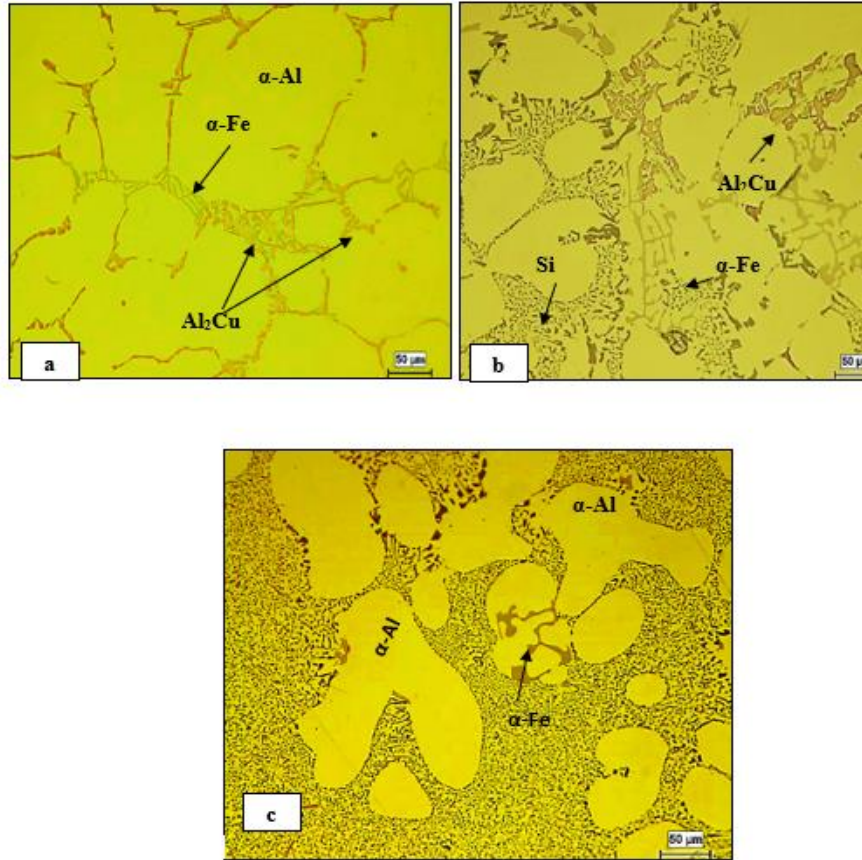


Figure 4-1 Optical microstructures of alloys in the as-cast condition: (a) HT200 alloy, (b) 319 alloy, (c) 356 alloy.

Table 4-1 Tensile properties of the studied alloys

<i>Alloy</i>	<i>UTS (MPa)</i>	<i>YS (MPa)</i>	<i>El%</i>
<i>Alloy A</i>	283	212	2.2
<i>Alloy B</i>	298	235	3.4
<i>Alloy C</i>	331	247	5.3
<i>Alloy D</i>	295	244	3.8
<i>Alloy E</i>	355	310	6.9

The as-cast HT200 alloy itself shows relatively good characteristics, with almost 96% of the yield strength of the 319 alloy after T7 treatment, but with a significantly low ultimate tensile strength and elongation. The T5 heat treatment of alloy B for 5 hours increased its elongation by 1.2%, coupled with a slight improvement in its ultimate tensile strength of about 5% and better improvement in the alloy yield strength by about 12%, from the original as-cast value (alloy A). In comparison, alloy C (in the T7 treated condition) showed real improvement in all three properties: the elongation increased by about 3% and both the yield strength and the ultimate tensile strength values increased by about 17 % above those obtained from alloy A. In terms of comparison between alloy HT200 and the commercial alloys, it can be noticed that the T7 heat-treated HT200 alloy (coded alloy C) reveals a comparable performance to the 319 alloy for the T7 treatment in terms of yield strength but with a higher percentage elongation. On the other hand, alloy C exhibits lower yield strength compared to the 356 alloy (T6 heat-treated) despite its comparable ultimate tensile strength and ductility values, which may be interpreted in terms of the relatively high Cu content (~6%, which is slightly higher than Cu concentration in A206 alloy [5]).

Figure 4-2 shows the precipitation density in alloys C and D. As mentioned previously, alloy C and alloy D were aged similarly at 250°C for 5 hours, revealing the effect of increased Cu content on the density of the particles in Figure 4- 2(b) compared to that seen in Figure 2(a). Also Figure 4-2(c) demonstrates the change in the inter-particle distance on going from T6 (alloy E) to T7 (alloy C) treatment and how this change would affect the alloy tensile strength shown in Table 4- 1 and schematically represented in Figure 4-3 [6].

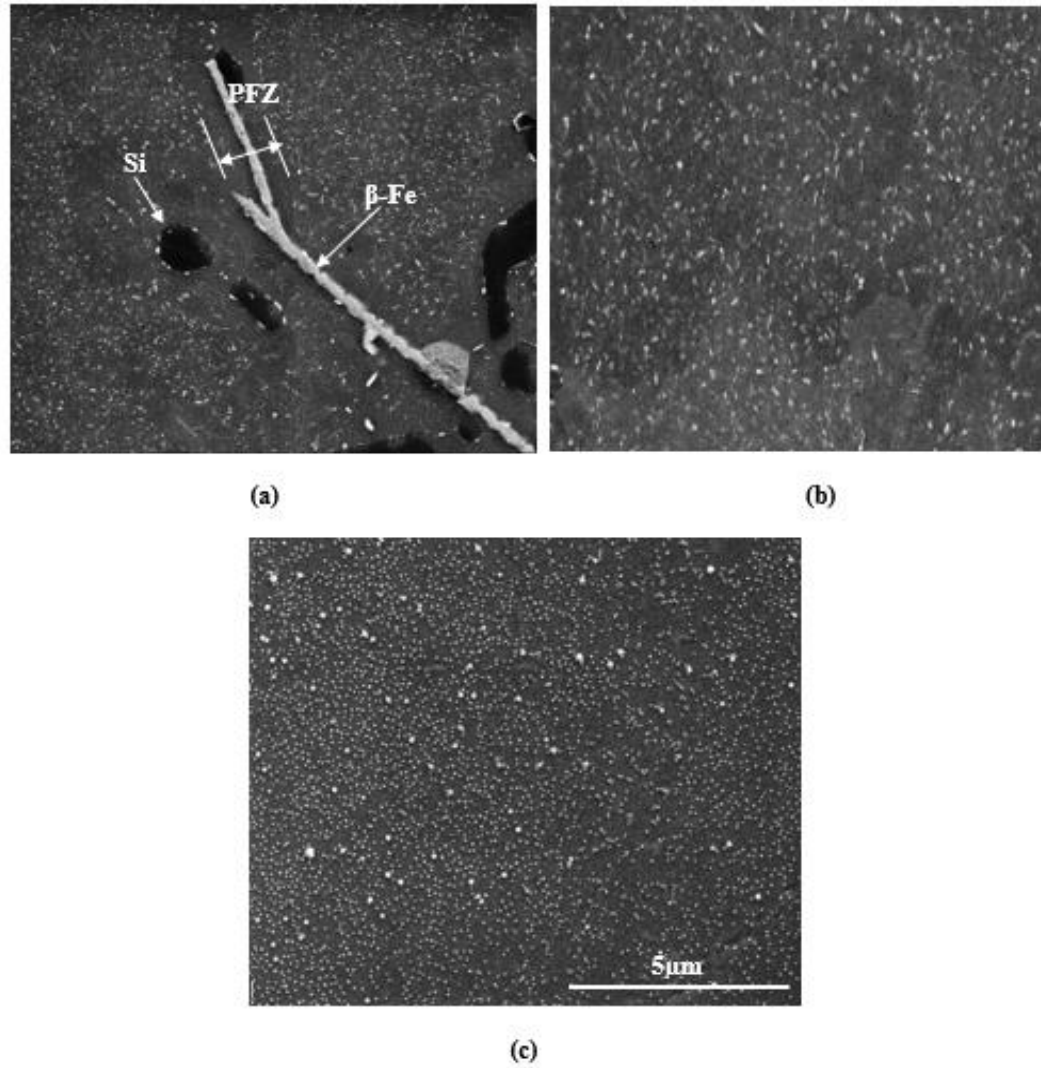


Figure 4-2 Backscattered electron images of: (a) alloy D; (b) alloy C in T7 condition, (c) alloy E in T6 condition. PFZ = precipitate free zones.

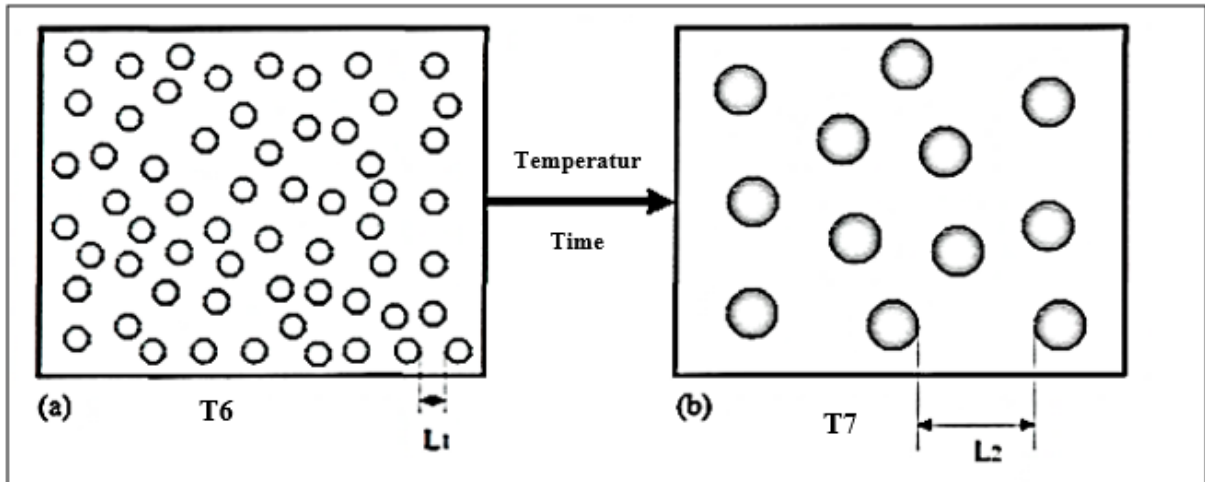


Figure 4-3 Schematic representation showing the influence of the increasing aging temperature on the size , density ,and inter-particle spacing of the hardening precipitates : (a) at a low aging temperature , and (b) at a high aging temperature (L1 and L2 indicate inter-particle spacing).

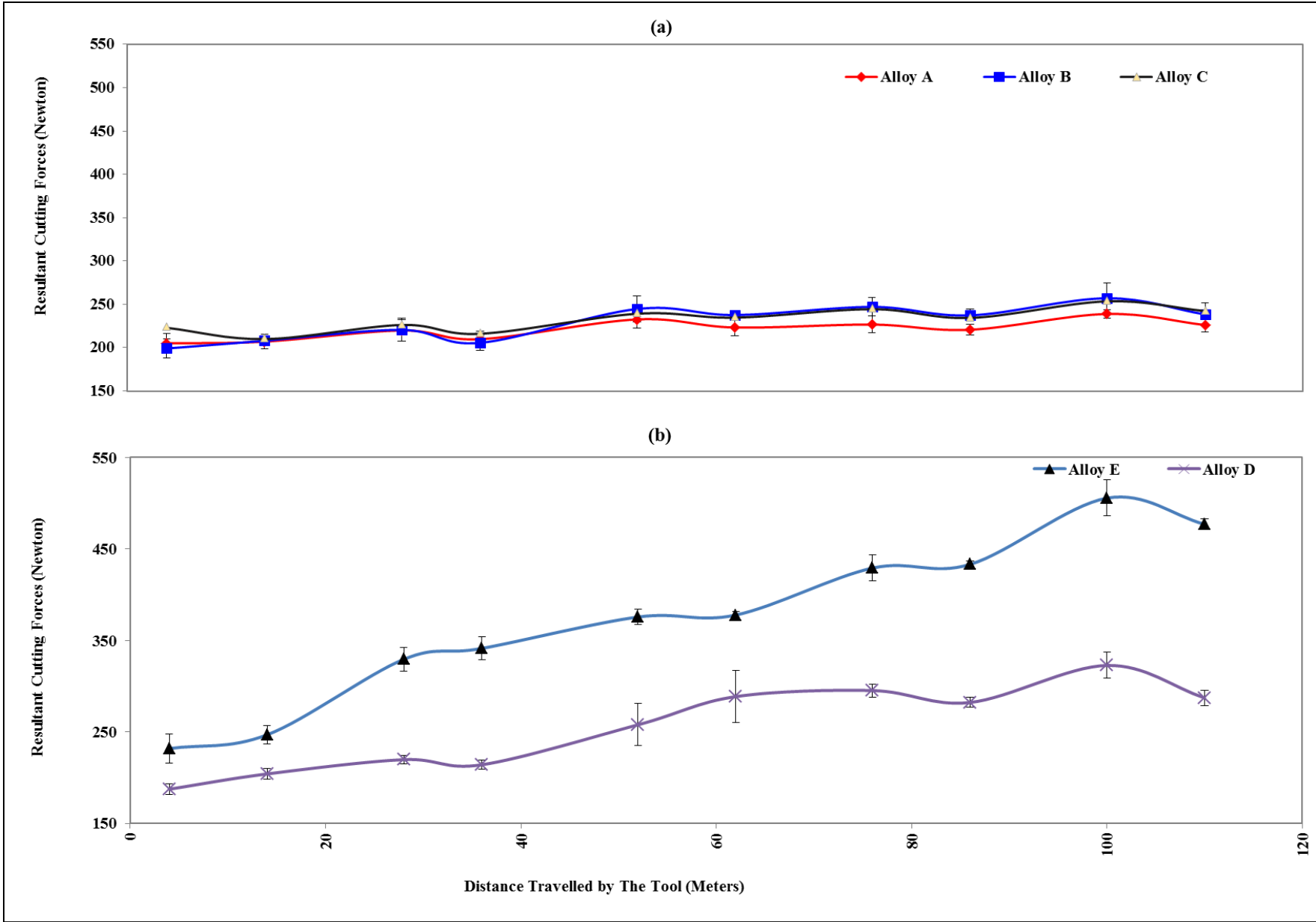
4.2.2 CUTTING FORCES AND TOOL WEAR

According to Zaghbani and Songmene [7], while the cutting forces during the machining of aluminum alloys are relatively low, they can nevertheless provide a good indicator for a comparison of different alloys under the same machining conditions. Songmene et al. [8] concluded that the machining of aluminum alloys is relatively easy as the cutting forces involved are low and the tool life is relatively high if there is no built-up edge or material adhesion problem. However, some problems may arise with the chip form and particle emissions. The review article of Praneeth and Naveen [9] on the machining of aluminum alloys reveals that machining of aluminum and its alloys is not usually a difficult task. Major problems are encountered only in alloys containing high Si contents (above 7.5 wt.%) or hard SiCp or Al₂O₃p particles.

In another review on machining of aluminum alloys by Santos et al. [10], it was reported that flank wear can generate excessive machining forces [11] during the milling of aluminum alloys, since flank wear increases the workpiece-tool contact area. The rate of flank wear will increase when the cutting speed increases. In other words, the higher the cutting speed, the shorter would be the tool life [12].

Although alloys A, B and C share the same chemical composition, each alloy was subjected to a different heat treatment. To determine the effects of heat treatment, a comparison of the machinability of the alloys under the same machining conditions was carried out. It was observed that alloys A, B and C exhibit the same trend with incremental variation in the resultant cutting force.

In Figure 4-4(a), alloy A, which was tested in the as-cast condition, showed the lowest cutting forces compared to alloys B and C. The highest cutting force in alloy A (238 N) was obtained after machining a distance of 120 m. Slight tool wear was observed on the cutting edge and the face of the cutting insert after machining 120 m of alloy A; the wear is minimal as the material is very soft, containing no hard particles that would grind the cutting edge of the insert (Figure 4-5).



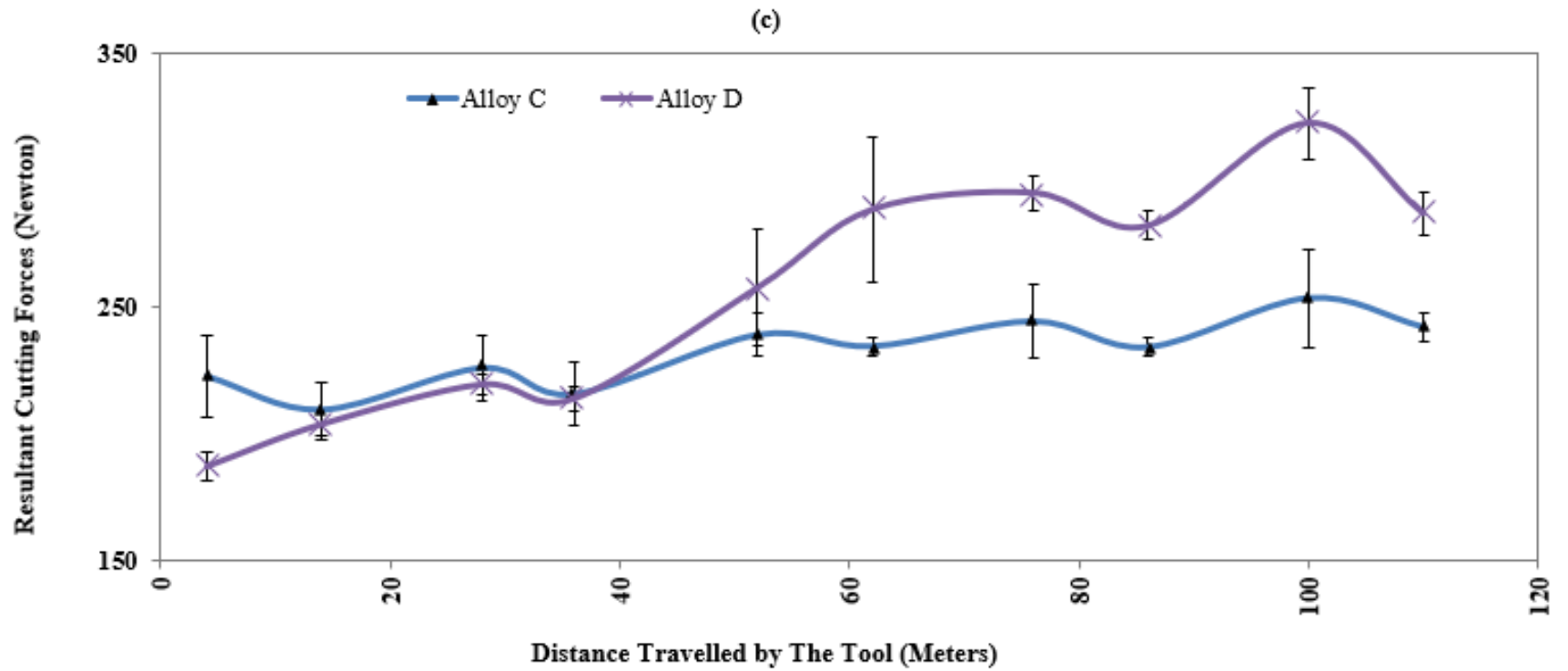


Figure 4-4 Resultant cutting forces obtained for (a) alloys A, B and C in the as-cast, T5 and T7 heat-treated conditions, respectively; Comparison of resultant cutting forces (b) for commercial alloys E and D, and (c) for alloy C with alloy D.

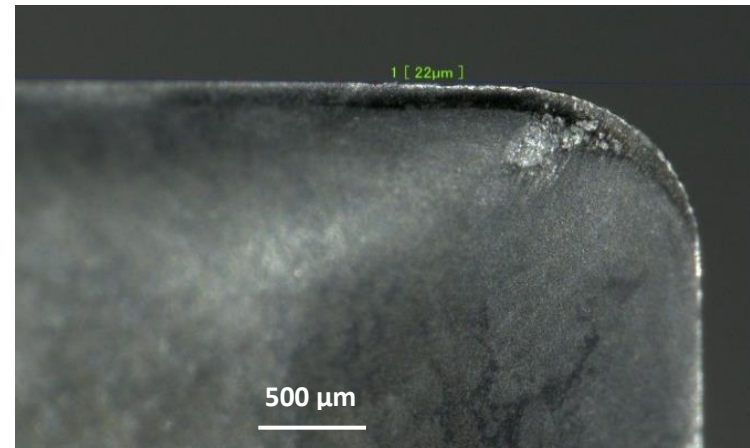
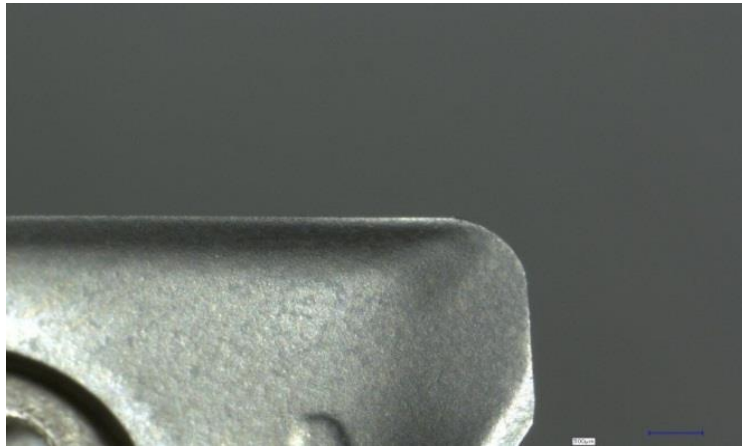
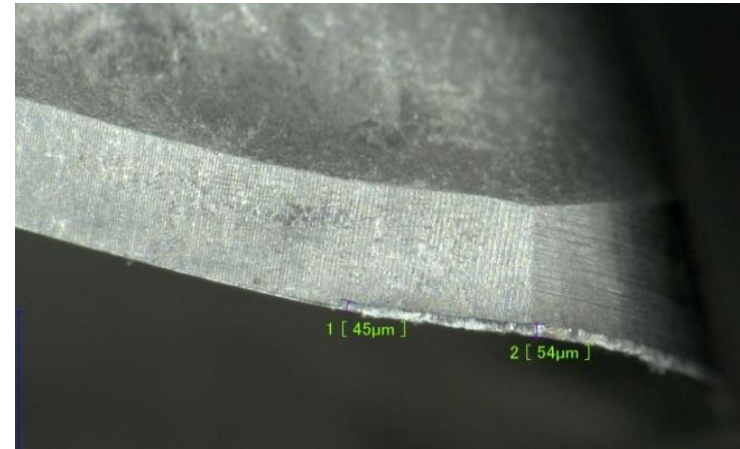
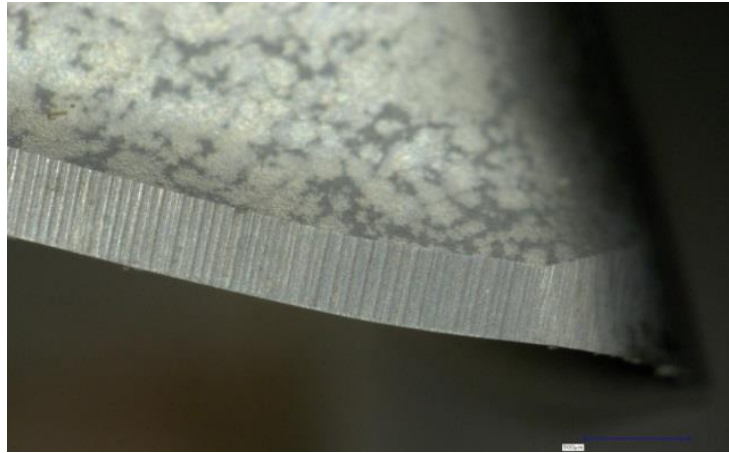


Figure 4-5(a) Cutting edge of new insert, (b) cutting edge after machining 120 m, (c) face of new insert, (d) face of the insert after machining 120 m in alloy A.

As shown in Figure 4-4(a) the cutting force exhibited by alloy C after machining of 120 m was 253 N, which is almost the same as for alloy B. This observation may be attributed to the overaging effect during the heat treatment process. Alloy C also does not exhibit noticeable tool wear, only a slight notch can be seen on the face side of the tool (Figure 4-6), which may be due to the presence of some inclusions within the machined surface. The face wear in alloy C was slightly more than that observed in alloy B.

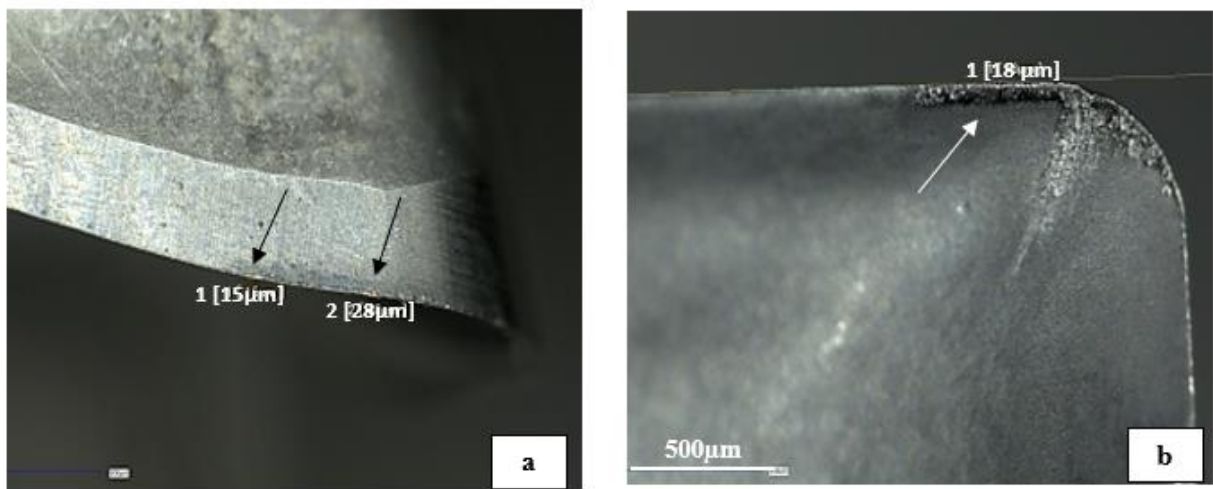


Figure 4-6 (a) Cutting edge of new insert (b) cutting edge after machining 120 m (c) face of new insert (d) face of the insert after machining 120 m - alloy C.

Alloy E recorded the maximum cutting forces among the five tested alloys (500 N after 120 m), particularly with respect to alloy D (275 N). Alloy E was T6 heat-treated (aged at 180°C, i.e., peak aged) while alloy D was T7 heat-treated, corresponding to the overaged condition. During overaging, the dissolution of fine precipitates occurs, with diffusion into the larger precipitates within the soft matrix. The large hard precipitates coarsen resulting in increased inter-particle spacing and material softening. The presence of Cu still improves the machinability of the alloy D (Figure 4-4).

At the peak aging condition in the case of alloy E, the alloy matrix is embedded with fine hard precipitates, as shown in Figure 4-2(c). The inter-particle spacing of these precipitates is decreased, resulting in a matrix having a high density of hard particles. These particles enhance the hardness as well as the tensile properties. The enhanced mechanical properties and the presence of hard silicon particles in alloy E result in an increase of the cutting forces required to shear the layers of the material. As the mechanical properties were enhanced, the material resistance to forming is increased, resulting in progressive wear at the cutting edges of the inserts. Tool wear is gradually increased, resulting in increased cutting forces. Any increase in cutting forces during a machining operation reflects a reduction in the tool life. The upcoming figures show the deformation that occurred in the cutting edges of the inserts used in the machining of both alloys D and E. The insert used to machine alloy E faced more wear than that used for alloy D. The wear along the cutting edge of the insert was found to be 136 μm for alloy E at point 2, and 94 μm for alloy D at point 2, as shown in Figure 4-7.

In Figure 4-4(c), alloy C, the new HT200 alloy, is compared with the commercial alloy D – alloy B319.0. Alloy C and D are having almost the same tensile properties as shown in the table 4-1. The tensile test results show that alloy C exhibits a UTS value of 309 MPa, a YS value of 291 MPa and percentage elongation of 4%, while alloy D displays a UTS value of 321 MPa, YS of 244 MPa and percentage elongation of 2.5 %. In alloy D, the cutting forces increase gradually especially after machining a distance of 40 m, where the effect of silicon particles is noted in the increase in cutting forces as seen in Figure 4-4(c). The cutting forces increased continuously, reaching a peak value of 322 N after machining 120 m. Alloy C shows an insignificant increase in the cutting force from 220 N to 253 N after 120m machining distance. The cutting inserts used to machine alloy C showed less tool wear compared to alloy D.

The tool wear observed for alloy C was 28 μm at point 2 on the cutting edge of the insert whereas it increased to 94 μm at point 2 on the cutting edge of the insert for alloy D. The difference in tool wear might be due to the low Si content of alloy C, namely 0.64 wt% compared to 6.5 wt% in alloy D. Therefore, the absence of hard Si particles reduces tool wear, suppresses the cutting forces and enhances the tool life. Alloy C has higher tensile properties and hardness due to the high Cu content present in the alloy 6.5 wt%, which is nearly double that of alloy D (3.5 wt%). In addition, the presence of copper aluminide in high percentage improves the machinability of alloy C and reduces the tool wear as shown in Figure 4-2.

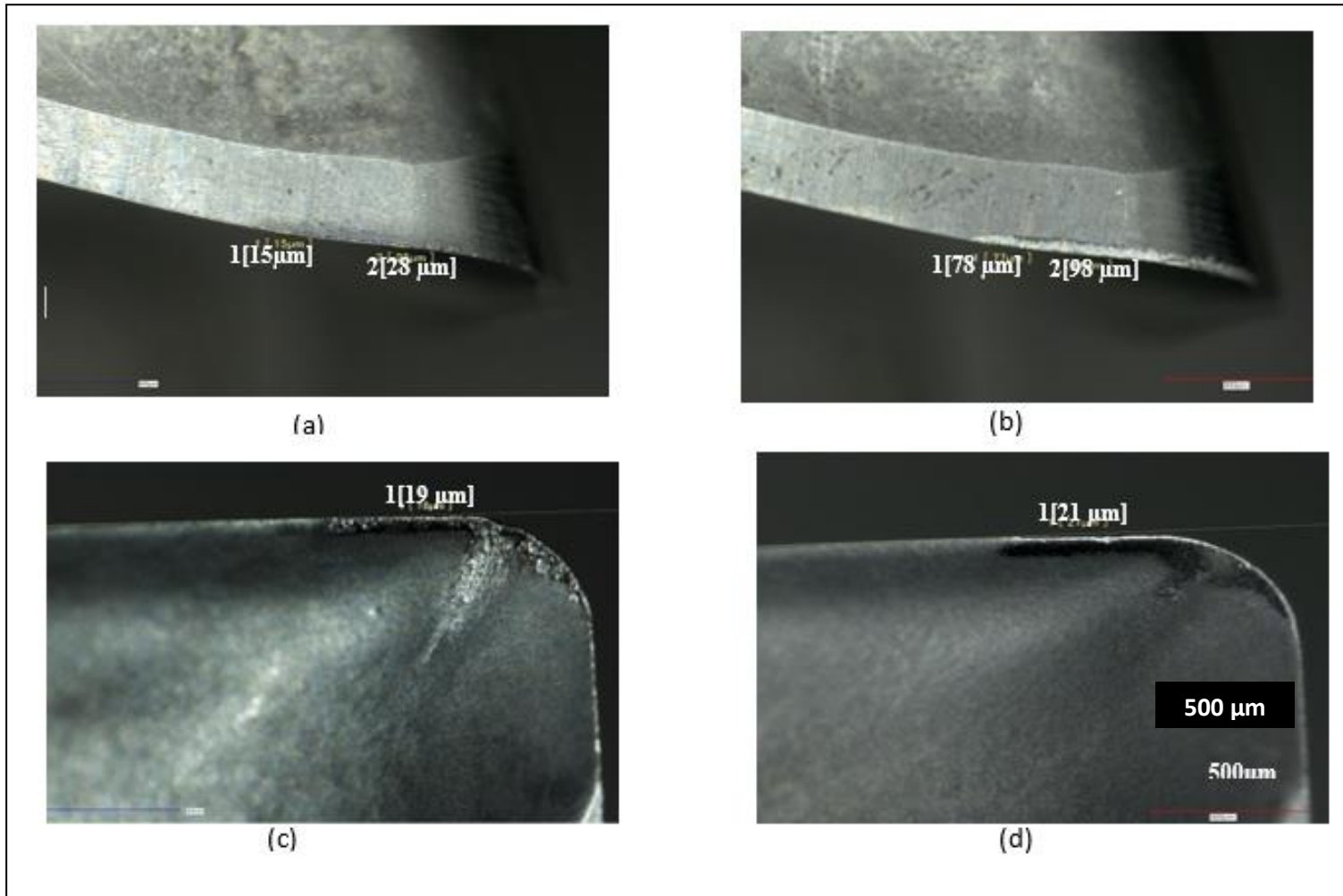


Figure 4-7 (a) Cutting edge after machining 120 m of alloy C, (b) cutting edge after machining 120 m of alloy D, (c) face of the insert after machining 120 m of alloy C, (d) face of the insert after machining 120 m of alloy D.

4.2.3 MEASUREMENT OF RESIDUAL STRESSES

Measurement of residual stresses was carried out on the blocks at the end of the milling process, using the X-ray technique. A portable X-ray unit was used for this purpose. Portable x-ray machines are characterized by their flexibility and ease of use. The compact system can perform in the laboratory, on the shop floor, or in the field [13]. Figure 4-8 displays a photograph of such a machine.

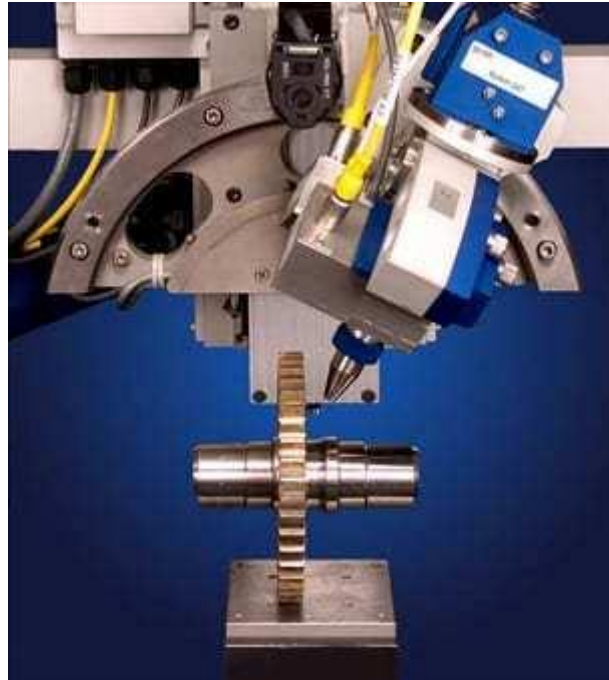


Figure 4-8 Portable X-ray machine [13].

Robinson and Redington [14] studied the influence of alloy composition on residual stresses in heat-treated aluminium alloys. Residual stress magnitudes are a function of the inherent strength of the alloy and the microstructural changes (precipitation) that occur during the heat treatment process. Near surface residual stresses were assessed using X-ray diffraction.

Robinson *et al.* [15] concluded that one of the unavoidable results arising from the heat treatment of precipitation-hardened aluminium alloys is the introduction of high residual stresses. Tang *et al.* [16] performed a study on residual stresses in milling of aluminium alloys. The authors concluded that a high cutting speed will induce tensile residual stresses on the surface of the workpiece and result in a shallow residual stress layer, and that a large feed rate has no effect on the superficial residual stress and results in deeper residual stresses beneath the surface.

Figure 4- 9 represents the residual stresses built up beneath the milling surface after 120m machining distance. As can be seen, regardless the applied heat treatment, the Al-Cu alloys revealed approximately the same values (36-52 MPa), which are nearly half of the stresses caused by the presence of hard particles in the Al-Si alloys. As in the case of cutting forces, the presence of Cu in B319.0 alloy played a significant role in reducing the severity of the accumulated stresses.

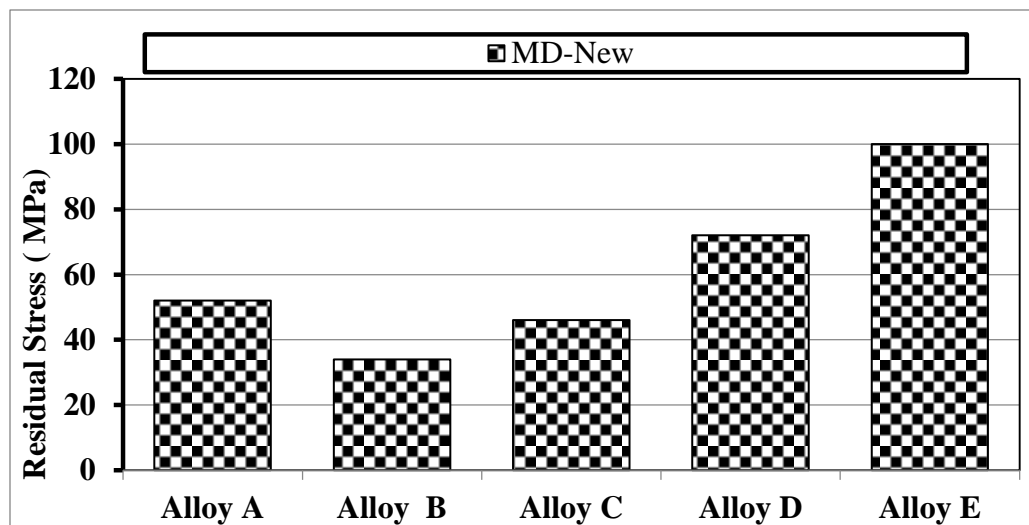


Figure 4-9 Residual stresses measured by x-ray diffraction technique in the milling direction.

The hardness of the five alloys are measured and evaluated at 10µm below the machined surface. The test is carried out using a weight of 50g .As showed in Table 4-2 Alloy C and E reveled the highest hardness values 93.5 HV and 123.4 HV respectively. This observation may be attributed to the enhanced strength and ductility of these two alloys as shown in Table 4-1.

Table 4-2: Evaluation of the Max hardness values HV at 10µm below the machined surface

Alloy	Max hardness, HV
A	81.5
B	75.6
C	93.5
D	81.4
E	123.4

4.2.4 SURFACE ROUGHNESS AND BURR FORMATION

Kumar *et al.* [17] emphasized the effect of machining parameters on the surface quality of aluminum alloy in CNC milling operations with HSS tools. The authors developed a multiple regression model with spindle speed, feed rate and depth of cut as the independent variables and the surface roughness parameter ‘Ra’ as the dependent variable. Lee *et al.* [18] performed a study on the surface shape and roughness of aluminum alloy used in heat exchangers, using ball end milling. In the machining field, the demand for machined pieces free from traces of surface roughness has gradually increased. This demand has led to the ability to design and machine complicated three-dimensional (3D) shapes. According to Gangopadhyay *et al.* [19], the main difficulty in machining aluminum

alloys with uncoated cemented carbide inserts lies in the formation of build-up layer (BUL) on the rake surface whereas Jomaa *et al.* [20] stressed on the importance of the cutting feed and the tool nose radius due to its strong influence on the surface finish of the workpiece. Suraratchai *et al.* [21] and Maya *et al.* [22] highlighted the importance of the machined surface roughness on the fatigue life of aluminum alloys.

Figure 4-10 demonstrates the criteria for measuring the surface roughness used in the present work, while Figure 4-11 shows the obtained results [5]. It is evident from Figure 4-11 that the presence of Si is the main parameter in increasing the surface roughness. The presence of Cu in alloy D seems to counter the Si effect to a limited extent. As the Al-Cu alloys do not have hard particles, the surface roughness is mainly related to the alloy strength. As inferred from Figure 4-12, the machined surfaces of Al-Cu alloys are relatively smooth after machining the distance of 120 m. In contrast, the presence of the Si hard particles in Al-Si alloys resulted in noticeable damage caused by possible removal of Si particles or surface cracking during the milling operation as pointed out by the white arrows in Figure 4-13.

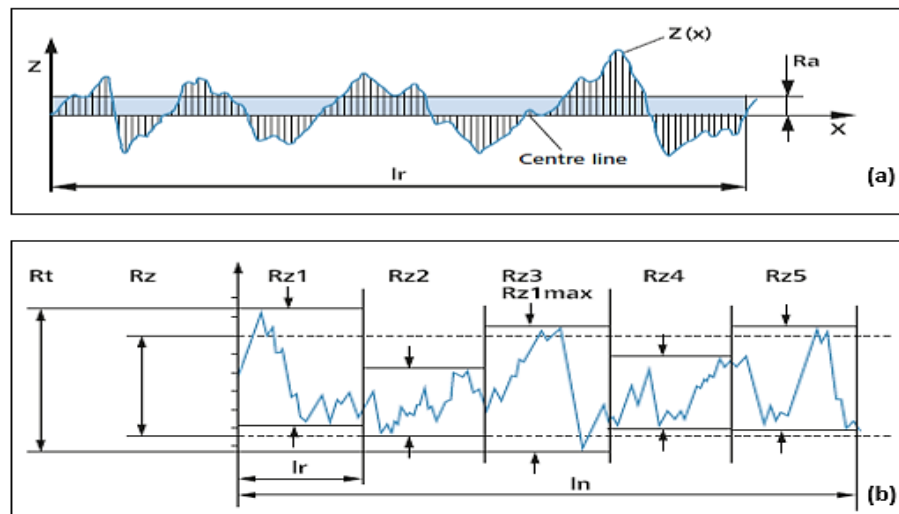


Figure 4-10 Criteria for defining the surface roughness:(a) Ra, (b) Rz, Rt according to ISO 4287.

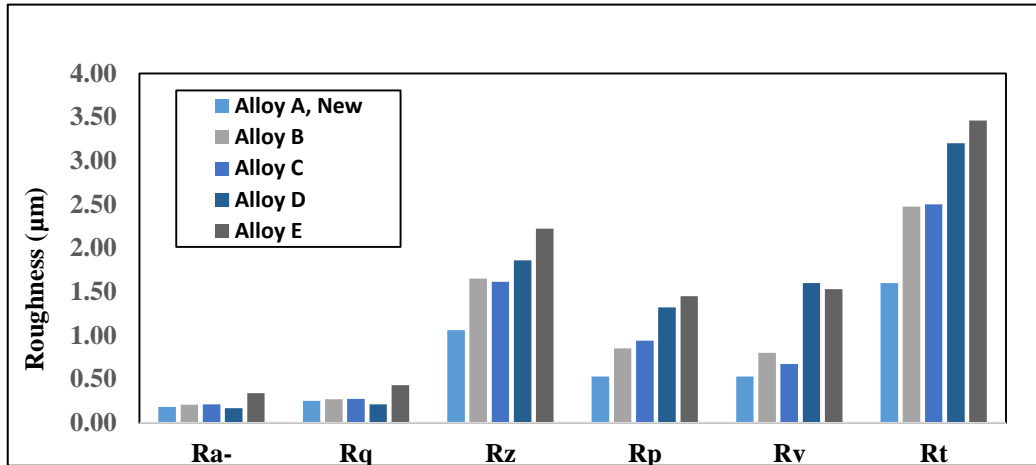


Figure 4-11 Measurements of surface roughness for the five alloys studied.

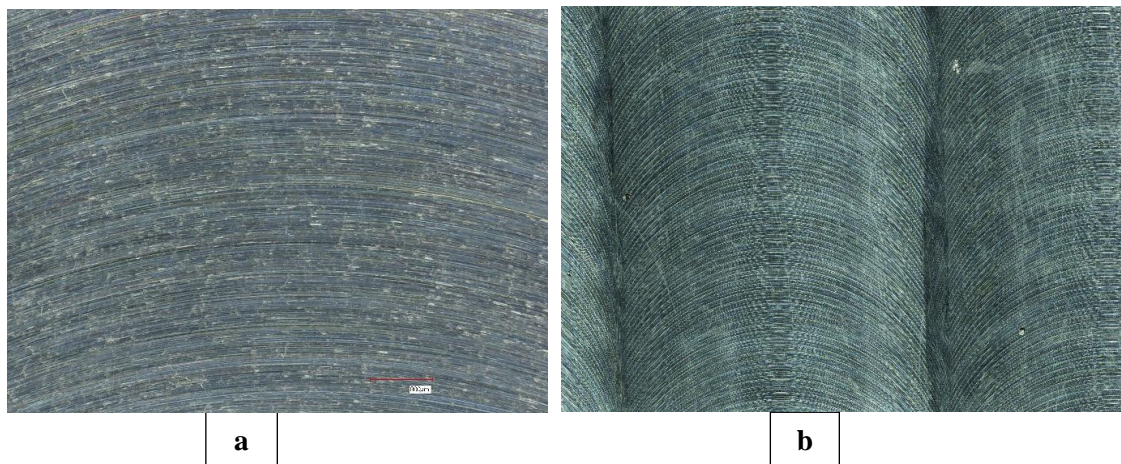


Figure 4-12 Surface roughness after milling for 120 m: (a) alloy A, (b) alloy C.

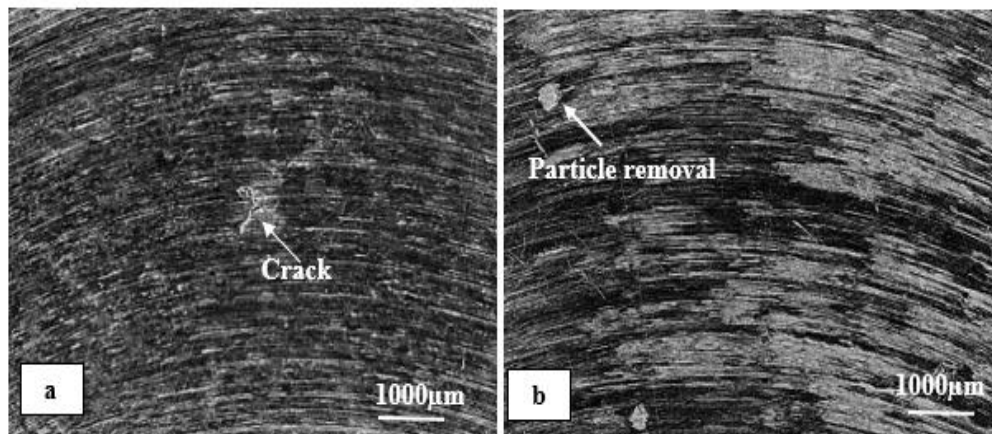


Figure 4-13 Surface roughness after milling for 120 m: (a) alloy D, (b) alloy E.

Niknam *et al.* [23] concluded that most aluminium alloys, whether wrought or cast, can experience burr formation during machining processes. The shape and the size of this burr will depend on the alloy composition and conditions, its mechanical properties, but also on type of machining operation, tooling used, machining parameters, and machining conditions and strategies. Using very low feed rates on a material with high ductility would generally lead to higher burr heights. Figure 4-14 shows burr formation after 120 m milling distance in (a) alloy C and (b) alloy E. The solid arrow in Figure 4-14(a) illustrates the starting edge of the block characterized by its smoothness. The broken arrow points to the opposite end where very tiny burrs adhered to the block edge due to alloy ductility. In the case of alloy E, burrs are thick and separated from the block due to its high hardness.

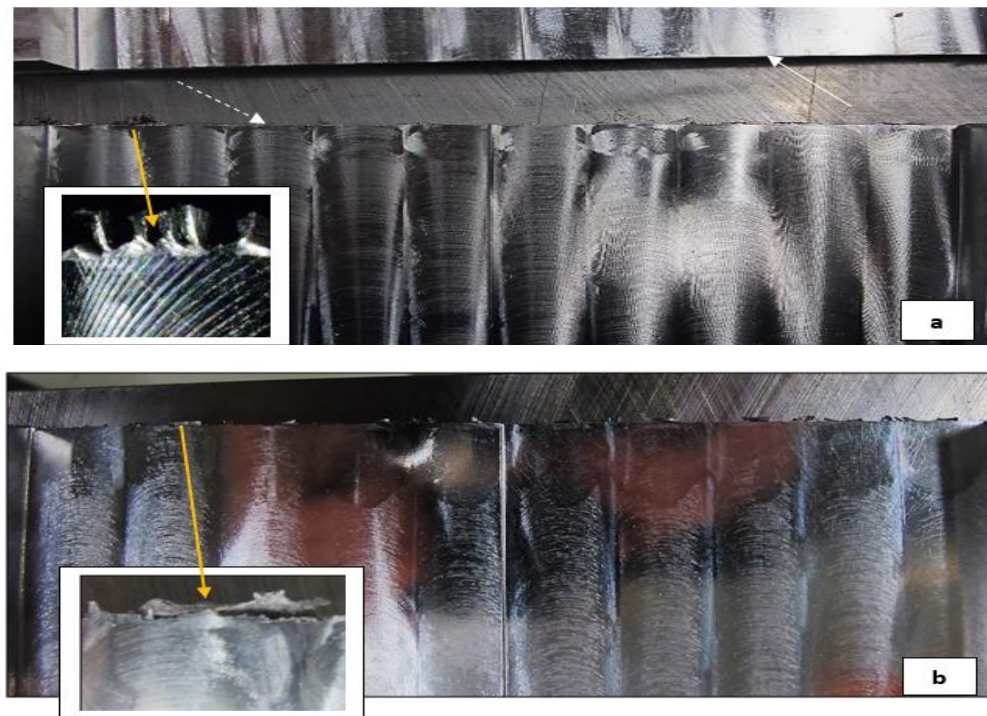


Figure 4-14 Burring formation after 120 m milling distance: (a) alloy C, (b) alloy E.

2.5 CHIP FORMATION

Barry and Byrne [23] and Haddag *et al.* [24] found that using orthogonal cutting tests in dry conditions, the BUE could be explained by the contact/friction change at the tool–work material interface during cutting. The ductility of aluminum alloy also promotes BUE formation. Xu *et al.* [25] investigated chip formation parameters of 6061-T6 aluminum alloy based on the high-speed orthogonal cutting model. The authors observed that chips mainly appeared as continuous chip, curling chip, and discontinuous chip. A high cutting speed was helpful to form ribbon chip. According to Kouadri *et al.* [26], the morphology of the chip depends on cutting parameters, tool geometry, the relative position of the tool-workpiece, and work material properties. In the literature, many research studies can be found on the impact of cutting conditions on the chip formation process and the mechanism of chip formation [27].

In all of the five alloys studied, the chips maintained a spiral form with shiny surfaces and no sign of burning, due to fluid showers employed during milling. Such chips can be seen in Figure 4-15. However, due to the high strength of alloy E, a few cracks were observed (see white arrows). Also, the edges are clearly rougher (blue arrow), compared to those obtained from the Al-Cu alloys.

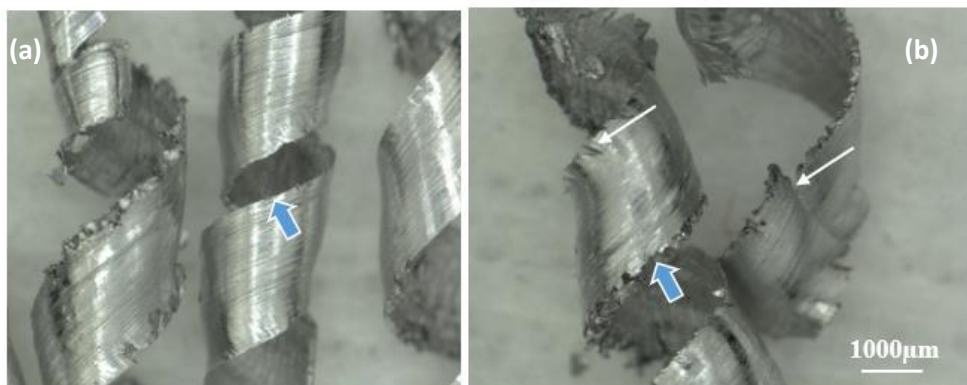


Figure 4-15 Chip shape after 120 m milling distance obtained from: (a) alloy C,(b) alloy E.

4.3 PART II - USE OF DULL INSERTS

4.3.1 TOOL SHAPE

As mentioned in Chapter 3 in the experimental procedures, of the inserts in order to observe the effect of dull inserts (when the inserts lose their sharpness during the milling process) on the applied forces and surface roughness. In order to physically simulate this condition, fresh inserts were passed over a white cast iron block to eliminate their sharpness. It should be mentioned here that the width of the sharp edge (Figure 4-5) is about 500 μm . Figure 4-16(a) shows the edge of a fresh insert as reference, compared to the dull tool presented in Figure 4-16(b) and 4-16(c). As can be seen, the cutting edge in Figure 4-16(c) is characterized by the formation of several deep cavities of irregular shape and size (maximum 428 μm) which is almost the entire width of the sharp tool (500 μm). In addition, it should be noted that part of the sharp tool remained undamaged.

Additionally, it should be noted that all dull tools are not alike in contrast to the fresh tools used before. Therefore, in this part of the study, the machining distance was limited to 14 m instead of 120 m used in the case of fresh inserts. All other machining parameters, however, were kept the same. Considering that the average hardness of white cast iron is ~450 BHN compared to the hardness of A356 alloy in the T6 condition ~105 BHN as was determined by El Sebaie *et al.* [28], it is not expected that machining alloy E, in spite of the presence of the hard Si phase (with a hardness of approximately 900-1000 HV), will significantly contribute towards increased damage of the tool, as shown in Figure 4-16(d).

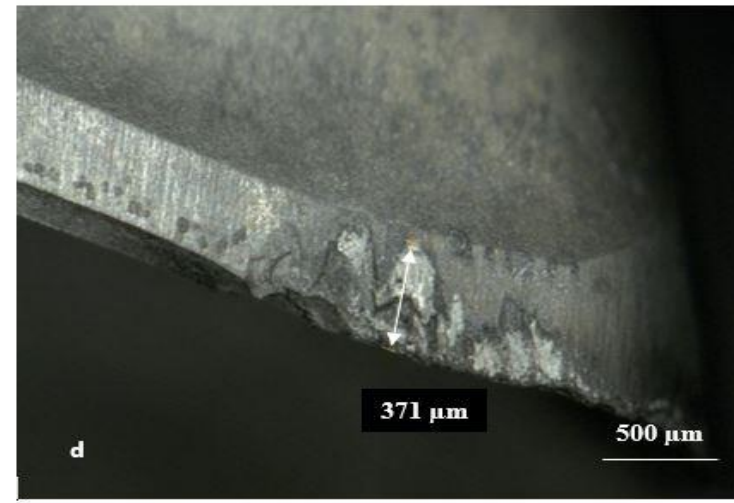
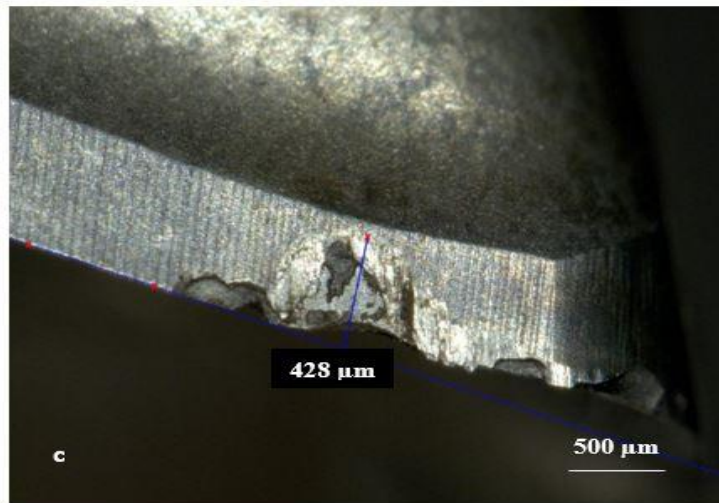
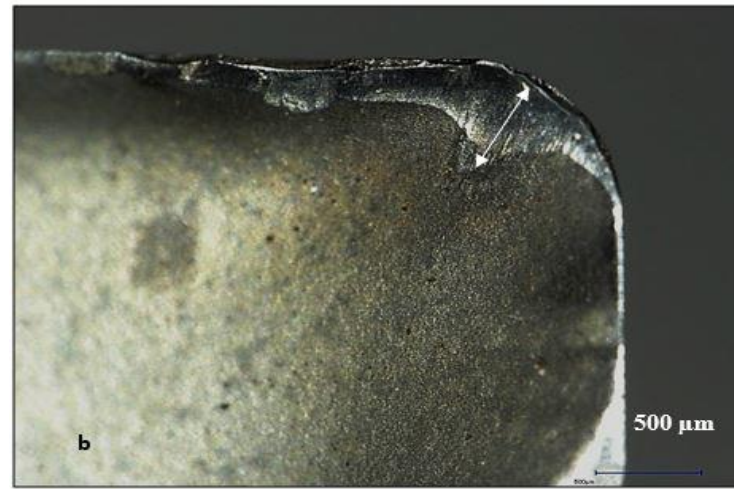
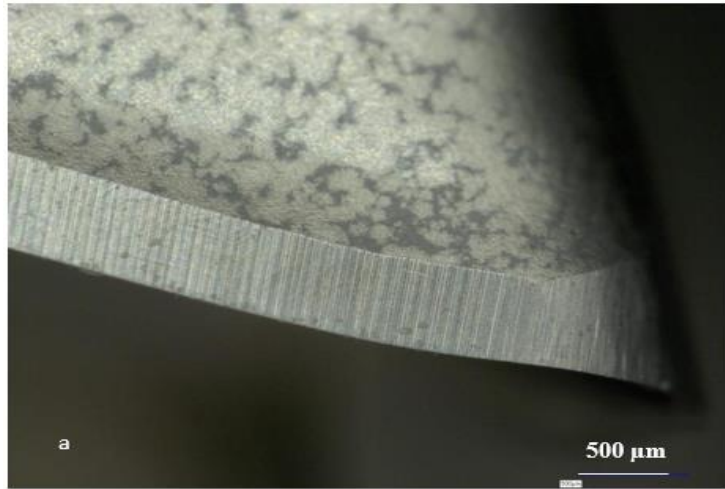


Figure 4-16 Shape of the cutting inserts for different conditions: (a) fresh tool, (b) dull tool- side, (c) dull tool- edge, and (d) dull tool after machining alloy E.

4.3.2 CUTTING FORCES

Figure 4-17 displays the cutting forces obtained using new and dull tools after 14 m of machining distance. Regardless of alloy composition, the forces required to machine the workpiece when applying dull inserts are ~40-50% higher than those required in the case of new inserts. The difference is made clear in the case of alloy E due to the resistance offered by both the eutectic Si particles and the alloy strength.

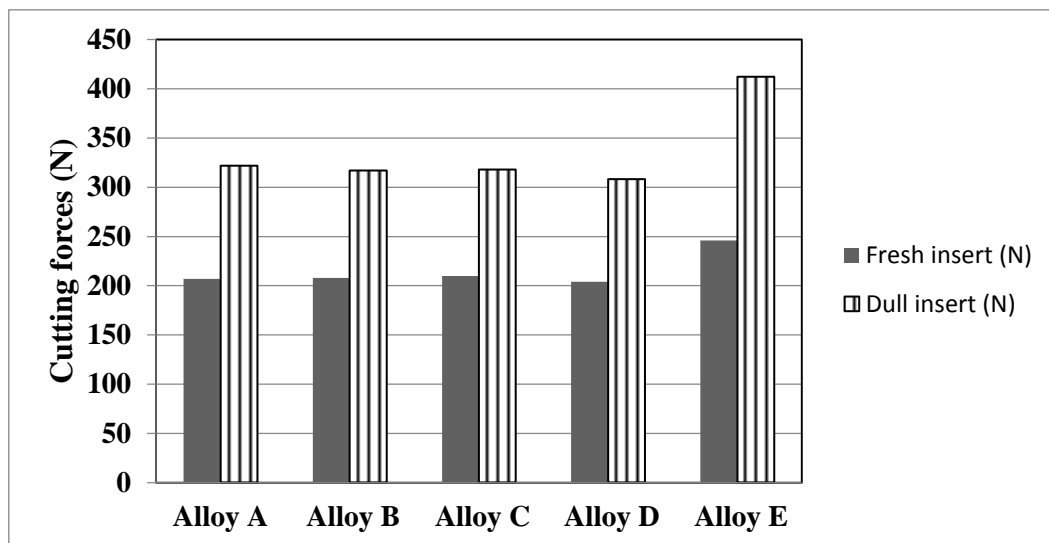


Figure 4-17 Cutting forces for both new and dull inserts (14 m of machining distance).

4.3.3 SURFACE ROUGHNESS

According to Barzani *et al.* [29], the surface roughness (Ra) is the most common index for determining surface quality in a machining process. Additionally, Ra is more common than the Rt and Rz values as it accounts for the averages of peaks and valleys on the surface of the workpiece. Figure 4-18(a) reveals the roughness profile obtained from alloy

E after 120 m of machining distance (with fresh inserts), exhibiting a large number of peaks with different heights. In comparison, Figure 4-18(b) presents the profile obtained from the same alloy using dull inserts after 14 m of machining distance, but for the same machined layer (1.2 mm). It is evident from Figure 4-18(b) that using dull inserts resulted in (i) less number of peaks, that (ii) all peaks are of more-or-less the same height and width, and (iii) the width of peaks are much larger than those seen in Figure 4-18(a). Based on Figure 18, the average Ra (new tool) is $\sim 0.184 \mu\text{m}$ compared to $1.056 \mu\text{m}$ reported for the dull tool.

In order to emphasize the effect of the quality of the inserts used on the surface roughness, five roughness parameters - namely Ra, Rq, Rv, Rp and Rt - have been plotted in Figure 4-19 for both new (120 m machining distance) and dull (14 m machining distance) inserts to obtain a wider image of how the presence of deep irregularities, shown in Figures 4-16(b) and 4-16(c), would affect the surface finishing. Apparently, the increased cutting forces reported in Figure 4-17 are reflected in the values of the five parameters, which follow the same trend. Considering the possibility that some of the debris may fill the cavities, it is expected that increasing the alloy strength through aging coupled with the use of showers of coolant would result in the removal of the debris during the course of the milling operation.

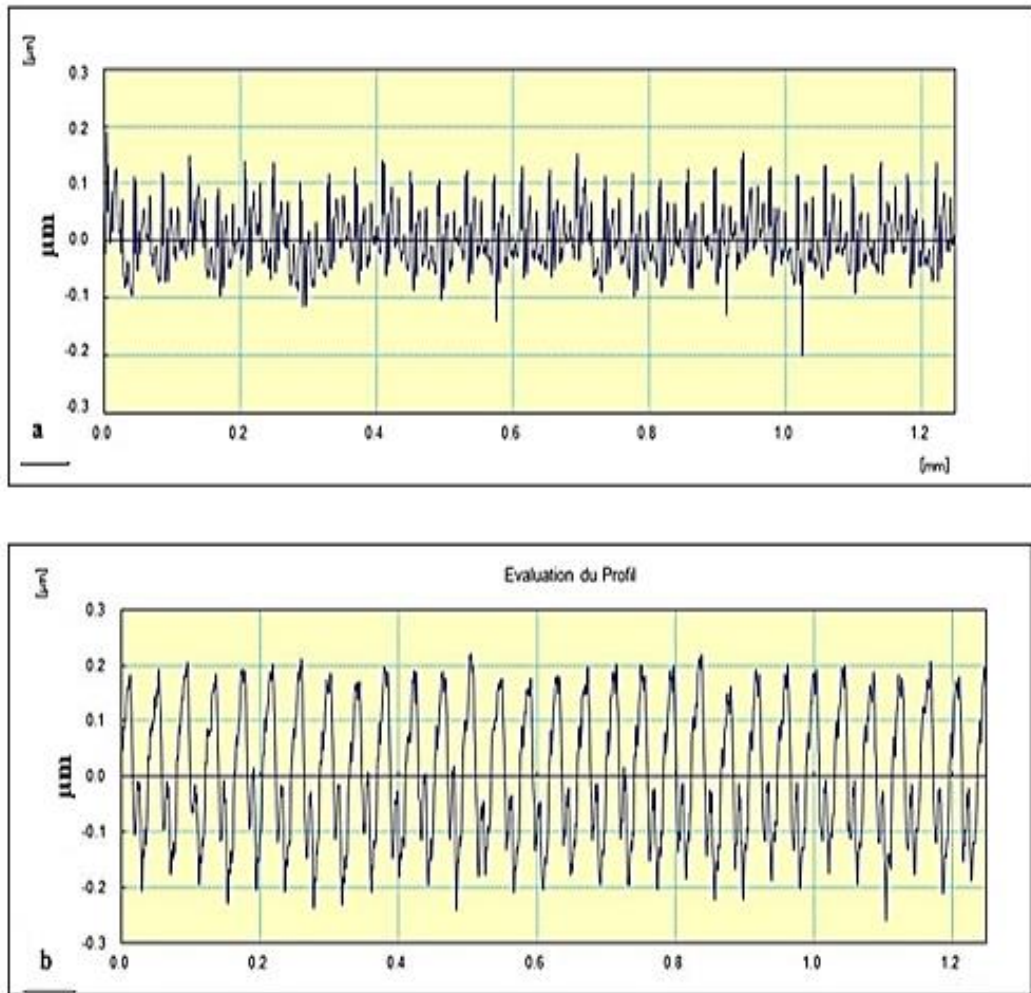


Figure 4-18 Profiles of the machining surface of alloy E: (a) fresh inserts - 120 m machining distance, and (b) dull inserts - 14 m machining distance.

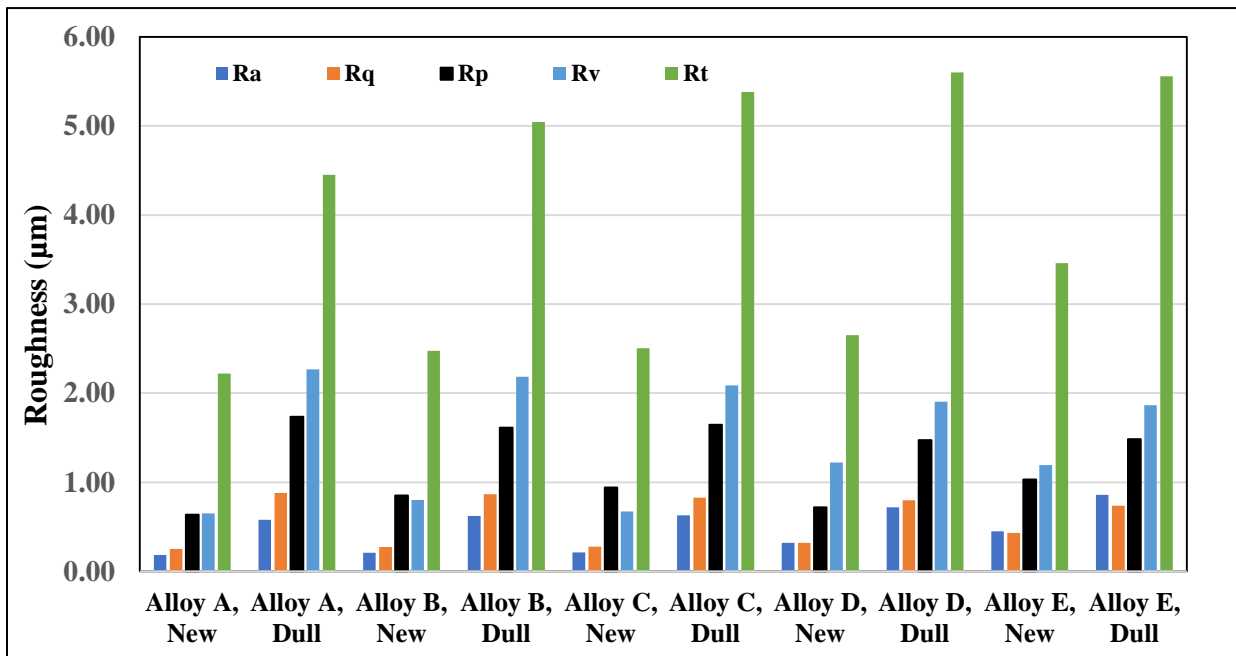


Figure 4-19 Comparison of roughness parameters for the five alloys using new inserts (120 m machining distance) and dull inserts (14 m machining distance).

4.3.4 SURFACE FINISH

The surface finish of the machined workpiece was examined using stereographic microscopy; the results are shown in Figure 4-20. Due to severe damage of the dull inserts, it is difficult to properly distinguish between the surface finishing of the three alloys. All surfaces are rough with multiple cracks. In other words, neither the alloy composition nor heat treatment type is relevant, which is consistent with the roughness measurements presented in Figure 4-18. In conformation with these observations, Figure 4-21 reveals the surface finish of alloy C (viewed by optical microscopy) and clearly illustrates the cracks created by the dull tool after only 14 m of machining length, compared to practically none in the case when new inserts were used for 120 m of machining distance.

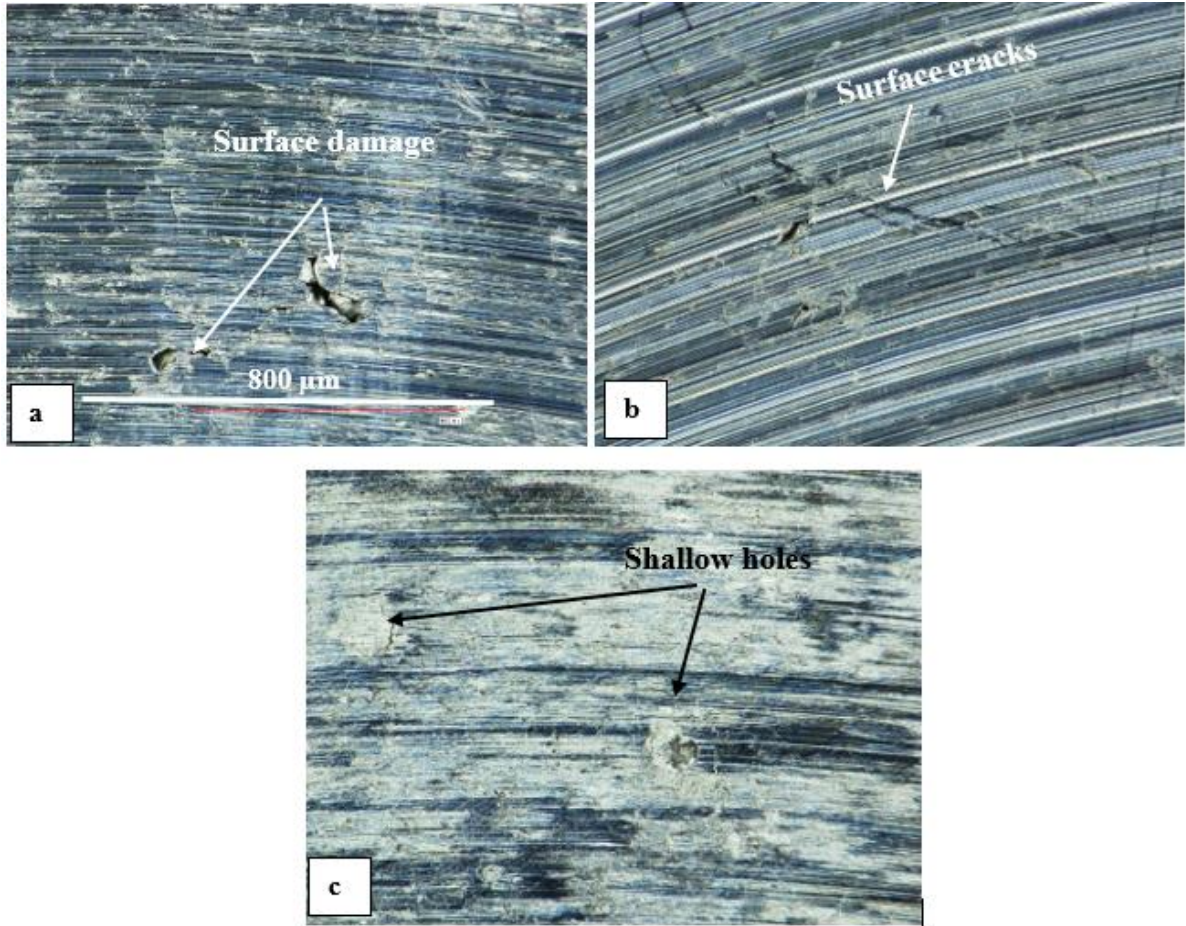


Figure 4-21 Surface finishing using dull inserts: (a) alloy A, (b) alloy C, (c) alloy E.

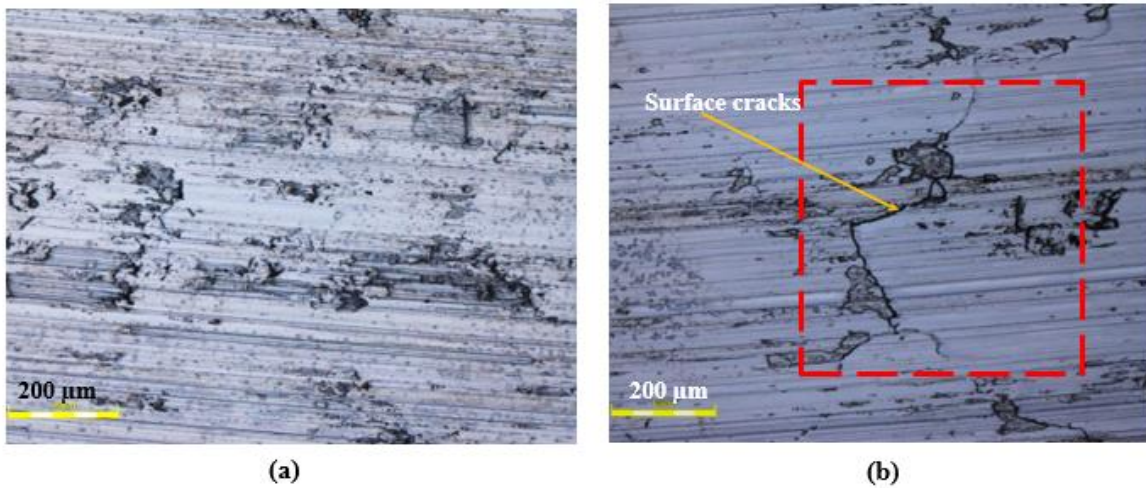


Figure 4-20 Comparison of surface finish of alloy C: (a) new inserts and (b) dull inserts.

4.3.5 RESIDUAL STRESSES

Figure 4-22 is an example of residual stresses cumulated after milling using dull tools (14 m machining distance) compared to those measured using new inserts (120 m machining distance). As can be seen the amount of residual stresses varies from one spot to another along the width of the block, depending on variation in the applied forces. In addition, the use of dull inserts causes fairly larger amounts of stresses due to the initial condition of the cutting tool shown in Figure 4-16. However, in all cases the residual stresses caused by the cutting tools are tension stresses whereas the stresses in the shoulders of the ingots (following heat treatment) are of compression type.

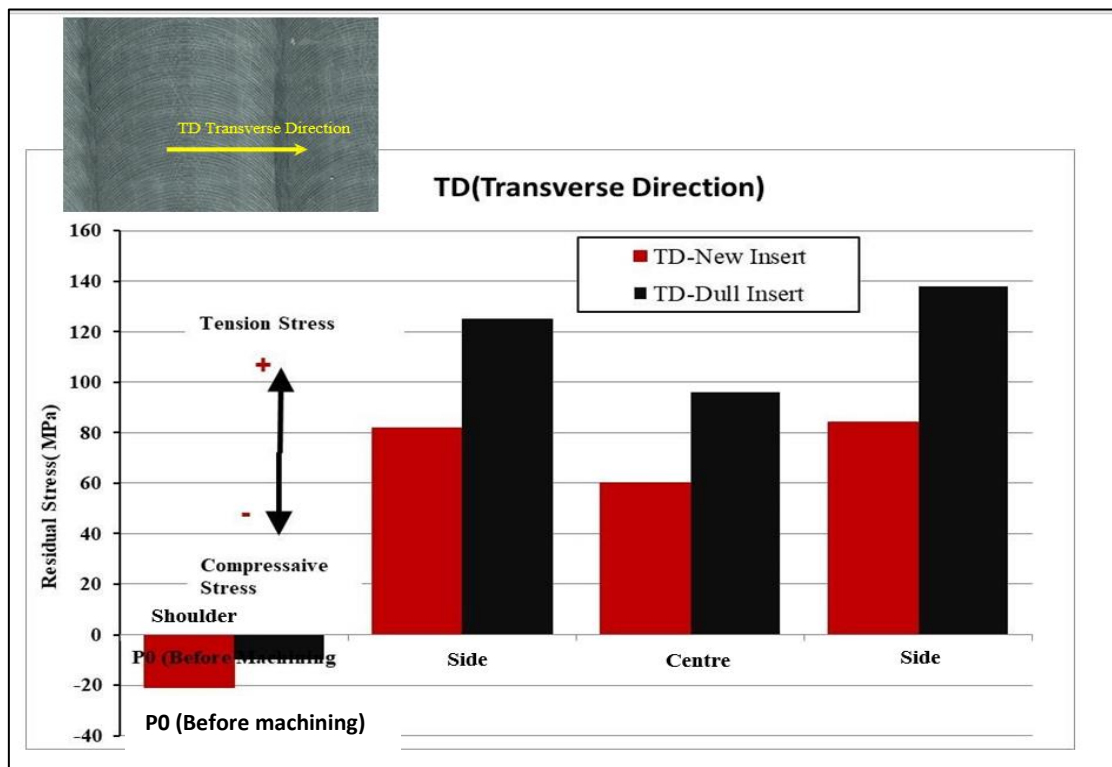


Figure 4-22 Residual stresses measured in the transverse direction for alloy C.

4.3.6 CHIP SHAPE AND BURRING

Since large amounts of coolant were employed, all chips are shiny, with no signs of burning, as demonstrated in Figure 4-23. It is interesting to note that in spite of the bad quality of the used inserts, the resulting chips are long and spiral shaped, however, with cracked edges due to the high-applied forces. The chips obtained from the three alloys A, C and E are identical, except for minor cracks in the case of alloy E (see white arrow).

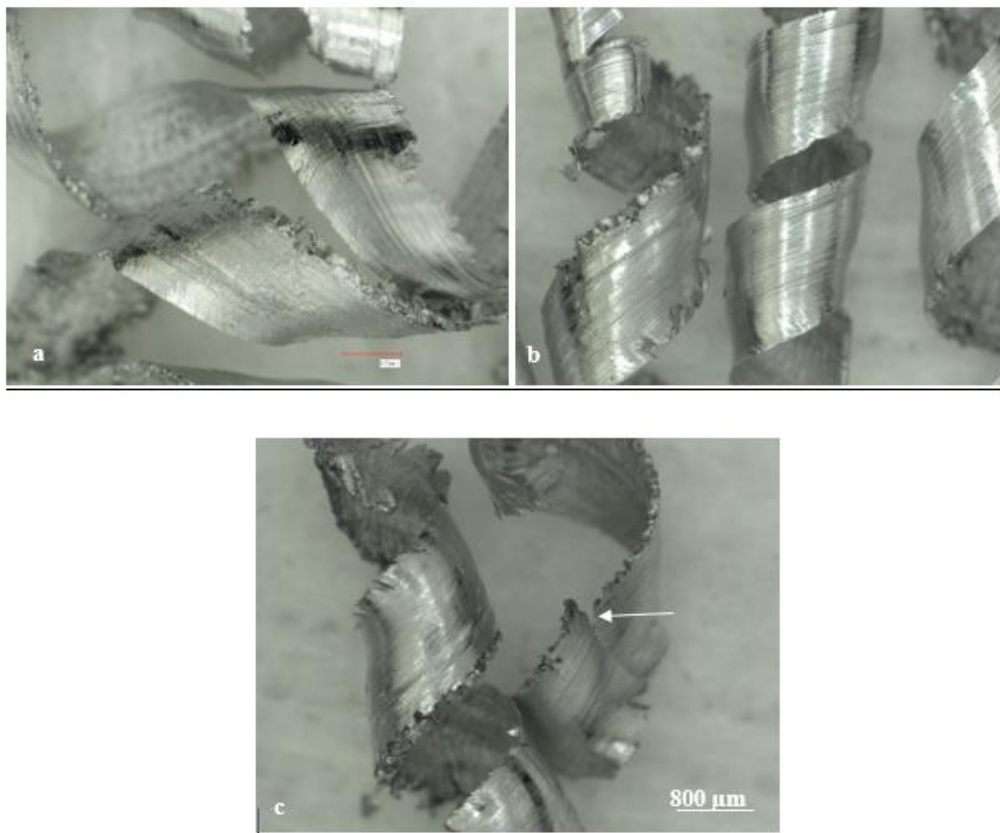


Figure 4-23 Shape of the chips obtained using dull inserts: (a) alloy A, (b) alloy C and (c) alloy E.

According to Niknam et al. [30], burrs forming during machining are defined as an extension of material beyond the workpiece edges, which should be limited rather than deburring them applying a subsequent operation [8]. Figure 4-24 shows examples of burr formation [31]. Figure 4-25 shows the type of burrs that formed during the milling of alloys C and E using dull tools. In both cases the debris are separated from the edge of the workpiece (positive burr).

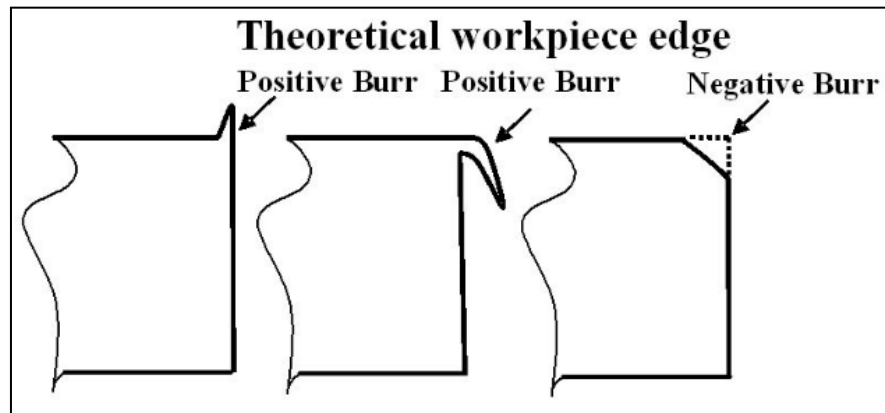


Figure 4-24 Examples of burr forms during milling operation [31].



(a)



(b)

Figure 4-25 Burr forms using dull tools: (a) alloy C, (b) alloy E

CHAPTER 5
CONCLUSIONS
AND
RECOMMENDATIONS FUTURE WORK

5 CONCLUSIONS

5.1 PART I - NEW INSERTS

Based on the results obtained in this study using new inserts, and after 120 m of machining distance, the following conclusions may be drawn:

- 1- The cutting forces of Al-Cu alloys (250 N) are much lower than those obtained for Al-Si alloys (500 N). The cutting forces for Al-Si-Cu alloys fall in between (~320 N) due to the presence of Cu.
- 2- The presence of a high Cu concentration in Al-Cu-Si may neutralize/minimize the abrasive tendency of the hard eutectic Si particles.
- 3- Copper leads to better surface finishing, compared to Al-Si alloys (Rt of 0.4 and 3.5 μm , respectively).
- 4- Another advantage of Al-Cu alloys over Al-Si alloys is the marked reduction in the residual stresses (50 MPa and 100 MPa, respectively).
- 5- Burrs, in the case of Al-Cu alloys, are normally adhered to the outer edges of the workpiece, whereas they are separated from the machined block in the case of Al-Si alloys.
- 6- Although chips are helical in all cases, with bright surfaces, the chips obtained from the Al-Si alloys reveal cracks with rough edges compared to the smooth surface of the chips in the case of Al-Cu alloys.

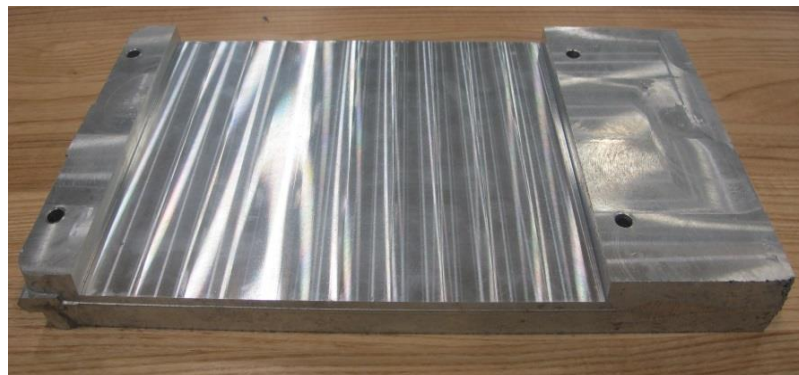
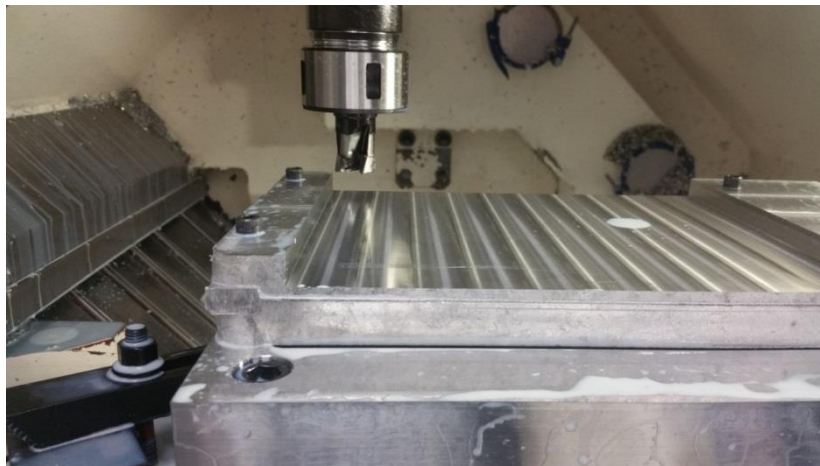
5.2 PART II - DULL INSERTS

- 1- The use of cast iron to reduce the sharpness of the new carbide inserts leads to severe damage of the insert and formation of deep cavities.
- 2- The shape of the dull inserts and cutting characteristics vary from one insert to another and hence it is difficult to produce reproducible results.
- 3- Due to the bad shape of the dull inserts, the cutting forces needed to machine 14 m of distance are 40-50% higher than those required to machine 120 m of cutting distance using new inserts.
- 4- The profile of surface roughness using dull tools is almost twice that of the profile obtained using new inserts. However, the signals are much wider in the former case with less number of peaks.
- 5- Due to the severe irregularities of the edges of the dull tools, neither the alloy composition nor the heat treatment is relevant.
- 6- The surface finish of all alloys is characterized by the presence of cracks and shallow holes.
- 7- Residual stresses vary along the width of the machined block. All stresses are of tension type compared to compression type in the un-machined shoulders. Due to the high-applied forces associated with the use of dull inserts.
- 8- The resulting residual stresses are almost twice those generated by new inserts in spite of the large difference in the machining distance in the two cases.
- 9- Due to the use of showers of coolant, the chips in all cases are shiny, with no signs of burning.
- 10- In all cases, the burrs were separated from the workpieces (positive burr).

RECOMMENDATIONS FOR FUTURE WORK

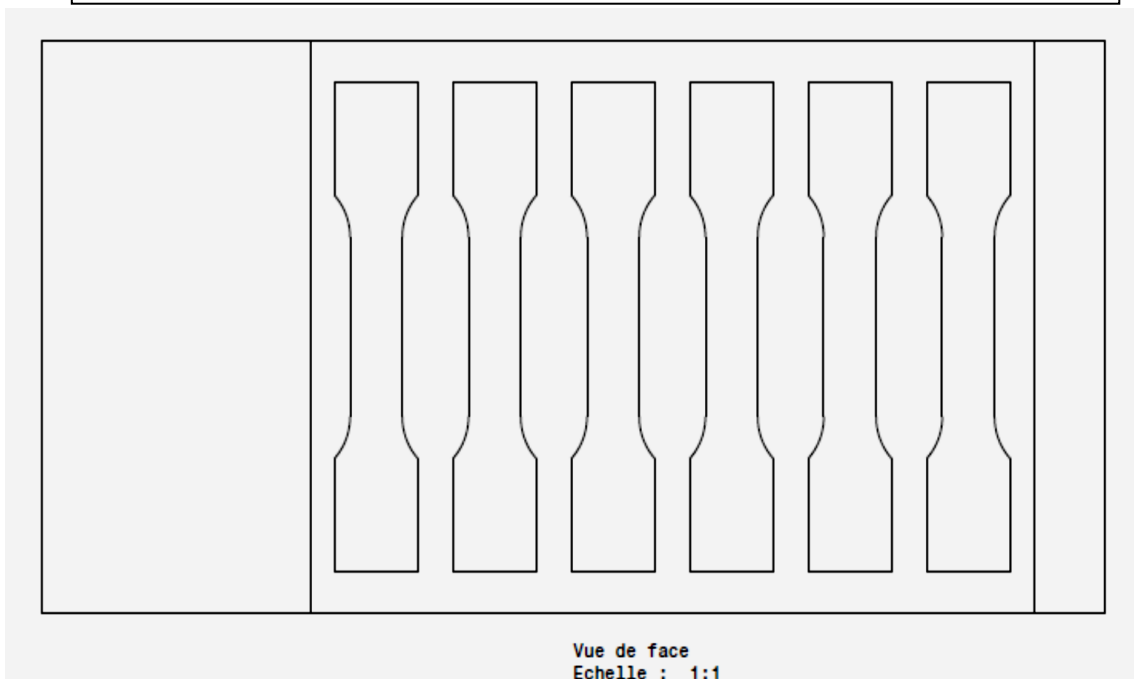
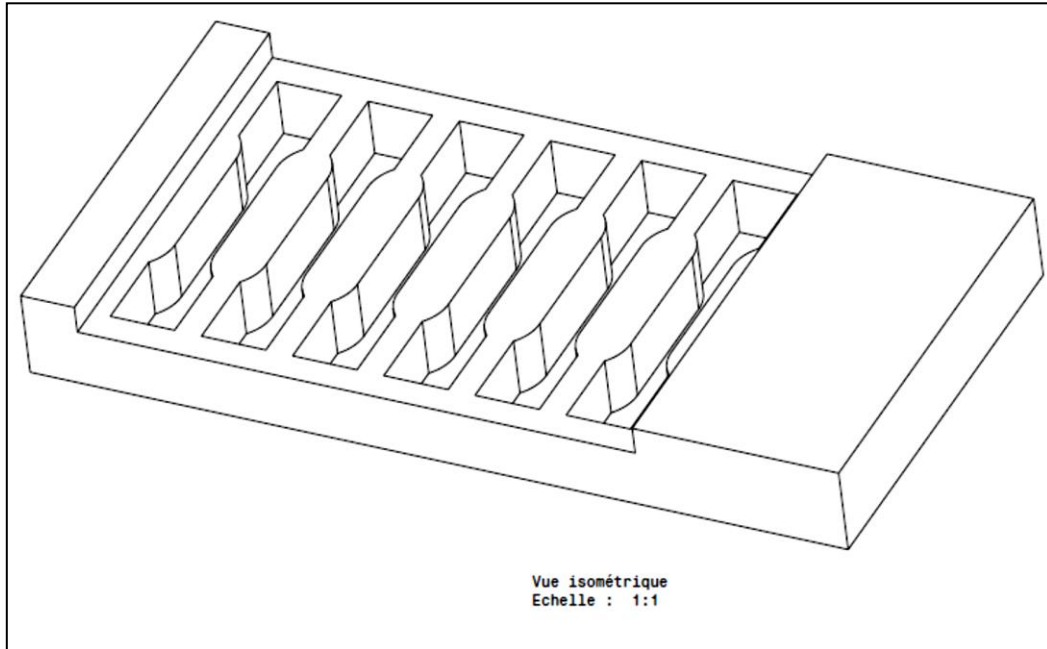
(1) Effect of depth of cut on surface characterization

The effects of radial depth-of-cut (0.5 mm and 2 mm) on the material damage and microstructure evolution beneath the machined surface will be investigated.



(2) Effect surface characterization on mechanical properties

The machined surface is significantly work-hardened due to the dominant mechanical loading. Four-point bending fatigue testing will be carried out to determine the fatigue life of milled Al-Cu alloys.



5.3 REFERENCES

- 1- A.M. Samuel, H.W. Doty, S. Valtierra and F.H. Samuel, New Method of Eutectic Silicon Modification in Cast Al–Si Alloys. *International Journal of Metalcasting*, vol. 11(3), 2017, 475-493.
- 2- H.R. Ammar, A.M. Samuel, F.H. Samuel, E.A. Simielli, J.C. Lin, and G.K. Sigworth, Effects of Mg-Addition, Sr-Modification and Solidification Rate on the Tensile Properties and Quality Index of 359 Type Al-Si-Mg Casting Alloys, in *Transactions of the American Foundry Society* vol. 119, 115th Metalcasting Congress, April 5 - 8, 2011 [Schaumburg, Illinois]. 2011, American Foundry Society: [Schaumburg, Illinois]. pp. 67-82.
- 3- F.J. Tavitias-Medrano, J.E. Gruzleski, F.H. Samuel, S. Valtierra and H.W. Doty, Effect of Mg and Sr-modification on the mechanical properties of 319-type aluminum cast alloys subjected to artificial aging, *Materials Science and Engineering A*, vol. 480 (1-2), 2008, 356-364.
- 4- G. Pucella,, A.M. Samuel, F.H. Samuel, H.W. Doty, S. Valtierra, Sludge formation in Sr-modified Al-11.5 Wt% Si diecasting alloys, *AFS Transactions*, vol. 107, 1999, 117-125.
- 5- H.K. Kamga, D. Larouche , M. Bournane, A. Rahem, Mechanical properties of aluminium–copper B206 alloys with iron and silicon additions, *International Journal of Cast Metals Research*, vol. 25, 2012, 15-25.
- 6- H.R. Ammar, A.M. Samuel, F.H. Samuel, E. Simielli, G.K. Sigworth, and J.C. Lin, Influence of aging parameters on the tensile properties and quality index of Al-9 pct Si-1.8 pct Cu-0.5 pct Mg 354-type casting alloys. *Metallurgical and Materials Transactions A*, vol. 43 (1), 2012, 61-73.
- 7- I. Zaghbani and V. Songmene, A force-temperature model including a constitutive law for Dry High Speed Milling of aluminium alloys, *Materials Processing Technology*, vol. 209, 2009, 2532–2544.
- 8- V. Songmene, R. Khettabi, I. Zaghbani, J. Kouam and A. Djebara, Machining and Machinability of Aluminum Alloys, *Aluminium Alloys, Theory and Applications*, Prof. Tibor Kvackaj (Ed.), ISBN: 978-953-307-244-9, InTech Open, Croatia (2011), pp. 377-400.
- 9- Jammula Praneeth1 , Narraa Naveen, “Machining of Aluminum alloys: a review” *International Journal for Research in Applied Science & Engineering Technology (IJRASET)* , Vol. 5 , Issue X , October 2017.
- 10-M. C. Santos Jr, A. R. Machado, W. F. Sales, M. A. S. Barrozo, E. O. Ezugwu, Machining of aluminum alloys: a review, *Int J Adv Manuf Technol*, 2016, DOI 10.1007/s00170-016-8431-9.

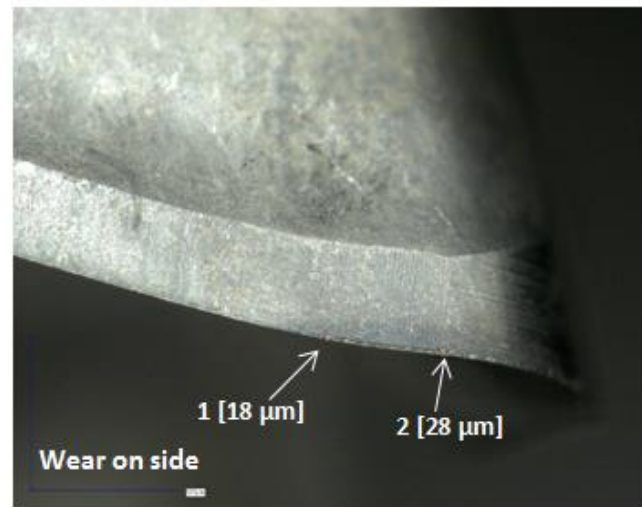
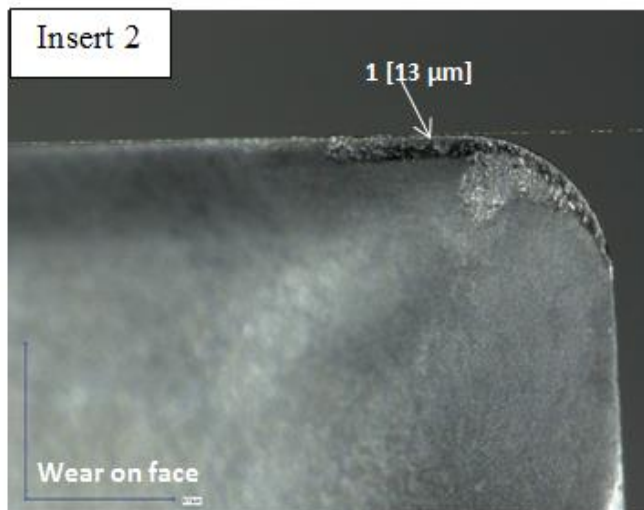
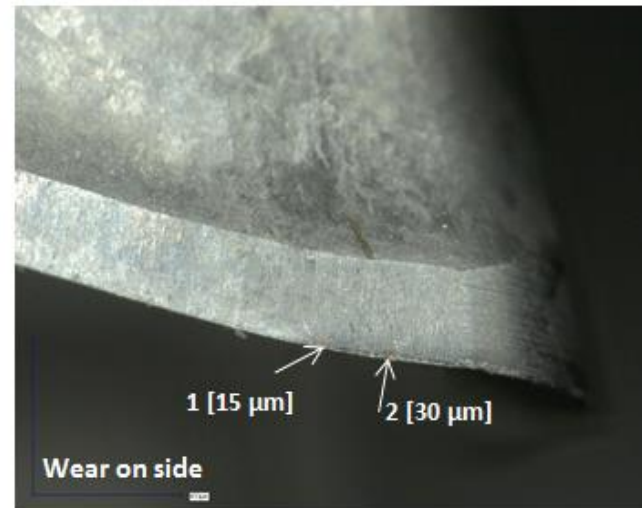
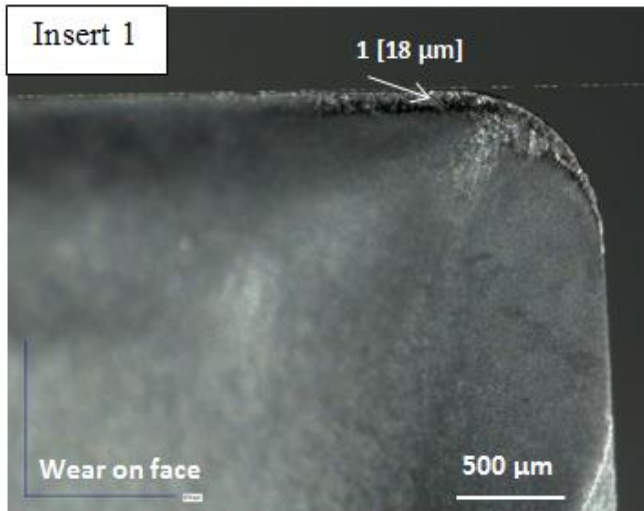
- 11- F.W. Taylor, "On the art of cutting metals", *ASME Trans.*, vol. 28, 1907, 31-350.
- 12- Y.C. Yen, J. Sohner, B. Lilly and T. Altan, Estimation of tool wear in orthogonal cutting using the finite element analysis, *Journal of Materials Processing Technology*, vol. 146, 2004, 82-91.
- 13-TEC Materials Testing, Knoxville, USA - X-Ray Diffraction Equipment and Testing, <https://www.tec-materialstesting.com>
- 14-J.S. Robinson and W. Redington, The influence of alloy composition on residual stresses in heat-treated aluminium alloys, *Materials Characterization*, vol. 105, 2015, 47-55.
- 15-J.S. Robinson, D.A. Tanner, C.E. Truman, A.M. Paradowska, R.C. Wimpory, The influence of quench sensitivity on residual stresses in the aluminium alloys 7010 and 7075, *Materials Characterization*, vol. 65, 2012, 73-85.
- 16- Z.T. Tang, Z.Q. Liu, Y.Z. Pan, Y. Wan, X. Ai, The influence of tool flank wear on residual stresses induced by milling aluminum alloy. *J Mater Process Technol*, vol. 209 (9), 2009, 4502–4508.
- 17- D.V. Kumar, T. Naveen, S. Naveenkumar, S. Sethupathi and S.Srinivasan, Surface Roughness Analysis in Machining of Aluminium Alloys (6061 & 6063), *International Research Journal of Engineering and Technology (IRJET)*, vol. 03 (04), 2016, 2814-2821.
- 18- E. Lee, Y Kim, H Jeong and H Chung, A study on the surface shape and roughness of aluminum alloy for heat exchanger using ball end milling, *Materials Science and Engineering*, vol. 88, 2015, 012048.
- 19- S. Gangopadhyay, J. Limido, C. Mabru and R. Chieragatti, Effect of cutting speed and surface chemistry of cutting tools on the formation of BUL or BUE and surface quality of the generated surface in dry turning of AA6005 aluminium alloy. *Mach. Sci. Technol.*, vol. 14, 2010, 208–223.
- 20- W. Jomaa, V. Songmene and P. Bocher, Surface Finish and Residual Stresses Induced by Orthogonal Dry Machining of AA7075-T651, *Materials*, vol. 7, 2014, 1603-1624; doi:10.3390/ma7031603.
- 21- M. Suraratchai, J. Limido, C. Mabru , R. Chieragatti, Modelling the influence of machined surface roughness on the fatigue life of aluminium alloy, *International Journal of Fatigue*, vol. 30, 2008, 2119–2126.
- 22- P.S. Maya, Geometrical characterization of surface roughness and its application to fatigue crack initiation. *Mater Sci Eng*, vol. 21, 1975, 57–62.
- 23- J. Barry and G. Byrne, The mechanisms of chip formation in machining hardened steels, *J. Manuf. Sci. Eng.*, 2002, vol. 124, 528–535.

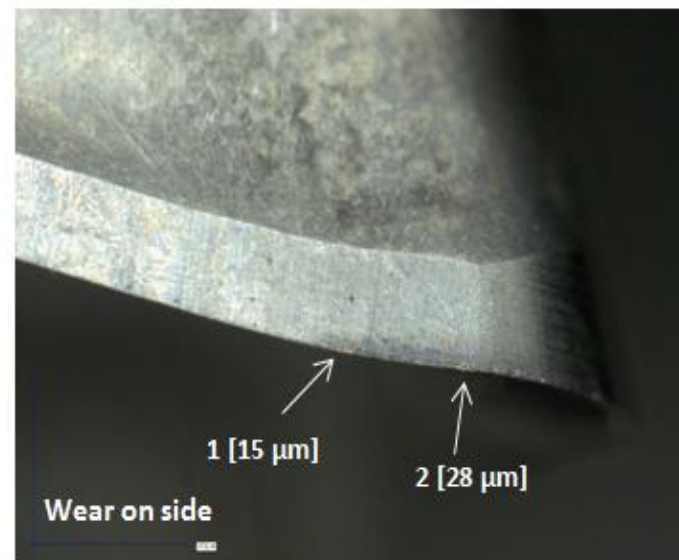
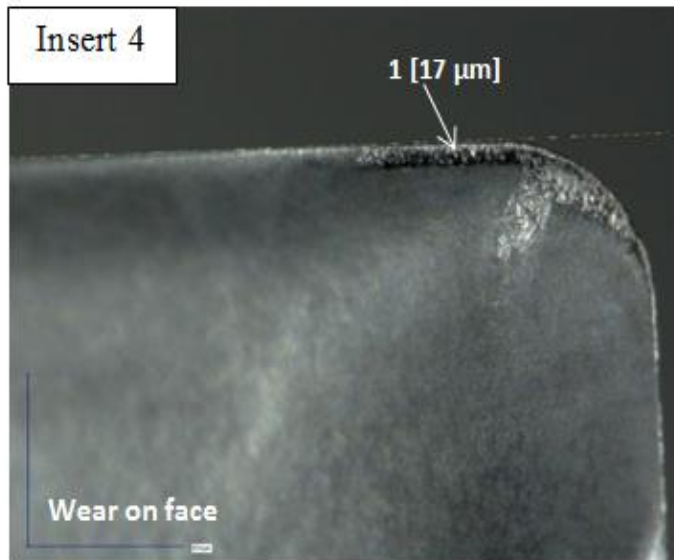
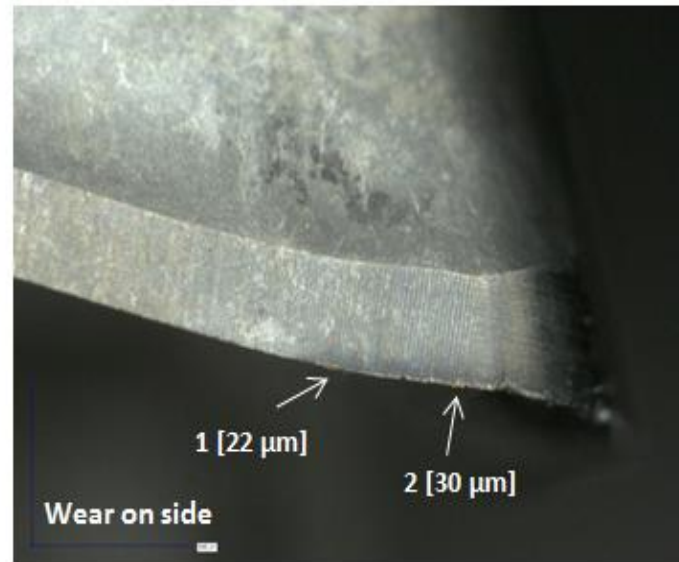
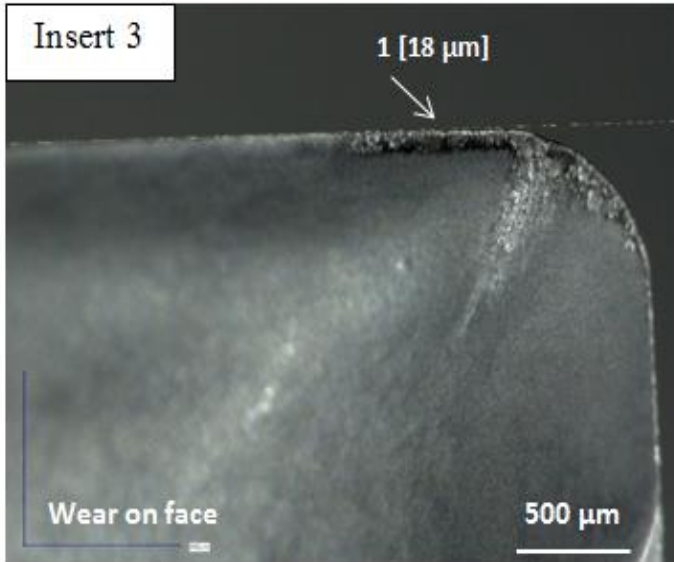
- 24- B. Haddag, S. Atlati, M. Nouari and A. Moufki, Dry Machining Aeronautical Aluminum Alloy AA2024-T351: Analysis of Cutting Forces, Chip Segmentation and Built-Up Edge Formation, *Metals* 2016, 6(9), 197; <https://doi.org/10.3390/met6090197>
- 25- D. Xu, P. Feng, W.Li, Y. Ma and B. Liu, Research on chip formation parameters of aluminum alloy 6061-T6 based on high-speed orthogonal cutting model, *Int. J. Adv. Manuf. Technol.*, vol. 72, 2014, 955–962.
- 26- S. Kouadri, K. Necib, S. Atlati, B. Haddag, M. Nouari, Quantification of the chip segmentation in metal machining: Application to machining the aeronautical aluminium alloy AA2024-T351 with cemented carbide tools WC-Co. *Int. J. Mach. Tools Manuf.*, vol. 64, 2013, 102–113.
- 27- P. Kovac and L. Sidjanin, Investigation of chip formation during milling, *Int. J. Production Economics*, vol. 51, 1997, 149-153.
- 28- O. Elsebaie, A.M. Samuel, F.H. Samuel and H.W. Doty, The effects of mischmetal, cooling rate and heat treatment on the hardness of A319.1, A356.2 and A413.1 AlSi casting alloys, *Materials Science and Engineering A*, vol. 486 (1-2), 2008, 241-252.
- 114
- 29- M.M. Barzani, S. Farahany and V. Songméné, Machinability characteristics, thermal and mechanical properties of Al-Mg₂Si in-situ composite with bismuth, *Measurement Journal of the International Measurement Confederation*, vol. 110, 2017, 263-274.
- 30- S. A. Niknam, A. Tiabi and V. Songméné, Burr Edge Occupancy: An Edge Finishing Index for Milling Machined Parts, *Transactions of the Canadian Society for Mechanical Engineering*, vol. 43 (2), 2019, 248-255.
- 31- B. Balout, V. Songmene and J. Masounave, An experimental study of dust generation during dry drilling of pre-cooled and pre-heated workpiece material, *Journal of Manufacturing Processes*, vol. 9, 2007, 23-34.

APPENDDICES

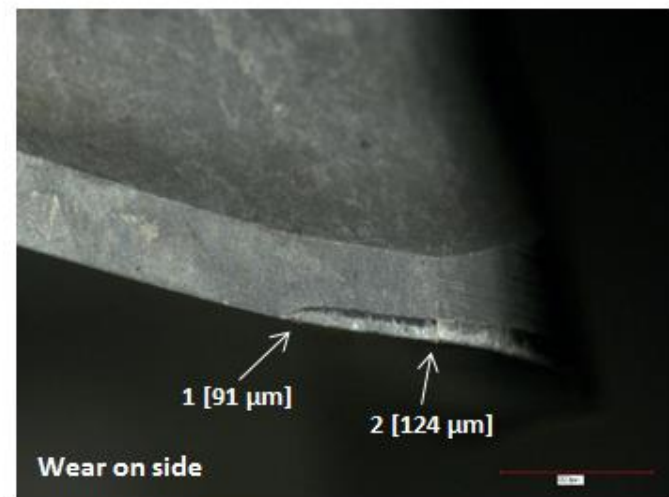
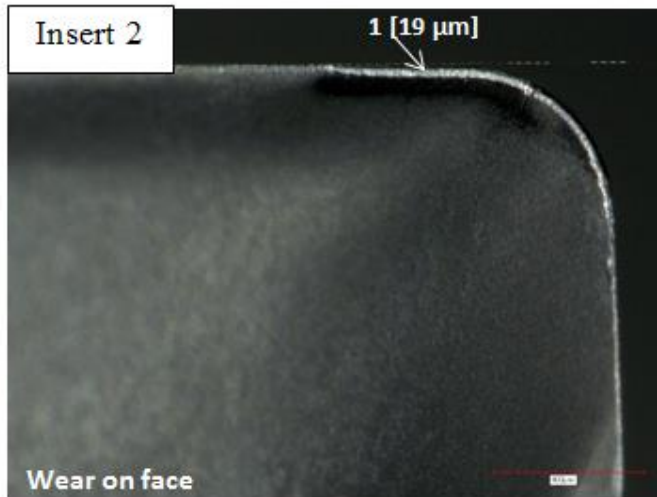
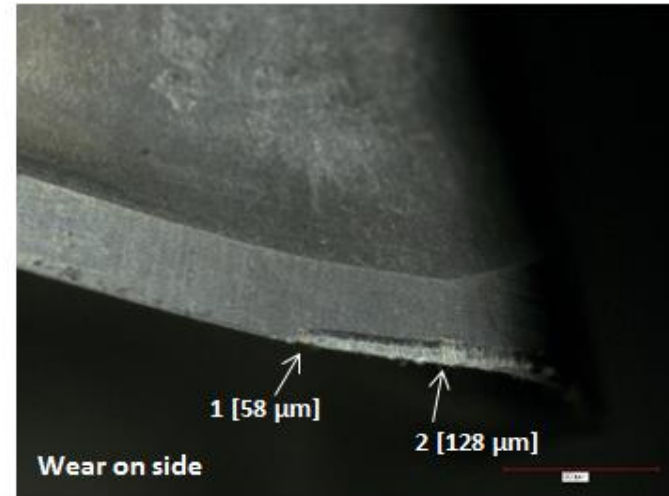
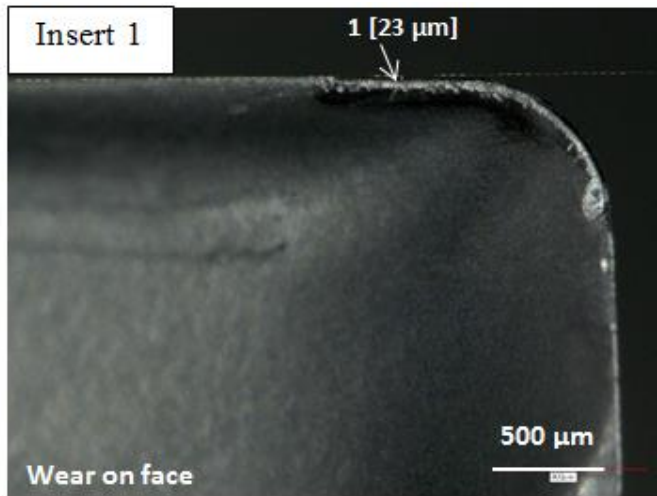
A- Wearing of milling tools used for alloys C and E

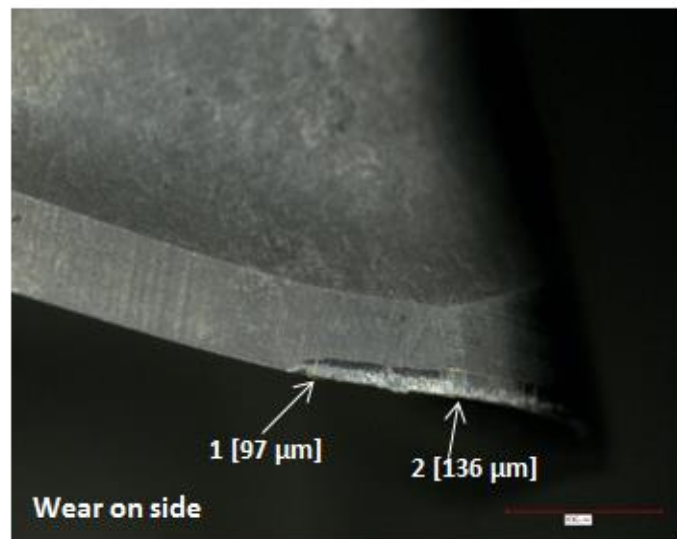
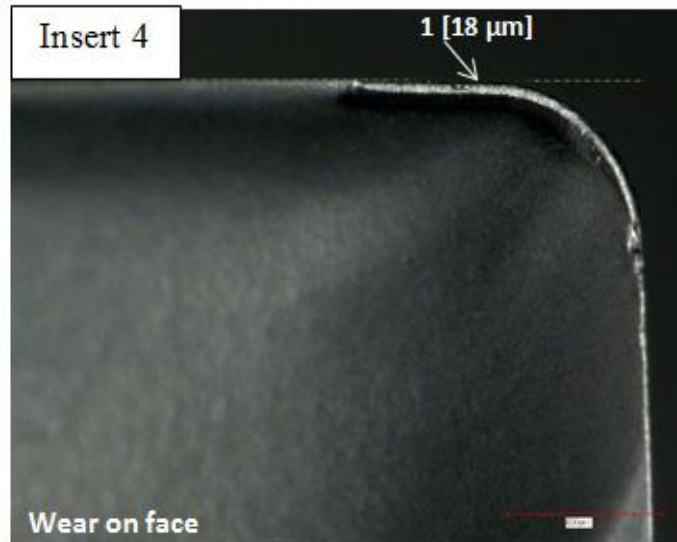
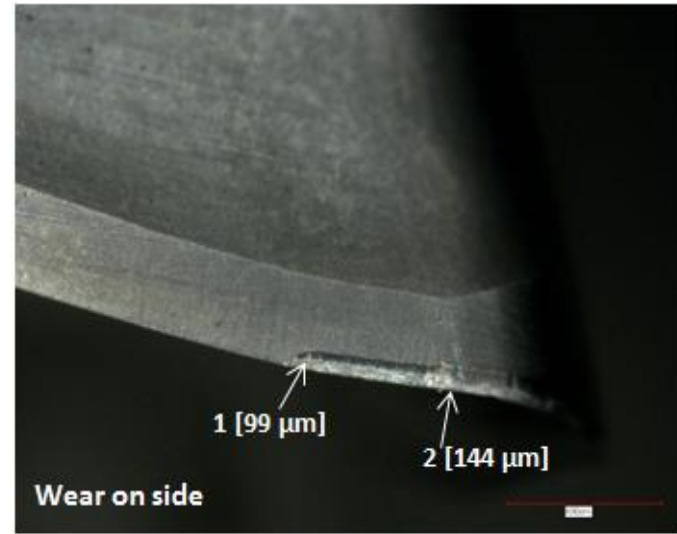
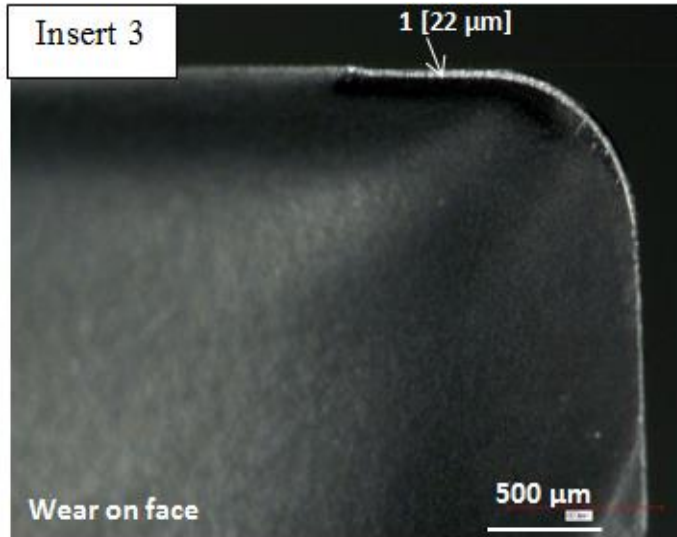
The pictures below show the wear of the 4 inserts used for the milling of alloy C after 110 m of cutting distance.





The images below show the wear of the 4 inserts used to perform the milling of the alloy E after 110 m of cutting distance.





B- Matlab code

```
clc ;
clear all;
close all ;
Name = 'ABCDE';

for Alloy = 1:5
    Old_Path=0;

    if Alloy ==1
        start =6;
        final =10;
    else
        start =1;
        final =5;
    end

    for Block =start:final
        for layer = 1:2
            filename = (['C:\Users\p2-1020.LABORATOIRE\Desktop\Nouveau
dossier\Alloy',Name(Alloy),'\Plaque',num2str(Block),'-
',num2str(layer),'\Plaque',num2str(Block),'_',num2str(layer),'.mdt']);
            load (filename);
            filename_01 =
eval(['Plaque',num2str(Block),'_',num2str(layer)]);

            time = filename_01(:,1);
            Fx12 = filename_01(:,2);
            Fx34 = filename_01(:,3);
            Fy14 = filename_01(:,4);
            Fy23 = filename_01(:,5);
            Fz1 = filename_01(:,6);
            Fz2 = filename_01(:,7);
            Fz3 = filename_01(:,8);
            Fz4 = filename_01(:,9);

%%%%%%%%%%%%%%FORCE CALCULATION%%%%%%%%%%%%%%
            Fx = Fx12 + Fx34;
            Fy = Fy14 + Fy23;
            Fz = Fz1+ Fz2 + Fz3 + Fz4;
            Fs = sqrt(Fx.*Fx + Fy.*Fy);
            Fr = sqrt(Fx.*Fx + Fy.*Fy + Fz.*Fz);
            frequency =10000;

            figure()
            plot(time,Fx,'b')
            title('Fx')
            figure()
            plot(time,Fy,'r')
            title('Fy')
            figure()
            plot(time,Fz,'g')
            title('Fz')
            figure()
```

```

        plot(time,Fs,'m')
        title('Fs')
        figure()
        plot(time,Fr,'c')
        title('Fr')

        x=1;%input('Is it OK?? Going to Frequency Alanysis?? [1
Continue with frequency Analysis / 0 Continue without frequency
Analysis]\n');
%           close all;
%%%%%%%%%%%%%%%%%%%%%%%%%%%%%%%%%%%%%%%%%%%%%%%%%%%%%%%%%%%%%%%%%%%%%%%%FREQUENCY ANALYSIS%%%%%%%%%%%%%%%%%%%%%%%%%%%%%%%%%%%%%%%%%%%%%%%%%%%%%%%%%%%%%%%%%%%%%%%%

        Frequency_Analysis(Fx,frequency,'Fx');
        Frequency_Analysis(Fy,frequency,'Fy');
        Frequency_Analysis(Fz,frequency,'Fz');
        Frequency_Analysis(Fs,frequency,'Fs');
        Frequency_Analysis(Fr,frequency,'Fr');
    end

%%%%%%%%%%%%%%%%%%%%%%%%%%%%%%%%%%%%%%%%%%%%%%%%%%%%%%%%%%%%%%%%%%%%%%%%CYCLE RECOGNITION
FUNCTION%%%%%%%%%%%%%%%%%%%%%%%%%%%%%%%%%%%%%%%%%%%%%%%%%%%%%%%%%%%%%%%%%%%%%%%%
        fprintf('Alloy %c ,Block %d , Layer %d
\n',Name(Alloy),Block,layer)
        [Std_Cycle] = Cycle_Recognition(time,Fy);
        Std_Cycle(:,2) = round(Std_Cycle(:,2));
        Peak_Std(Alloy,Block,layer) = (length(Std_Cycle)-1)/2;

%%%%%%%%%%%%%%%%%%%%%%%%%%%%%%%%%%%%%%%%%%%%%%%%%%%%%%%%%%%%%%%%%%%%%%%%FILTRATION FUNCTION%%%%%%%%%%%%%%%%%%%%%%%%%%%%%%%%%%%%%%%%%%%%%%%%%%%%%%%%%%%%%%%%%%%%%%%%
    while 1
        x=1;%input('Type of Filteration\n');
        y=3000;%input('Frequency / Range of Filteration\n');
        z=1;%input('Range of Filteration\n');

        [FFx] = Flexible_Filteration(Fx,x,y,z);
        [FFy] = Flexible_Filteration(Fy,x,y,z);
        [FFz] = Flexible_Filteration(Fz,x,y,z);

        figure()
        plot(time,Fx,'b',time,FFx,'r')
        title('Fx')
        figure()
        plot(time,Fy,'b',time,FFy,'r')
        title('Fy')
        figure()
        plot(time,Fz,'b',time,FFz,'r')
        title('Fz')

        s=1;%input('\n Does Filteration fit??\n');
%           close all;
        if s==1
            break;
        else
            error('Error in Filteration')
        end
    end

```

```

end

%%%%%%%%%%%%%%%%%%%%%%%%%%%%%%%%%%%%%%%%%%%%%%%%%%%%%%%%%%%%%%%%%%%%%%%%CORRECTION FUNCTION%%%%%%%%%%%%%%%%%%%%%%%%%%%%%%%%%%%%%%%%%%%%%%%%%%%%%%%%%%%%%%%%%%%%%%%%
[Org_Fx] = Flexible_Filteration(Fx,1,20,1);
[Org_Fy] = Flexible_Filteration(Fy,1,20,1);
[Org_Fz] = Flexible_Filteration(Fz,1,20,1);

[Cor_FFx] = Force_Correction(FFx,Std_Cycle,Org_Fx);
[Cor_FFy] = Force_Correction(FFy,Std_Cycle,Org_Fy);
[Cor_FFz] = Force_Correction(FFz,Std_Cycle,Org_Fz);

figure();
plot(time,Fx,'b',time,FFx,'r',time,Cor_FFx,'g')
title('Fx')

figure();
plot(time,Fy,'b',time,FFy,'r',time,Cor_FFy,'g')
title('Fy')

figure();
plot(time,Fz,'b',time,FFz,'r',time,Cor_FFz,'g')
title('Fz')

s=1;%input('\n Does Correction fit??\n');
close all;
if s~=1
    error('Error in Correction')
end

Cor_FFx = sqrt(Cor_FFx.*Cor_FFx + Cor_FFy.*Cor_FFy);
Cor_FFy = sqrt(Cor_FFx.*Cor_FFx + Cor_FFy.*Cor_FFy +
Cor_FFz.*Cor_FFz);

%%%%%%%%%%%%%%%%%%%%%%%%%%%%%%%%%%%%%%%%%%%%%%%%%%%%%%%%%%%%%%%%%%%%%%%%PEAK EXTRACTION FUNCTION%%%%%%%%%%%%%%%%%%%%%%%%%%%%%%%%%%%%%%%%%%%%%%%%%%%%%%%%%%%%%%%%%%%%%%%%
while 1
    fprintf('Fx\n')
    Final_Peak_Fx = peak_Ext(time,Cor_FFx,Std_Cycle);
    figure();

plot(time,Fx,'y',time,Cor_FFx,'b',Final_Peak_Fx(:,4)/frequency,Final_P
eak_Fx(:,2),'r',Final_Peak_Fx(:,4)/frequency,Final_Peak_Fx(:,3),'m')
title('Fx');
x=input('Does The Peak Extraction fits Logically for
Fx??[1,-1]\n');
if x == 1
    close all
    break;
end
end

while 1
    fprintf('Fy\n')
    Final_Peak_Fy = peak_Ext(time,Cor_FFy,Std_Cycle);
    figure();

```

```

plot(time,Fy,'y',time,Cor_FFy,'b',Final_Peak_Fy(:,4)/frequency,Final_P
eak_Fy(:,2),'r',Final_Peak_Fy(:,4)/frequency,Final_Peak_Fy(:,3),'m')
title('Fy');
x=input('Does The Peak Extraction fits Logically for
Fy??[1,-1]\n');
    if x ==      1
        close all
        break;
    end
end

while 1
    fprintf('Fz\n')
    Final_Peak_Fz = peak_Ext(time,Cor_FFz,Std_Cycle);
    figure();

plot(time,Fz,'y',time,Cor_FFz,'b',Final_Peak_Fz(:,4)/frequency,Final_P
eak_Fz(:,2),'r',Final_Peak_Fz(:,4)/frequency,Final_Peak_Fz(:,3),'m')
title('Fz');
x=input('Does The Peak Extraction fits Logically for
Fz??[1,-1]\n');
    if x ==      1
        close all
        break;
    end
end

while 1
    fprintf('Fs\n')
    Final_Peak_Fs = peak_Ext(time,Cor_FFf,Std_Cycle);
    figure();

plot(time,Fs,'y',time,Cor_FFf,'b',Final_Peak_Fs(:,4)/frequency,Final_P
eak_Fs(:,2),'r',Final_Peak_Fs(:,4)/frequency,Final_Peak_Fs(:,3),'m')
title('Fs');
x=input('Does The Peak Extraction fits Logically for
Fs??[1,-1]\n');
    if x ==      1
        close all
        break;
    end
end

while 1
    fprintf('Fr\n')
    Final_Peak_Fr = peak_Ext(time,Cor_FFf,Std_Cycle);
    figure();

plot(time,Fr,'y',time,Cor_FFf,'b',Final_Peak_Fr(:,4)/frequency,Final_P
eak_Fr(:,2),'r',Final_Peak_Fr(:,4)/frequency,Final_Peak_Fr(:,3),'m')
title('Fr');
x=input('Does The Peak Extraction fits Logically for
Fr??[1,-1]\n');

```

```

        if x == 1
            close all
            break;
        end
    end
end

%%%%%%%%%%%%%%%%%%%%%%%%%%%%%%%%%%%%%%%%%%%%%%%%%%%%%%%%%%%%%%%%%%%%%%%%%DATA MERGING%%%%%%%%%%%%%%%%%%%%%%%%%%%%%%%%%%%%%%%%%%%%%%%%%%%%%%%%%%%%%%%%%%%%%%%%%
Path = Old_Path + (length(Std_Cycle)-1)/2;
for i=Old_Path + 1: Path
    Final_Fx(i,1,Alloy) = i;
    Final_Fx(i,2,Alloy) = Final_Peak_Fx(i-Old_Path,2);
    Final_Fx(i,3,Alloy) = Final_Peak_Fx(i-Old_Path,3);

    Final_Fy(i,1,Alloy) = i;
    Final_Fy(i,2,Alloy) = Final_Peak_Fy(i-Old_Path,2);
    Final_Fy(i,3,Alloy) = Final_Peak_Fy(i-Old_Path,3);

    Final_Fz(i,1,Alloy) = i;
    Final_Fz(i,2,Alloy) = Final_Peak_Fz(i-Old_Path,2);
    Final_Fz(i,3,Alloy) = Final_Peak_Fz(i-Old_Path,3);

    Final_Fs(i,1,Alloy) = i;
    Final_Fs(i,2,Alloy) = Final_Peak_Fs(i-Old_Path,2);
    Final_Fs(i,3,Alloy) = Final_Peak_Fs(i-Old_Path,3);

    Final_Fr(i,1,Alloy) = i;
    Final_Fr(i,2,Alloy) = Final_Peak_Fr(i-Old_Path,2);
    Final_Fr(i,3,Alloy) = Final_Peak_Fr(i-Old_Path,3);
end
Old_Path = Path;

clearvars -except Name Alloy Block layer Final_Fx Final_Fy
Final_Fz Final_Fs Final_Fr Old_Path Path Peak_Std
end
end
end

figure()
plot(Final_Fr(:,1,1),Final_Fr(:,2,1),'b*',Final_Fr(:,1,2),Final_Fr(:,2,2),
'r*',Final_Fr(:,1,3),Final_Fr(:,2,3),'g*',Final_Fr(:,1,4),Final_Fr
(:,2,4),'m*',Final_Fr(:,1,5),Final_Fr(:,2,5),'k*')
legend('Alloy A','Alloy B','Alloy C','Alloy D','Alloy E')
title('Fr')

xlswrite('C:\Users\p2-1020.LABORATOIRE\Desktop\Nouveau
dossier\Force_Finalx.xls', Final_Fx(:, :, 1), 'Alloy A', 'A1')
xlswrite('C:\Users\p2-1020.LABORATOIRE\Desktop\Nouveau
dossier\Force_Finalx.xls', Final_Fx(:, :, 2), 'Alloy B', 'A1')
xlswrite('C:\Users\p2-1020.LABORATOIRE\Desktop\Nouveau
dossier\Force_Finalx.xls', Final_Fx(:, :, 3), 'Alloy C', 'A1')
xlswrite('C:\Users\p2-1020.LABORATOIRE\Desktop\Nouveau
dossier\Force_Finalx.xls', Final_Fx(:, :, 4), 'Alloy D', 'A1')
xlswrite('C:\Users\p2-1020.LABORATOIRE\Desktop\Nouveau
dossier\Force_Finalx.xls', Final_Fx(:, :, 5), 'Alloy E', 'A1')

```

```
xlswrite('C:\Users\p2-1020.LABORATOIRE\Desktop\Nouveau dossier\Force_Finaly.xls', Final_Fy(:, :, 1), 'Alloy A', 'A1')
xlswrite('C:\Users\p2-1020.LABORATOIRE\Desktop\Nouveau dossier\Force_Finaly.xls', Final_Fy(:, :, 2), 'Alloy B', 'A1')
xlswrite('C:\Users\p2-1020.LABORATOIRE\Desktop\Nouveau dossier\Force_Finaly.xls', Final_Fy(:, :, 3), 'Alloy C', 'A1')
xlswrite('C:\Users\p2-1020.LABORATOIRE\Desktop\Nouveau dossier\Force_Finaly.xls', Final_Fy(:, :, 4), 'Alloy D', 'A1')
xlswrite('C:\Users\p2-1020.LABORATOIRE\Desktop\Nouveau dossier\Force_Finaly.xls', Final_Fy(:, :, 5), 'Alloy E', 'A1')
```

```
xlswrite('C:\Users\p2-1020.LABORATOIRE\Desktop\Nouveau dossier\Force_Finalz.xls', Final_Fz(:, :, 1), 'Alloy A', 'A1')
xlswrite('C:\Users\p2-1020.LABORATOIRE\Desktop\Nouveau dossier\Force_Finalz.xls', Final_Fz(:, :, 2), 'Alloy B', 'A1')
xlswrite('C:\Users\p2-1020.LABORATOIRE\Desktop\Nouveau dossier\Force_Finalz.xls', Final_Fz(:, :, 3), 'Alloy C', 'A1')
xlswrite('C:\Users\p2-1020.LABORATOIRE\Desktop\Nouveau dossier\Force_Finalz.xls', Final_Fz(:, :, 4), 'Alloy D', 'A1')
xlswrite('C:\Users\p2-1020.LABORATOIRE\Desktop\Nouveau dossier\Force_Finalz.xls', Final_Fz(:, :, 5), 'Alloy E', 'A1')
```

```
xlswrite('C:\Users\p2-1020.LABORATOIRE\Desktop\Nouveau dossier\Force_Finalfs.xls', Final_Fs(:, :, 1), 'Alloy A', 'A1')
xlswrite('C:\Users\p2-1020.LABORATOIRE\Desktop\Nouveau dossier\Force_Finalfs.xls', Final_Fs(:, :, 2), 'Alloy B', 'A1')
xlswrite('C:\Users\p2-1020.LABORATOIRE\Desktop\Nouveau dossier\Force_Finalfs.xls', Final_Fs(:, :, 3), 'Alloy C', 'A1')
xlswrite('C:\Users\p2-1020.LABORATOIRE\Desktop\Nouveau dossier\Force_Finalfs.xls', Final_Fs(:, :, 4), 'Alloy D', 'A1')
xlswrite('C:\Users\p2-1020.LABORATOIRE\Desktop\Nouveau dossier\Force_Finalfs.xls', Final_Fs(:, :, 5), 'Alloy E', 'A1')
```

```
xlswrite('C:\Users\p2-1020.LABORATOIRE\Desktop\Nouveau dossier\Force_Finalr.xls', Final_Fr(:, :, 1), 'Alloy A', 'A1')
xlswrite('C:\Users\p2-1020.LABORATOIRE\Desktop\Nouveau dossier\Force_Finalr.xls', Final_Fr(:, :, 2), 'Alloy B', 'A1')
xlswrite('C:\Users\p2-1020.LABORATOIRE\Desktop\Nouveau dossier\Force_Finalr.xls', Final_Fr(:, :, 3), 'Alloy C', 'A1')
xlswrite('C:\Users\p2-1020.LABORATOIRE\Desktop\Nouveau dossier\Force_Finalr.xls', Final_Fr(:, :, 4), 'Alloy D', 'A1')
xlswrite('C:\Users\p2-1020.LABORATOIRE\Desktop\Nouveau dossier\Force_Finalr.xls', Final_Fr(:, :, 5), 'Alloy E', 'A1')
```

%%%

%%%**NOISE FREQUENCY ANALYSIS**%%%

```
function Frequency_Analysis(Process,frequency,tit)

NS_Process = fft(Process);
NSR_Process = fftshift(NS_Process);
f = linspace(-frequency/2,frequency/2,length(Process));

figure();
plot(f,abs(NSR_Process),'b');
title(sprintf('%s',tit))

end
```

%%%**FILTERATION FUNCTION**%%%

```
function [F_Process] = Flexible_Filteration(Process,type,Range,Loop)
History = Process;
%%Type of filteration
if type == 1
```

%%% **Using Digital Filter Techniques**%%%

```
    Fil_01 = designfilt('lowpassiir', 'PassbandFrequency', Range,
'StopbandFrequency', 1.05*Range, 'PassbandRipple', 1,
'StopbandAttenuation', 2, 'SampleRate', 10000);
    F_Process = filtfilt(Fil_01,Process);
```

```
elseif type == 2
```

%%% **Smoothing Using Dynamic Avrage**%%%

```
    Dyn_avrrate = Range;
    Dyn_Coeff = ones(1, Dyn_avrrate)/Dyn_avrrate;

    for i=1:Loop
        F_Process = filter(Dyn_Coeff, 1, Process);
        Process = F_Process;
    end
```

```
elseif type == 3
```

%%% **Smoothing Using Savitzky-Golay**%%%

```
    for i=1:Loop
        F_Process = sgolayfilt(Process,5,Range);
        Process = F_Process;
    end
```

```

elseif type ==4

%%%%%%%%%%%%%%%%%%%%%%%%%%%%%%%%%%%%%%%%%%%%%%%%%%%%%%%%%%%%%%%%%%%%%%%% Spiking Removal using Median Filter Technique%%%%%%%%%%%%%%%%%%%%%%%%%%%%%%%%%%%%%%%%%%%%%%%%%%%%%%%%%%%%%%%%%%%%%%%%
    for i=1:Loop
        F_Process = medfilt1(Process,Range);
        Process = F_Process;
    end
end

end

%%%%%%%%%%%%%%%%%%%%%%%%%%%%%%%%%%%%%%%%%%%%%%%%%%%%%%%%%%%%%%%%%%%%%%%%CYCLE RECOGNITION FUNCTION%%%%%%%%%%%%%%%%%%%%%%%%%%%%%%%%%%%%%%%%%%%%%%%%%%%%%%%%%%%%%%%%%%%%%%%%

function [Std_Cycle] = Cycle_Recognition(time,Fy)
%%%%%%%%%%%%%%%%%%%%%%%%%%%%%%%%%%%%%%%%%%%%%%%%%%%%%%%%%%%%%%%%%%%%%%%%STANDARDIZATION%%%%%%%%%%%%%%%%%%%%%%%%%%%%%%%%%%%%%%%%%%%%%%%%%%%%%%%%%%%%%%%%%%%%%%%%
%%%%%%%%%%%%%%%%%%%%%%%%%%%%%%%%%%%%%%%%%%%%%%%%%%%%%%%%%%%%%%%%%%%%%%%%
frequency = 10000;
Fil_01 = designfilt('lowpassfir', 'PassbandFrequency', 1,
'StopbandFrequency', 1.1, 'PassbandRipple', 1, 'StopbandAttenuation',
2, 'SampleRate', 10000);
F_Process = filtfilt(Fil_01,Fy);
PeakHight = mean(F_Process);

[Bottom(:,1), Bottom(:,2)] = findpeaks(-1*F_Process, 'MinPeakHeight', -
30, 'MinPeakDistance', 5000);
[CPM_Peak(:,1), CPM_Peak(:,2)] =
findpeaks(F_Process, 'MinPeakHeight', PeakHight, 'MinPeakDistance', 5000);

Bottom(:,1) = -1*Bottom(:,1);
for i=1:length(Bottom)
    CPM_Bottom(i+1,1) = Bottom(i,1);
    CPM_Bottom(i+1,2) = Bottom(i,2);
end
CPM_Bottom(1,1) = 0;
CPM_Bottom(1,2) = 1;
CPM_Bottom(length(Bottom)+2,1) = 0;
CPM_Bottom(length(Bottom)+2,2) = length(F_Process);

Index = length(CPM_Peak) + length(CPM_Bottom);
CPM_Peak(length(CPM_Peak)+1,2) = length(F_Process)+10;

%%%%%%%%%%%%%%%%%%%%%%%%%%%%%%%%%%%%%%%%%%%%%%%%%%%%%%%%%%%%%%%%%%%%%%%%CREATING UNIFIED MATRIX%%%%%%%%%%%%%%%%%%%%%%%%%%%%%%%%%%%%%%%%%%%%%%%%%%%%%%%%%%%%%%%%%%%%%%%%
j=1;
i=1;
for n=1:Index
    if CPM_Peak(j,2) < CPM_Bottom(i,2)
        Unified_Matrix(n,1) = CPM_Peak(j,1);
        Unified_Matrix(n,2) = CPM_Peak(j,2);
        j=j+1;
    elseif CPM_Peak(j,2) > CPM_Bottom(i,2)
        Unified_Matrix(n,1) = CPM_Bottom(i,1);
        Unified_Matrix(n,2) = CPM_Bottom(i,2);
        i=i+1;
    end
end

```

```

        end
    end

    %%%%%%%%%%%%%%%%%%%%%%%%%%%%%%%%%%%%%%%%%%%%%%%%%%%%%%%%%%%%%%%%%%%%%%%%%%MATRIX REDUCTION%%%%%%%%%%%%%%%%%%%%%%%%%%%%%%%%%%%%%%%%%%%%%%%%%%%%%%%%%%%%%%%%%%%%%%%%%

    Avr_Sum = 0;
    Loc_Sum = 0;
    Counter = 0;
    SCC = 1;
    for i=1:length(Unified_Matrix)
        Avr_Sum = Avr_Sum + Unified_Matrix(i,1);
        Loc_Sum = Loc_Sum + Unified_Matrix(i,2);
        Counter = Counter+1;
        if i== length(Unified_Matrix)
            Avr_Sum = Avr_Sum/Counter;
            Loc_Sum = Loc_Sum/Counter;
            Std_Cycle(SCC,1) = Avr_Sum;
            Std_Cycle(SCC,2) = Loc_Sum;

            elseif (Unified_Matrix(i,1) < PeakHight && Unified_Matrix(i+1,1) >
            PeakHight) || (Unified_Matrix(i,1) > PeakHight &&
            Unified_Matrix(i+1,1) < PeakHight)
                Avr_Sum = Avr_Sum/Counter;
                Loc_Sum = Loc_Sum/Counter;
                Std_Cycle(SCC,1) = Avr_Sum;
                Std_Cycle(SCC,2) = Loc_Sum;

                Avr_Sum = 0;
                Loc_Sum = 0;
                Counter =0;
                SCC = SCC+1;
        end
    end

    figure();
    plot(time,F_Process)
    hold on
    for i=1:length(Std_Cycle)
        line([Std_Cycle(i,2)/frequency Std_Cycle(i,2)/frequency],[ylim])
    end
    x=1;%input('\n Does Standard Cycle fit??\n');
    if x == -1
        error('Error in Standard Cycle Recognition')
    end
end
end

```

%%CORRECTION FUNCTION%%

```
function [Cor_Force] = Force_Correction(Force,Std_Cycle,Origin)
n=3;
for i=1: length(Force)
    if i < Std_Cycle(n,2)
        Cor_Force(i) = Force(i) - Origin(Std_Cycle(n-2,2));
    elseif i== length(Force) || n== length(Std_Cycle)
        Cor_Force(i) = Force(i) - Origin(Std_Cycle(n-2,2));
    else
        n=n+2;
        Cor_Force(i) = Force(i) - Origin(Std_Cycle(n-2,2));
    end
end
end
end
```

%%PEAK EXTRACTION FUNCTION%%

```
function Final_Peak = peak_Ext(time,Cor_FF,Std_Cycle)

Fil_01 = designfilt('lowpassiir', 'PassbandFrequency', 20,
'StopbandFrequency', 1.05*20, 'PassbandRipple', 1,
'StopbandAttenuation', 2, 'SampleRate', 10000);
F_Process = filtfilt(Fil_01,Cor_FF);

Percent = input('\n Minimum Peak Percentage of Max Height for The
Force = \n');
for n=3:2:length(Std_Cycle)
    limit = Percent*(max(Cor_FF(Std_Cycle(n-2,2):Std_Cycle(n,2)-1))-
F_Process(Std_Cycle(n-1,2))) + F_Process(Std_Cycle(n-1,2));
    [Peak_Fz(:,1),Peak_Fz(:,2)] = findpeaks(Cor_FF(Std_Cycle(n-
2,2):Std_Cycle(n,2)-
1),'MinPeakDistance',200,'MinPeakProminence',0,'MinPeakHeight',limit,'
Threshold',0);

    Final_Peak((n-1)/2,1) = (n-1)/2;
    Final_Peak((n-1)/2,2) = mean(Peak_Fz(:,1));
    Final_Peak((n-1)/2,3) = max(Peak_Fz(:,1));
    Final_Peak((n-1)/2,4) = Std_Cycle(n-1,2);

    clear Peak_Fz
end
end
end
```